Quantum Measurement and Cloning of States

By

Anirudh Reddy

A thesis Submitted to the Jawaharlal Nehru University
for the degree of Doctor of Philosophy
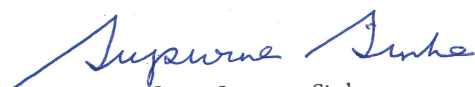
Theoretical Physics
Raman Research Institute
Bangalore, India
May 2018

To my mom and my dad.

Author's declaration

I, hereby, declare that this thesis is composed independently by me at Raman Research Institute, Bangalore, India, under the supervision of Prof. Supurna Sinha. The subject matter presented has not been previously formed the basis of the award of any degree, diploma, associateship, fellowship or another similar title in any other university. I also declare that I have run it through the *Turnitin* plagiarism software.

Professor Supurna Sinha

Theoretical Physics
Raman Research Institute
Bangalore - 560080
India.

Anirudh Reddy

Certificate

This is to certify that the thesis entitled *"Quantum Measurement and Cloning of States"* submitted by Anirudh Reddy for the award of the degree of doctor of philosophy of Jawaharlal Nehru University is his original work. This has not been published or submitted to any other University for any other Degree or Diploma.

Professor Ravi Subrahmanyam

(Center Chairperson)
Director
Raman Research Institute
Bangalore - 560080
India.

Professor Supurna Sinha

(Thesis Supervisor)

Quantum Measurement and Cloning of States

Synopsis

In this thesis aspects of quantum measurement and cloning of states are explored. Quantum cloning has been a subject of interest for a long time, starting with the *no-cloning theorem*. The no-cloning theorem states that it is impossible to create an identical copy of an arbitrary quantum state. While perfect copying is not possible, one can consider imperfect copying. In such a scenario, one can copy all quantum states at the same level of imperfection and achieve optimal quantum cloning. Optimal cloning can be realised using atom-photon interactions, where one tries to copy photon polarisation states. Even this corresponds to a highly idealised situation, free from sources of noise that are generally present in a laboratory. Our aim is to study atom-photon interactions with the introduction of thermal noise in the atomic system, the photonic system and both, thereby studying to what extent the thermal noise corrupts the cloning process by comparing the initial and final states using the concept of fidelity.

The no-cloning theorem has been extended to classical systems. There does exist a classical no-cloning theorem. Even though in our everyday experience we do see copying of classical information (for instance, a photocopying machine), not much is known about the physics behind it. Aaron Feynes has studied classical cloning using symplectic maps and shown that the no-cloning theorem in classical systems occurs as a result of a too restrictive definition of the cloning process. We generate explicit cloning maps which facilitate classical cloning. In addition, we come up with a procedure to generate Hamiltonians pertaining to cloning maps. We also study the corruption of classical cloning in the presence of thermal noise, which transforms a deterministic system to a statistical mechanical system.

An issue closely related to cloning of states is quantum measurement since one needs to compare the original state with the state obtained at the output of a measurement. We study the quantum measurement process under coarse graining using a Stern-Gerlach setup. We calculate the exact wave function of a Stern-Gerlach setup using the Feynman path integral approach. Coarse graining is done by considering a lower limit on the size of a pixel on the screen, which is used to detect the silver atom. We then look at the information extracted in a coarse quantum measurement.

Finally the issues of distinguishability and discrimination of quantum states are studied from an operational point of view. There exist different metrics for the comparison of quantum states. We consider the relative entropy for the construction of the metric (Bogoliubov-Kubo-Mori metric), discussing its connection with Likelihood theory. One problem with measurements in quantum systems is we have only probabilities to compare two states. By optimising the measurement basis with respect to the distinguishability of two quantum states we end up with the Bures-Hestrom metric. Using the Cramer-Rao bound we show that the BKM metric is superior to the BH metric in comparing any two quantum states. We also come up with a measurement strategy involving measurements on multiple qubits at a time (which gives us a practical way to realize the BKM metric) to beat the BH metric.

The thesis is structured as follows. In Chapter *I* we give an overview on the aspects of quantum cloning and classical cloning. We also discuss the quantum measurement process and discuss different approaches towards understanding the quantum measurement process. In Chapter *II* we study cloning of quantum states and study how thermal noise leads to a corruption of the cloning process. We then look at the classical limit of the quantum cloning process. We also look at the classical cloning process with the idea of generating a Hamiltonian for realising the process operationally. Then we study how classical cloning is affected when we replace a delta function by a function with a finite spread. In Chapter *III* we consider a Stern-Gerlach setup to analyse the idea of resource limitation in a quantum measurement. We study resource limitation in the form of the size of the pixels on the screen used for detection of silver atoms. Then we calculate the average information extracted per event un-

der coarse graining. In Chapter *IV* we come up with a strategy to realise the BH metric experimentally by optimising the measurement direction with respect to the states being discriminated and show that the BKM metric is superior in distinguishing two quantum states. We propose a strategy to realise the BKM metric experimentally by measuring multiple qubits at a time. In Chapter *V* we present a way to extract the maximum information from an unknown quantum state using a strategy similar to the one mentioned in Chapter IV. We finally end the thesis in Chapter *VI* with some concluding remarks and future directions.

List Of Publications

Articles Published in journals/unpublished eprints.

1. Anirudh Reddy, Joseph Samuel, Kumar Shivam, and Supurna Sinha. Coarse quantum measurement: An analysis of the Stern-Gerlach experiment. Physics Letters A, 380(11):1135 - 1140, 2016.

2. Kumar Shivam, Anirudh Reddy, Joseph Samuel, and Supurna Sinha. Entropy and Geometry of Quantum States. International Journal of Quantum Information, Vol. 16, No. 4 (2018) 1850032 (17 pages).

3. Anirudh Reddy, Joseph Samuel, and Supurna Sinha A Physical Perspective on Classical Cloning, Arxiv:1810.12080

Contents

List of Figures

Acknowledgement

Foremost, I would like to express my sincere gratitude to my advisor Prof. Supurna Sinha for the continuous support of my Ph.D study and research, for her patience, motivation, enthusiasm, and immense knowledge. Her guidance helped me throughout my PhD. research and writing of this thesis.

Besides my advisor, I would like to thank the rest of my thesis committee: Prof. Joseph Samuel, and Prof. Shiv Sethi, for their encouragement and insightful comments.

I would also like to thank the library and admin. staff Manju, Radha, Marisa, and Mahadev.

I thank my fellow labmate in the Theoretical Physics Group: Kumar Shivam, for the stimulating discussions, for the sleepless nights we were working to-

"Colorless green ideas sleep furiously."

Noam Chomsky

1

Introduction

"A Mathematical Theory of Communication" by Claude Shannon[2] has revolutionised information theory and the process of communication. Prior to Shannon's work, it was widely believed that error-free transmission of information was not possible. Shannon, using his theory, has shown that it is possible to achieve error-free transmission if the Information entropy (entropy) of the sig-

nal is less than the channel capacity. The Channel capacity depends upon the properties of the channel that cause noise[3]. He achieved this by quantifying the information entropy, by removing the subjectivity involved[4]. The entropy of a signal or any physical system, in general, is defined as the ignorance of the observer or randomness in the system. Mathematically,

$$H = -\sum_i p_i \log p_i. \tag{1.1}$$

The units for measuring entropy in base two is a *bit*, in base e is a *nat*.

This definition of information entropy has helped in many areas such as data transmission, data compression, statistical mechanics[4], thermodynamics[5,6], quantum mechanics[7], and many other fields. For understanding data compression, consider a random variable with non-uniform distribution over the possible outcomes. While encoding the data, either we can use the same description length for all the possible outcomes; or we can use shorter description for the high probability outcomes and longer description for the lower probability outcomes, thus the average description length is reduced and also the entropy of the signal. This way of assigning different lengths allows us to send the signal, error-free, in a low capacity channel.

The definition of information entropy is related to the definition of entropy in statistical mechanics $(-k_B \sum_i p_i \ln p_i)$. This connection establishes that the information entropy is physical, not just a mathematical concept, using Maxwell's

demon[5]. Landauer has even established a relation between information theory and thermodynamics in 1961[5], famously known as Landauer's principle. Landauer's principle states that the minimum energy one has to spend in order to erase one bit of information is $k_B T \ln 2$, where k_B is the Boltzmann's constant and T is the temperature.

The study of information theory using quantum mechanics is quantum information. A definition of entropy exists in the case of quantum states, similar to the one defined earlier, called the Von Neumann entropy[8]

$$S = -\text{Tr}(\rho \ln \rho) = -\sum_i \lambda_i \ln \lambda_i, \tag{1.2}$$

where ρ is the density matrix, λ_is are the eigenvalues of the density matrix.

Many aspects of classical information and computation have been subjected to quantum mechanical treatment: for instance, quantum computation using quantum gates, quantum circuits and algorithms. In the case of quantum information, we have a qubit, qutrit, and qudit, etc. *Qubit* (quantum bit) is a fundamental concept in quantum information analogous to a *bit* in classical information. A qubit is an arbitrary state of a two-level system, that can be written as a linear combination or superposition of the basis states,

$$|\psi\rangle = \alpha\,|0\rangle + \beta\,|1\rangle. \tag{1.3}$$

Similarly, a qutrit is an arbitrary state in a three-level system, and a qudit is a state in an n-level system.

Quantum computation is a process where a qubit undergoes changes while passing through a quantum gate (analogous to a classical gate). We have a quantum NOT (X) gate similar to the classical one. Here $|0\rangle$ and $|1\rangle$ are flipped under the operation as expected, but the operation is special because it preserves the linearity of quantum mechanics when applied on a superposition state,

$$X(\alpha |0\rangle + \beta |1\rangle) = \alpha |1\rangle + \beta |0\rangle .\tag{1.4}$$

Because of the linearity of quantum mechanics, for all the finite dimensional quantum systems, operators and states can be represented using matrices. Hence, the above equation can be rewritten as $X \begin{pmatrix} \alpha \\ \beta \end{pmatrix} = \begin{pmatrix} \beta \\ \alpha \end{pmatrix}$, where $X = \begin{pmatrix} 0 & 1 \\ 1 & 0 \end{pmatrix}$. This is an example of a gate which is present in both classical and quantum computations. There are some gates which are present only in the quantum context, but not in the classical context, such as , Z gate, $Hadamard(H)$ gate, etc. Mathematically,

$$Z = \begin{pmatrix} 1 & 0 \\ 0 & -1 \end{pmatrix} \implies Z(\alpha |0\rangle + \beta |1\rangle) = \alpha |0\rangle - \beta |1\rangle ,$$

$$H = \frac{1}{\sqrt{2}} \begin{pmatrix} 1 & 1 \\ 1 & -1 \end{pmatrix} \implies H(\alpha \ket{0} + \beta \ket{1}) = \alpha \frac{\ket{0} + \ket{1}}{\sqrt{2}} + \beta \frac{\ket{0} - \ket{1}}{\sqrt{2}}.$$

To generalise, let us discuss quantum gates on multiple qubits. One such gate is *Controlled*-NOT (CNOT) gate. CNOT gate is regarded as a generalised XOR gate (classical). But a notable difference between these two is, CNOT gate is reversible while XOR gate is not. CNOT gate requires two input qubits. First one is the control qubit and the second one is the target qubit. The operation of this gate can be described as: if $\ket{0}$ is chosen as the control qubit, then the target qubit is unaltered. If $\ket{1}$ is chosen as the control qubit, then the target qubit is flipped. This can be seen as, $\ket{00} \rightarrow \ket{00}, \ket{01} \rightarrow \ket{01}, \ket{10} \rightarrow \ket{11}, \ket{11} \rightarrow \ket{10}$. In matrix form, it can be written as

$$U_{\text{CNOT}} = \begin{pmatrix} 1 & 0 & 0 & 0 \\ 0 & 1 & 0 & 0 \\ 0 & 0 & 0 & 1 \\ 0 & 0 & 1 & 0 \end{pmatrix}. \tag{1.5}$$

This gate is not restricted to the two qubit case; it can be generalised to n qubits. One of the applications of the CNOT gate is the creation of the *Bell states*. This can be achieved by first applying the Hadamard gate on the control qubit and

then passing the qubit through the CNOT gate. This gives us the Bell states.

$\lvert 00 \rangle$	$\frac{\lvert 00 \rangle + \lvert 11 \rangle}{\sqrt{2}}$
$\lvert 01 \rangle$	$\frac{\lvert 01 \rangle + \lvert 10 \rangle}{\sqrt{2}}$
$\lvert 10 \rangle$	$\frac{\lvert 00 \rangle - \lvert 11 \rangle}{\sqrt{2}}$
$\lvert 11 \rangle$	$\frac{\lvert 01 \rangle - \lvert 10 \rangle}{\sqrt{2}}$

One of the applications of the Bell states is quantum teleportation. Quantum teleportation[9] is a process by which a state of a qubit is teleported, just by sharing an entangled pair and a classical message. For achieving this, it is not required to send a physical qubit through a quantum channel.

Quantum algorithms have been developed, using quantum gates, to solve problems which require an enormous amount of classical computation facility. These algorithms can be applied in the areas such as searching, quantum simulations, cryptography, etc. Simulating a quantum system using classical computers becomes an exceedingly complicated task, because of the complexity involved in quantum systems. Simulation of a quantum system using a quantum computer would reduce the complexity considerably.

Quantum parallelism is the reason for quantum algorithms to perform faster than classical ones. Loosely speaking, quantum parallelism is a feature of quantum algorithms, which enables quantum computers to evaluate the value of a function at different values simultaneously. One of the problems in classical computation is unstructured search. If the search has to be made in a space of

size N elements, time taken using classical computers will be of the order of N. There are quantum algorithms, such as Grover's algorithm[10], Deutsch's algorithm[11], etc., for which time scales are of the order $\sqrt{N}$.

One of the powerful applications of quantum computers is Shor's algorithm[12], developed by Peter Shor. Shor's algorithm is used for integer factorisation. To understand the power of this algorithm considering factorising an n-bit integer, a classical algorithm would take $\exp\{O(n^{1/3}(\log(n))^{2/3})\}$ operations, whereas Shor's algorithm would take $O(n^2 \log n \log \log n)$.

One of the basic differences between classical information and quantum information is the no-cloning theorem[13,14], which provides greater security in a communication channel. It is a key ingredient in quantum cryptography. This also allows us to detect the presence of an eavesdropper in the communication channel. The no-cloning theorem states that copying an arbitrary quantum state is not possible.

The discovery of the no-cloning theorem is a story in itself. It started with a paper entitled "FLASH - A superluminal communicator based upon a new kind of measurement"[15] by Nick Herbert. A process was discussed in the paper which would allow faster than light communication, thereby violating causality. Asher Peres, one of the referees of the paper, suggested publication, despite knowing it was wrong because he believed it would invoke interest in finding the error leading to a better understanding of physics. This has led to the discovery of the

no-cloning theorem. Describing these events Asher Peres[16] wrote

"This is the story of my own personal contribution to the no-cloning theorem[13,14], made public for the first time after more than twenty years. [...] It was obvious to me that the paper could not be correct because it violated the special theory of relativity. However, I was sure this was also obvious to the author. Anyway, nothing in the argument had any relation to relativity, so that the error had to be elsewhere. [...] I recommended to the editor of Foundations of Physics that this paper be published[15]. I wrote that it was obviously wrong, but I expected that it would elicit considerable interest and that finding the error would lead to significant progress in our understanding of physics. Soon afterwards, Wootters and Zurek[13] and Dieks[14] published, almost simultaneously, their versions of the no-cloning theorem. The tantalising title "A single quantum cannot be cloned" was contributed by John Wheeler. How the present paper got its name is another story.

There was another referee, GianCarlo Ghirardi, who recommended to reject Herbert's paper. His anonymous referee's report contained an argument which was a special case of the theorem in references[13,14]. Perhaps Ghirardi thought that his objections were so obvious that they did not deserve to be published in the form of an article (he did

publish them the following year[17]). Other objections were raised by Glauber, and then by many other authors whom I am unable to cite, because of space limitations."

No-Cloning Theorem:

Let us assume there exist a unitary operator and a machine that clone:

$$U \left| \phi \right\rangle_s \left| 0 \right\rangle_b \left| M \right\rangle = \left| \phi \right\rangle_s \left| \phi \right\rangle_b \left| M(\phi) \right\rangle, \tag{1.6}$$

$$U \left| \psi \right\rangle_s \left| 0 \right\rangle_b \left| M \right\rangle = \left| \psi \right\rangle_s \left| \psi \right\rangle_b \left| M(\psi) \right\rangle, \tag{1.7}$$

where $\left| \phi \right\rangle_s$, $\left| \psi \right\rangle_s$ are the original states to be copied, $\left| 0 \right\rangle_b$ is the blank state and $\left| M \right\rangle$ is the machine state. Now let us check the output for a superposition state, $\left| s \right\rangle_s = \alpha \left| \phi \right\rangle_s + \beta \left| \psi \right\rangle_s$,

$$U \left| s \right\rangle_s \left| 0 \right\rangle_b \left| M \right\rangle = \alpha \left| \phi \right\rangle_s \left| \phi \right\rangle_b \left| M(\phi) \right\rangle + \beta \left| \psi \right\rangle_s \left| \psi \right\rangle_b \left| M(\psi) \right\rangle. \tag{1.8}$$

In contrast, the expected outcome of a perfect cloning machine would be $U \left| s \right\rangle_s \left| 0 \right\rangle_b \left| M \right\rangle = \left| s \right\rangle_s \left| s \right\rangle_b \left| M(\phi, \psi) \right\rangle$. By taking the inner product between equations (1.6) and (1.7), we can say that $\left| \phi \right\rangle$ and $\left| \psi \right\rangle$ are either the same state or orthogonal to one another. This proves that there do not exist a unitary operator and a machine that clone an arbitrary state and if a cloning machine does

exist it can only copy orthogonal states.

There was no development in the area of cloning until 1996 when Bužek and Hillery[18] came up with the concept of imperfect cloning. They argued that the cloning procedure is dependent upon the input state, i.e., it copies the states $|\phi\rangle$ and $|\psi\rangle$ perfectly, while the copies of the superposition states are imperfect. They came up with the concept of a universal quantum-copying machine, which is independent of the input state. In other words, it copies all the states imperfectly, but the degree of imperfection is independent of the input state. They came up with the following transformations

$$U \left|\psi_+\right\rangle_s \left|0\right\rangle_b \left|M\right\rangle = \left|\psi_+\right\rangle_s \left|\psi_+\right\rangle_b \left|M(\psi_+)\right\rangle + \left(\left|\psi_+\right\rangle_s \left|\psi_-\right\rangle_b + \left|\psi_-\right\rangle_s \left|\psi_+\right\rangle_b\right) \left|N(\psi_+)\right\rangle,$$

$$U \left|\psi_-\right\rangle_s \left|0\right\rangle_b \left|M\right\rangle = \left|\psi_-\right\rangle_s \left|\psi_-\right\rangle_b \left|M(\psi_-)\right\rangle + \left(\left|\psi_+\right\rangle_s \left|\psi_-\right\rangle_b + \left|\psi_-\right\rangle_s \left|\psi_+\right\rangle_b\right) \left|N(\psi_-)\right\rangle,$$

where $|\psi_+\rangle$ and $|\psi_-\rangle$ are basis states in a qubit system. If we observe, in this process, along with the clone we are also producing some noise, which makes the cloning process imperfect. For calculating the imperfection, they used the Hilbert-Schmidt distance between the actual output and the ideal output states. The Hilbert-Schmidt distance between two density matrices (ρ and σ) is defined as

$$D(\rho, \sigma) = \text{Tr}\left[(\rho - \sigma)^2\right]. \tag{1.9}$$

For the imperfection to be the same for all the states, this distance has to be constant over all of state space, i.e., the distance is constant with respect to α and β for the superposition state $(|s\rangle = \alpha|\psi_+\rangle + \beta|\psi_-\rangle)$. Here, we calculate the distance between the ideal output and the actual output. By making this distance independent of α and β, we get

$$U|\psi_+\rangle_s|0\rangle_b|M\rangle = \sqrt{\frac{2}{3}}|\psi_+\rangle_s|\psi_+\rangle_b|\uparrow\rangle + \sqrt{\frac{1}{3}}|+\rangle|\downarrow\rangle, \quad \text{(1.10)}$$

$$U|\psi_-\rangle_s|0\rangle_b|M\rangle = \sqrt{\frac{2}{3}}|\psi_-\rangle_s|\psi_-\rangle_b|\uparrow\rangle + \sqrt{\frac{1}{3}}|+\rangle|\downarrow\rangle, \quad \text{(1.11)}$$

where, $|+\rangle = \frac{1}{\sqrt{2}}(|10\rangle + |01\rangle)$, $|\uparrow\rangle$ and $|\downarrow\rangle$ are the orthonormal basis states of the machine. The distance between the ideal and the actual outputs comes out to be 2/9. A perfect cloning machine takes one state as input and gives us two perfect output states (identical to the input state), this machine takes one input and two identical output states (not same as the input state), i.e., the original state gets corrupted.

Subsequent research work on cloning has shifted to using fidelity for measuring the imperfectness of the clone. Fidelity is defined as,

$$f = \langle\psi|\rho^{out}|\psi\rangle \quad \text{(1.12)}$$

Where, $|\psi\rangle$ = original qubit, ρ^{out} = reduced density matrix of one of the clones

after tracing out the original state and the machine state. Corresponding to the Hilbert-Schmidt distance 2/9, the fidelity comes out to be 5/6. The cloning procedure that produces imperfect clones has come to be known as optimal cloning.

This process has not been restricted to the study of only one input, one output systems or qubits. Gisin and Massar[19] have generalised this concept to N identical input qubits and M final copies (which include the input qubits), where fidelity is

$$f = \frac{NM + M + N}{M(N + 2)}.$$

(1.13)

The value 5/6 can be recovered by substituting $N = 1$ and $M = 2$.

Later, Werner[20] has generalised this result to a d dimensional system,

$$f = \frac{N}{M} + \frac{(M - N)(N + 1)}{M(d + N)}.$$

(1.14)

This formula gives us the accuracy with which a quantum state can be copied under ideal situation and this value cannot be surpassed.

One of the ways to realise an Universal Quantum Cloning Machine (UQCM) is to clone polarisation state of a photon using stimulated emissions. This process was proposed by Kempe et al[21]., Simon et al[22]. and experimentally realised by Fasel et al[23]., Lamas-Linares et al[24]. These processes use certain types of three-

level atomic systems (V or Λ) interacting with photonic modes. These photonic modes correspond to the atomic transitions, thereby cloning the polarisation state of the photon. A detailed description of the system and calculations are provided in the second chapter of this thesis.

Fan et al[25]., have studied the higher dimensional case of a similar system. A few other interesting papers in this direction involve "Improving the Fidelity of Quantum Cloning by Fast Cycling away the Unwanted Transition" by Agarwal et al[26]., and "Proposal for Inverting the Quantum Cloning of Photons" by Raeisi et al[27].

Research on quantum cloning has not been restricted to only UCQM. There have been studies on asymmetric cloning[28,29,30], where the fidelities of the output clones are not the same. There are studies on state-dependent cloning[31], where the idea is to simply make the best possible clones of any two arbitrary states. People have even explored the concept of cloning entangled states[32], continuous variable states[33], etc.

The idea of cloning has not been restricted to the quantum case. Daffertshofer et al.[1] and Aaron Fenyes[34] have worked on the idea of cloning a classical state. Although this might seem like a trivial process, the physics behind is not straight forward. The studies on classical cloning process have been very limited and restricted to a purely mathematical approach. In their paper[1], Daffertshofer et al. have worked on classical no-cloning theorem in phase space on probability dis-

tributions using Liouvillian dynamics. Aaron Fenyes discussed classical cloning from the point of view of symplectic geometry[34].

Quantum cloning is associated with many problems such as quantum measurements, state estimation, etc. While the no-cloning theorem may appear to be a disadvantage, it provides security in the context of quantum cryptography. This prevents an eavesdropper from making a copy of the quantum state that is shared through a quantum channel. One of the earliest quantum cryptography protocols was developed by Bennett and Brassard in 1984 known as the BB84 protocol[35].

No problem in quantum mechanics is complete without discussing the measurement problem. All measurements in quantum mechanics are associated with measuring an observable (operator $\hat{O}$), which is associated with a physical quantity like position ($\hat{x}$) or momentum ($-i\hbar\frac{\partial}{\partial x}$). Let us assume that the observable $\hat{O}$ has eigenstates $|o_i\rangle$, with eigenvalues o_i, i.e., $\hat{O}|o_i\rangle = o_i|o_i\rangle$, $i = 1, 2, ..d$, where d is the dimension of the system. Eigenvectors of any observable form a complete set of orthonormal basis. Consider a system prepared in the state

$$|\psi\rangle = \sum_i c_i |o_i\rangle, \ \sum_i |c_i|^2 = 1, \tag{1.15}$$

where c_is are complex numbers. When the observable $\hat{O}$ of the system is mea-

sured, it will reveal one of the eigenvalues (o_i) with the probabilities given by $P(o_i) = |c_i|^2$. Subsequently the state $|\psi\rangle$ is destroyed or collapsed and is not available for further investigation. This is one of the early interpretations developed in quantum mechanics known as the Copenhagen interpretation[36], where the wavefunction gives the complete description of the quantum system. This theory only predicts the probabilities of the outcomes.

Subsequently, other interpretations have been developed trying to explain the collapse of the wavefunction. The Von Neumann-Wigner interpretation[8] states that if a system in a state $|\psi\rangle$ results in a value of the observable o_i, then the state of the system immediately after the measurement is $|o_i\rangle$. This can be rewritten in terms of projection operators ($\hat{P}_i = |o_i\rangle\langle o_i|$), where the state after the measurement is given by $\dfrac{\hat{P}_i|\psi\rangle}{\sqrt{\langle\psi|\hat{P}_i|\psi\rangle}}$. This postulate can be easily verified by making immediate measurements on the system, which will give the same value o_i after repeated measurements.

Decoherence[37] further explains that loss of coherence in the system is caused by its interaction with the measuring apparatus. There are a few theories that are not dependent on the presence of an observer. These include Bohmian mechanics[38] and Many-worlds interpretation[39]. There are many collapse models[40] trying to explain what causes the collapse. One of the latest developments in this area is quantum measure theory[41,42] which talks about the histories and quantum measure associated with them rather than the probabilities.

The outline of the thesis is as follows:

In Chapter *II* we study cloning of quantum states and study how thermal noise leads to a corruption of the cloning process. We then look at the classical limit of the quantum cloning process. We also look at the classical cloning process with the idea of generating a Hamiltonian for realising the process operationally. Then we study how classical cloning is affected when we replace a delta function by a function with a finite spread.

In Chapter *III* we consider a Stern-Gerlach setup to analyse the idea of resource limitation in a quantum measurement. We study resource limitation in the form of the size of the pixels on the screen used for detection of silver atoms. Then we calculate the average information extracted per event under coarse graining.

In Chapter *IV* we come up with a strategy to realise the BH metric experimentally by optimising the measurement direction with respect to the states being discriminated and show that the BKM metric is superior in distinguishing two quantum states. We propose a strategy to realise the BKM metric experimentally by measuring multiple qubits at a time.

In Chapter *V* we present a way to extract the maximum information from an unknown quantum state using a strategy similar to the one mentioned in Chapter IV.

We finally end the thesis in Chapter *VI* with some concluding remarks.

2

Classical and Quantum Cloning

Copying information is a central aspect of information theory. While one can make an exact copy of classical information, it is not the same in the case of quantum information. In other words, we cannot make an exact replica of an arbitrary qubit, which is a direct result of the no-cloning theorem[13,14]. This is because of linearity and unitarity of quantum mechanics.

Here we use an atom-photon system [22,24] for studying the cloning process. In this system, achievement of a perfect clone is obstructed by the presence of spontaneous emission.

Initially, our system consists of a Fermionic oscillator (the atom) and a Bosonic oscillator (the photon). After the atom-photon interaction, we end up with two Bosonic oscillators (two photons). The atom is in a 3 level system (1 ground state with energy g and 2 degenerate excited states with energy e). $|e_1\rangle$ and $|e_2\rangle$ are coupled to polarization states ($\tilde{a}_1$ and $\tilde{a}_2$) of photon which are orthogonal to one another (See Fig. 2.1).

$|10\rangle$ represents a photon in $\tilde{a}_1$ polarization state.

$|01\rangle$ represents a photon in $\tilde{a}_2$ polarization state.

So an arbitrary photon in superposition can be represented as $(c_1 a_2^\dagger + c_2 a_1^\dagger) |0\rangle = c_1 |01\rangle + c_2 |10\rangle$.

$$|0\rangle = |00\rangle \quad \text{and} \quad |c_1|^2 + |c_2|^2 = 1 \qquad (2.1)$$

$a_1^\dagger$ — creation operator for $\tilde{a}_1$.

$a_2^\dagger$ — creation operator for $\tilde{a}_2$.

Since we are dealing with interaction between an atom and photons, we can
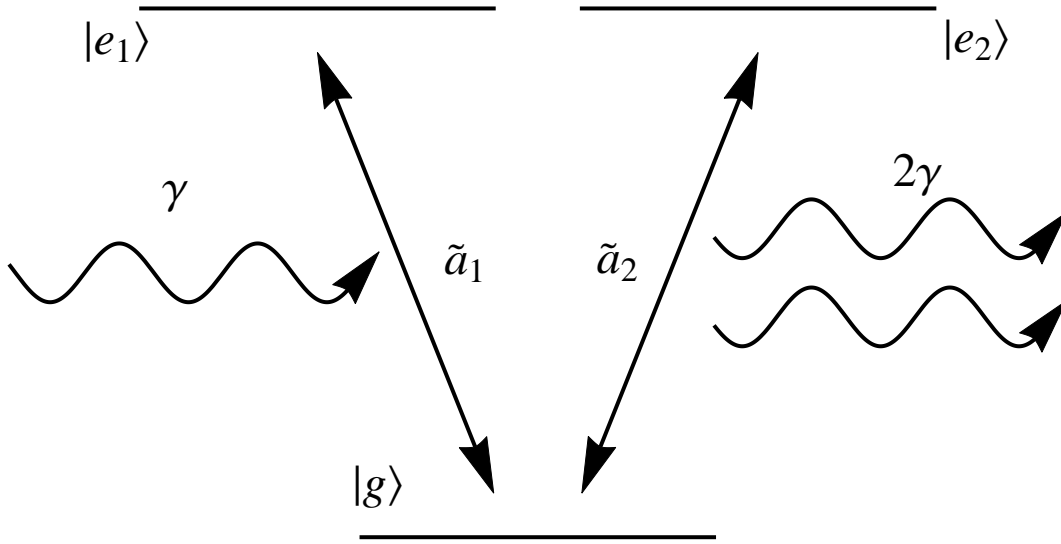
Figure 2.1: The configuration of the atomic system interacting with the photons.

write an interaction Hamiltonian[22],

$$\hat{H}^{int} = \gamma(\sigma_{1+}a_1 + \sigma_{2+}a_2 + \sigma_{1-}a_1^\dagger + \sigma_{2-}a_2^\dagger) \tag{2.2}$$

$$\sigma_{1+} = |e_1\rangle\langle g|, \sigma_{2+} = |e_2\rangle\langle g| \tag{2.3}$$

$$\sigma_{1-} = \sigma_{1+}^\dagger, \sigma_{2-} = \sigma_{2+}^\dagger \tag{2.4}$$

where γ is the transition rate and γt is the scaled time.

The Number operator is given by,

$$\hat{N} = \hat{N}_1 + \hat{N}_2 \tag{2.5}$$

where,

$$\hat{N}_1 = \sigma_{1+}\sigma_{1-} + a_1^\dagger a_1 \text{ and } \hat{N}_2 = \sigma_{2+}\sigma_{2-} + a_2^\dagger a_2 \tag{2.6}$$

$$[\hat{N}_1, \hat{H}^{int}] = 0 \text{ and } [\hat{N}_2, \hat{H}^{int}] = 0 \tag{2.7}$$

Here $\hat{N}$ is conserved and both $\hat{N}_1, \hat{N}_2$ are conserved separately.

The initial atomic state is

$$\rho_{atom} = \frac{1}{2}(|e_1\rangle \langle e_1| + |e_2\rangle \langle e_2|) \tag{2.8}$$

The initial photon state is $c_1 |01\rangle + c_2 |10\rangle = (c_1 a_2^\dagger + c_2 a_1^\dagger) |0\rangle = |\psi\rangle$.

We choose this Hamiltonian and the initial atomic state because they are invariant under simultaneous unitary transformations of $(a_1^\dagger, a_2^\dagger)$ and $(|e_1\rangle, |e_2\rangle)$.

Now by listing out all possible input and output states of the combined atom-photon state and by looking at the conservation of number, we can study the evolution of all states.

		N_1	N_2
$|e_2\rangle$	$|01\rangle$	0	2
$|e_1\rangle$	$|10\rangle$	2	0
$|g\rangle$	$|20\rangle$	2	0
$|g\rangle$	$|11\rangle$	1	1
$|g\rangle$	$|02\rangle$	0	2
$|e_1\rangle$	$|01\rangle$	1	1
$|e_2\rangle$	$|10\rangle$	1	1

This list consists of spontaneous and stimulated emissions. Accordingly, we divide the Hamiltonian also into three different parts, which become the blocks of the total Hamiltonian.

Spontaneous emission:

$$
\hat{H}_1 =
\begin{array}{c}
\\
\langle g11| \\
\langle e_1 01| \\
\langle e_2 10|
\end{array}
\begin{array}{c}
|g11\rangle \quad |e_1 01\rangle \quad |e_2 10\rangle \\
\left(
\begin{array}{ccc}
0 & \gamma & \gamma \\
\gamma & 0 & 0 \\
\gamma & 0 & 0
\end{array}
\right)
\end{array}
\qquad (2.9)
$$

Stimulated emission:

$$
\hat{H}_2 =
\begin{array}{cc}
& |g20\rangle \quad |e_1 10\rangle \\
\begin{array}{c} \langle g20| \\ \langle e_1 10| \end{array} &
\begin{pmatrix} 0 & \sqrt{2}\gamma \\ \sqrt{2}\gamma & 0 \end{pmatrix}
\end{array}
\tag{2.10}
$$

$$
\hat{H}_3 =
\begin{array}{cc}
& |g02\rangle \quad |e_2 01\rangle \\
\begin{array}{c} \langle g02| \\ \langle e_2 01| \end{array} &
\begin{pmatrix} 0 & \sqrt{2}\gamma \\ \sqrt{2}\gamma & 0 \end{pmatrix}
\end{array}
\tag{2.11}
$$

Thus the total Hamiltonian is of the form

$$
\hat{H}^{int} = \begin{bmatrix} \hat{H}_1 & 0 & 0 \\ 0 & \hat{H}_2 & 0 \\ 0 & 0 & \hat{H}_3 \end{bmatrix}
\tag{2.12}
$$

Using this Hamiltonian we calculate the evolution operator U of the combined system

$$
U = e^{\frac{-iHt}{\hbar}}
\tag{2.13}
$$

The initial state of the combined atom-photon system is given by the tensor

product of the individual systems (the atom and the photons).

$$\rho(0) = \frac{1}{2}\left(|e_1\rangle\langle e_1| + |e_2\rangle\langle e_2|\right) \otimes |\psi\rangle\langle\psi| \tag{2.14}$$

We time evolve the above state using the evolution operator U.

$$\rho(t) = U^\dagger \rho(0) U \tag{2.15}$$

After evolving, we trace out the atomic degrees of freedom from the total density matrix to get the reduced density matrix of the photon.

$$\rho^{red}(t) = \text{Tr}_{atom}[\rho(t)] \tag{2.16}$$

$$\rho^{red}(t) = \begin{array}{c} \\ |11\rangle \\ |01\rangle \\ |10\rangle \\ |20\rangle \\ |02\rangle \end{array} \begin{array}{cc} \langle 11| \quad\quad \langle 01| \;\; \langle 10| \quad\quad \langle 20| \quad\quad\quad \langle 02| \\ \begin{pmatrix} \frac{1}{4}\sin^2\left(\frac{\sqrt{2}\gamma t}{\hbar}\right) & 0 & 0 & \frac{c_1 c_2}{2\sqrt{2}}\sin^2\left(\frac{\sqrt{2}\gamma t}{\hbar}\right) & \frac{c_1 c_2}{2\sqrt{2}}\sin^2\left(\frac{\sqrt{2}\gamma t}{\hbar}\right) \\ 0 & a & b & 0 & 0 \\ 0 & b & a & 0 & 0 \\ \frac{c_1 c_2}{2\sqrt{2}}\sin^2\left(\frac{\sqrt{2}\gamma t}{\hbar}\right) & 0 & 0 & \frac{c_2^2}{2}\sin^2\left(\frac{\sqrt{2}\gamma t}{\hbar}\right) & 0 \\ \frac{c_1 c_2}{2\sqrt{2}}\sin^2\left(\frac{\sqrt{2}\gamma t}{\hbar}\right) & 0 & 0 & 0 & \frac{c_1^2}{2}\sin^2\left(\frac{\sqrt{2}\gamma t}{\hbar}\right) \end{pmatrix} \end{array}$$
$$\tag{2.17}$$

where, $a = \frac{4c_1^2 + 1}{8}\cos^2\left(\frac{\sqrt{2}\gamma t}{\hbar}\right) + \frac{c_1^2 - c_2^2}{4}\cos\left(\frac{\sqrt{2}\gamma t}{\hbar}\right) + \frac{1}{8}$, $b = \frac{c_1 c_2}{2}\cos\left(\frac{\sqrt{2}\gamma t}{\hbar}\right)\left(1 + \cos\left(\frac{\sqrt{2}\gamma t}{\hbar}\right)\right)$.

For the calculation of fidelity, we need an ideal output to compare with the

output state that we obtain. The ideal output is given by $|\chi\rangle = |\psi\rangle \otimes |\psi\rangle$.

The commonly used definition of fidelity used in the literature[22,20,19,24], is given by

$$
\begin{aligned}
f^{(1)} &= \sum_{\substack{k+l\geq 2}}^{M+1} \left(\frac{k}{k+l}\right) \frac{p(k,l)}{1-p(0,1)-p(1,0)} \\
&= \frac{p(2,0) + \frac{1}{2}p(1,0)}{1-p(0,1)-p(1,0)}
\end{aligned}
$$

$$
f^{(1)} = \frac{5}{6}. \tag{2.18}
$$

where,

$$
p(k,l) = \langle 0,0| \frac{b_1^k b_2^l}{\sqrt{k!l!}} \rho^{red}(t) \frac{b_1^{\dagger k} b_2^{\dagger l}}{\sqrt{k!l!}} |0,0\rangle ,
$$

$$
b_1^\dagger = c_1 a_2^\dagger + c_2 a_1^\dagger \text{ and } b_2^\dagger = c_1 a_2^\dagger - c_2 a_1^\dagger.
$$

We use a new definition of fidelity,

$$
\begin{aligned}
f^{(2)} &= \langle \chi| \rho^{red}(t) |\chi\rangle \\
&= \frac{1}{2} \sin^2\left(\frac{\sqrt{2}\gamma t}{\hbar}\right)
\end{aligned}
$$

The optimal value corresponds to $f^{(2)} = \frac{1}{2}$, obtained at time, $t = \frac{(2k+1)\pi}{2} \frac{\hbar}{\sqrt{2}\gamma}$.

24

The difference between the two definitions of fidelity is that while $f^{(1)}$ compares the input state with only one of the output states, equivalent to $\langle \psi | \rho | \psi \rangle$ (here ρ represents one output state), $f^{(2)}$ compares the ideal output states i.e, two perfect copies, with the two output states (includes both the input and the cloned states).

2.1 Non-Ideal cloning: Role of thermal noise in the cloning process

Till this point we have considered an ideal situation where there is no noise in the system. We now go beyond earlier work by introducing thermal noise to the system. Thermal noise is introduced first in the atomic system, where the atom is in a population inverted state. Next we send in a thermal photon along with the input photon. These act as thermal noise at the machine level and the input level respectively. This leads us to the study of effects of temperature on the cloning process.

Effects of temperature on quantum cloning[43] in an abstract system was earlier studied by Baghbanzandeh and Rezakhani. In their system they dealt with a static model where time scales do not appear i.e, they did not deal with the dynamics of the process. Also their process of cloning is not universal as the fidelity is dependent on the input state. As it will be made clear later in the chapter our approach to the problem deals with the dynamics and is universal.

2.1.1   Atom in a Thermal State

In the previous section, we have taken the initial atomic state to be the population inverted state. Here we consider the atom in a thermal state, which introduces noise and corrupts the cloning process.

$$\rho_i = \frac{e^{-\beta_1 e}(|e_1\rangle\langle e_2| + |e_1\rangle\langle e_2|) + e^{-\beta_1 g}|g\rangle\langle g|}{Z} \tag{2.19}$$

where, $Z = 2e^{-\beta_1 e} + e^{-\beta_1 g}$, $\beta_1 = 1/(k_B T)$.

Along with the states mentioned earlier, we have to add four more states to complete the set of all possible states. The states listed below pertain to absorption of the photon.

		N_1	N_2
$|g\rangle$	$|10\rangle$	1	0
$|e_1\rangle$	$|00\rangle$	1	0
$|g\rangle$	$|01\rangle$	0	1
$|e_2\rangle$	$|00\rangle$	0	1

We thus write the Hamiltonian corresponding to the process of absorption in

26

two blocks as follows,

$$
\hat{H}_4 = \begin{array}{c} \quad\quad |g10\rangle \quad |e_1 00\rangle \\ \begin{array}{c} \langle g10| \\ \langle e_1 00| \end{array} \begin{pmatrix} 0 & \gamma \\ \gamma & 0 \end{pmatrix} \end{array}
\tag{2.20}
$$

$$
\hat{H}_5 = \begin{array}{c} \quad\quad |g01\rangle \quad |e_2 00\rangle \\ \begin{array}{c} \langle g01| \\ \langle e_2 00| \end{array} \begin{pmatrix} 0 & \gamma \\ \gamma & 0 \end{pmatrix} \end{array}
\tag{2.21}
$$

Finally, the total Hamiltonian is

$$
\hat{H}^{int} = \begin{bmatrix} \hat{H}_1 & 0 & 0 & 0 & 0 \\ 0 & \hat{H}_2 & 0 & 0 & 0 \\ 0 & 0 & \hat{H}_3 & 0 & 0 \\ 0 & 0 & 0 & \hat{H}_4 & 0 \\ 0 & 0 & 0 & 0 & \hat{H}_5 \end{bmatrix}
\tag{2.22}
$$

The initial state of the combined system is given by

$$
\rho(0) = \left(\frac{e^{-\beta_1 e}(|e_1\rangle \langle e_2| + |e_1\rangle \langle e_2|) + e^{-\beta_1 g} |g\rangle \langle g|}{Z} \right) \otimes |\psi\rangle \langle \psi|
\tag{2.23}
$$

We evolve the above state with the evolution operator corresponding to the

Hamiltonian from (2.22).

$$\rho^{red}(t) = \mathrm{Tr}_{atom}[\rho(t)] = \langle e_1| \rho(t) |e_1\rangle + \langle e_2| \rho(t) |e_2\rangle + \langle g| \rho(t) |g\rangle \quad (2.24)$$

Similar to the previous section we calculate the fidelities:

$$f^{(1)} = \frac{p(2,0) + \frac{1}{2}p(1,0)}{1 - p(0,1) - p(1,0) - p(0,0)} \quad (2.25)$$

$$f^{(1)} = \frac{5}{6} \quad (2.26)$$

$$f^{(2)} = \frac{e^{-\beta_1 e}}{Z} \sin^2\left(\frac{\sqrt{2}\gamma t}{\hbar}\right) \quad (2.27)$$

The optimal value corresponds to $f^{(2)} = \frac{e^{-\beta_1 e}}{Z}$.

We can see that $f^{(1)}$ *does not distinguish* between a population inverted and a thermal state. This is counterintuitive since we expect a thermal state to corrupt the cloning process. Therefore we restrict our analysis to $f^{(2)}$ since it indeed distinguishes between these two cases and thus captures the physics of the cloning process better that $f^{(1)}$. We, therefore, restrict our analysis to $f^{(2)}$ in the following sections.

In this section, we introduce noise at the input by sending a thermal photon along with the photon that needs to be copied. The state for a photon in thermal state (Fock space) can be written as

$$\rho = \sum_n e^{-\beta n} |n\rangle \langle n| . \tag{2.28}$$

Since in our case we work with two polarisation modes we take the tensor product of the two modes to write the full state.

$$\rho = (1-x)^2 \sum_{n_1} x^{n_1} |n_1\rangle \langle n_1| \otimes \sum_{n_2} x^{n_2} |n_2\rangle \langle n_2| , \tag{2.29}$$

where, $x = e^{-\beta(e-g)}$. This can be written as follows

$$\rho = (1-x)^2 \sum_{n=0}^{\infty} \left(x^n \sum_{r=0}^{n} |n-r,r\rangle \langle n-r,r| \right) , \tag{2.30}$$

where, $n = n_1 + n_2$. We solve this by converting the Hamiltonian and density matrices into a block diagonal form and solve only for those blocks which provide non-zero fidelity. We use conservation conditions on N, N_1 and N_2 for forming the blocks.

We display a few special cases. For $n = 1$ and $n_1 = 1, n_2 = 0$

$$\hat{H}_1 = \begin{array}{c} \\ \langle e_1 00| \\ \langle g10| \end{array} \overset{\displaystyle |e_1 00\rangle \quad |g10\rangle}{\begin{pmatrix} 0 & \gamma \\ \gamma & 0 \end{pmatrix}}. \tag{2.31}$$

For $n = 1$ and $n_1 = 0, n_2 = 1$

$$\hat{H}_2 = \begin{array}{c} \\ \langle e_2 00| \\ \langle g01| \end{array} \overset{\displaystyle |e_2 00\rangle \quad |g01\rangle}{\begin{pmatrix} 0 & \gamma \\ \gamma & 0 \end{pmatrix}}. \tag{2.32}$$

Similarly we write the Hamiltonians for $n = 2$ and $n = 3$. These values of n provide all the blocks of the total Hamiltonian that are required for the evaluation of fidelity.

Since a thermal state acts as a noise source, the total state can be written as a convex combination of the input state and the thermal state.

$$\rho(0) = \frac{\rho_{th} + \rho_{in}}{2} \tag{2.33}$$

We can do the calculations separately for ρ_{th} and ρ_{in} and add the results for obtaining the total fidelity. The fidelity for cloning a photon state with thermal noise at the input level is given by

$$f^{(2)} = \frac{f^{(2)}_{(th)} + f^{(2)}_{(in)}}{2} \tag{2.34}$$

$$= \frac{(1-x)^2}{2} \left(\frac{x^2}{3} \left(1 + 2\cos^2 \frac{\sqrt{3}\gamma t}{\hbar} \right) + \frac{x}{2} \sin^2 \frac{\sqrt{2}\gamma t}{\hbar} \right) + \frac{1}{4} \sin^2 \frac{\sqrt{2}\gamma t}{\hbar}.$$

2.1.3 Both Atom and Photon in Thermal States

Here we introduce thermal noise at both the input and the machine level i.e, a thermal photon and an atom in a thermal state. We calculate the fidelity of the cloning process as done in previous cases.

$$f^{(2)} = \langle \chi | \rho^{red}(t) | \chi \rangle, \tag{2.35}$$

where $|\chi\rangle = |\psi\rangle \otimes |\psi\rangle$.

The total density matrix before interaction is written as

$$\rho = \rho_{at} \otimes \left(\frac{\rho_{th} + \rho_{in}}{2} \right) \tag{2.36}$$

where, ρ_{at} is the density matrix for an atom in a thermal state, ρ_{th} is the density matrix for a photon in a thermal state and ρ_{in} is the density matrix for the input photon. Like in the earlier case we calculate fidelity for a thermal photon and the input photon separately. The total fidelity is given by

$$
\begin{aligned}
f^{(2)} \;=\; & \frac{e^{-\beta_1 e}}{Z}(1-x)^2 \left(\frac{x^2}{3}\left(1 + 2\cos^2\frac{\sqrt{3}\gamma t}{\hbar}\right) + \frac{x}{2}\sin^2\frac{\sqrt{2}\gamma t}{\hbar} \right) \\
& + \frac{e^{-\beta_1 g}}{2Z}(1-x)^2 x^2 \left(\cos^2\frac{\sqrt{2}\gamma t}{\hbar} + \frac{4x}{3}\sin^2\frac{\sqrt{3}\gamma t}{\hbar} \right) \\
& + \frac{e^{-\beta_1 e}}{2Z}\sin^2\left(\frac{\sqrt{2}\gamma t}{\hbar} \right)
\end{aligned}
\tag{2.37}
$$

Figure 2.2 shows a comparison between fidelities for all the four cases calculated. This is just a qualitative comparison between fidelities, where $\gamma = 1, \hbar = 1$.

2.2 CLASSICAL LIMIT OF THE QUANTUM CLONING PROCESS

Till this point we have studied how temperature corrupts the quantum cloning process. Here we look at the classical limit of the process by taking both the number of input states (N) and the number of copies (M) to infinity.

So far we have restricted to a system for which $N = 1$ and $M = 2$. Let us calculate the fidelity for $N = 2$ and $M = 3$ i.e, two input photons and one atom in the excited state. The fidelities ($f^{(1)}$ and $f^{(2)}$) for this system are given by
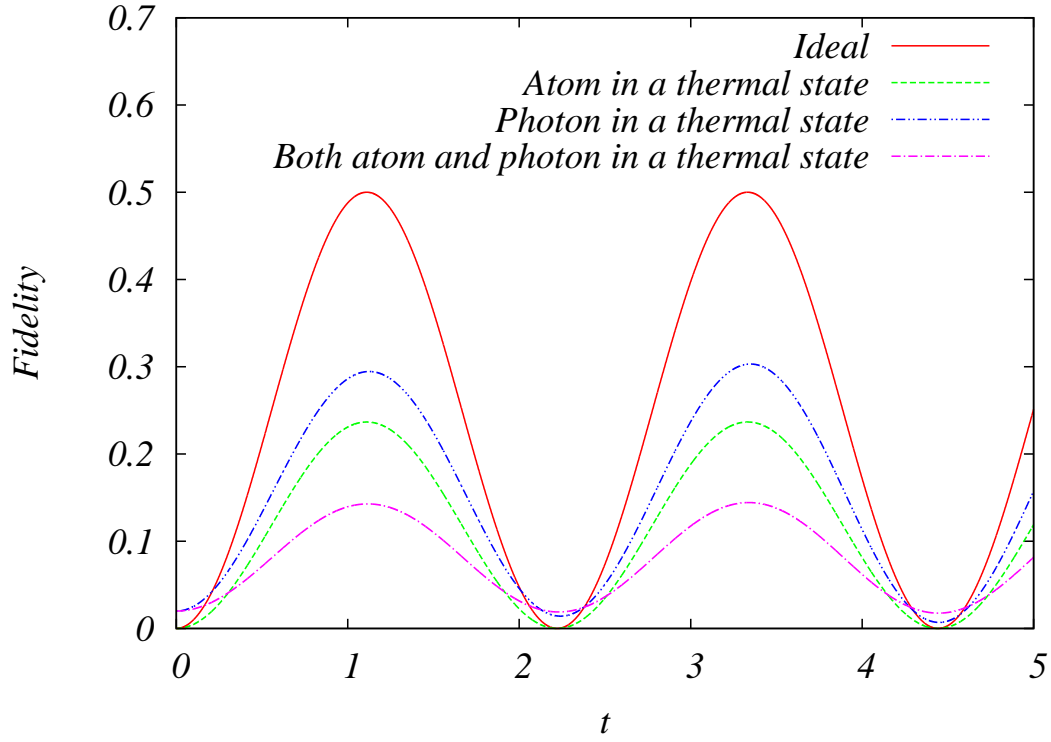
Figure 2.2: Comparison of fidelities after corruption with the ideal case as a function of time.

$$f^{(1)} = \frac{p(3,0) + \frac{2}{3}p(2,1) + \frac{1}{3}p(1,2)}{1 - p(2,0) - p(0,2) - p(1,1)}, \qquad (2.38)$$

$$f^{(2)} = \langle \chi | \rho^{red}(t) | \chi \rangle. \qquad (2.39)$$

By taking the input state of two photons as $\rho_{in} = \frac{1}{\sqrt{2}}(c_1 |01\rangle + c_2 |10\rangle) \otimes$

$(c_1 \ket{01} + c_2 \ket{10})$, we evolve the system unitarily. This gives us the fidelities

$$f^{(1)} = \frac{11}{12} \text{ and } f^{(2)} = \frac{1}{2} \sin^2 \left(\frac{\sqrt{3}\gamma t}{\hbar} \right) \qquad (2.40)$$

The fidelity $f^{(1)}$ for the atom-photon system agrees with the formula $f = \frac{NM+N+M}{M(N+2)}$, which is defined for any arbitrary quantum system. In contrast, the maximum of $f^{(2)}$ is $\frac{1}{2}$, which is the same as the case of $N = 1$ and $M = 2$, implying $f^{(2)}$ does not capture the roles of N and M effectively. Hence we restrict ourselves to calculating $f^{(1)}$ for analysing the classical limit.

For taking the limit of $N \to \infty$ and $M \to \infty$, we consider $M = rN$, where r is a finite number and greater than one. The reason behind choosing this condition is that the number of additional copies produced also does reach the limit of infinity.

$$\begin{aligned}
\lim_{N\to\infty, M\to\infty} f^{(1)} &= \lim_{N\to\infty, M\to\infty} \frac{NM + N + M}{M(N+2)}, \\
&= \lim_{N\to\infty} \frac{rN + r + 1}{rN + 2r}, \\
&= \lim_{N\to\infty} \frac{N + \frac{r+1}{r}}{N + 2}, \\
&= 1. \qquad (2.41)
\end{aligned}$$

This tells us that perfect cloning of a state is possible in the classical limit. One

more way of approaching the classical limit is by first taking $M \to \infty$ and then $N \to \infty$.

$$
\begin{aligned}
\lim_{M \to \infty} f^{(1)} &= \lim_{M \to \infty} \frac{NM + N + M}{M(N+2)}, \\
&= \lim_{M \to \infty} \frac{N+1}{N+2}
\end{aligned}
\tag{2.42}
$$

This approaches one as N goes to infinity.

2.3 CLASSICAL CLONING

Wootters and Zurek's[13] work on the no-cloning theorem has led to extensive research on the quantum cloning process and its physical implications. While the studies in the quantum regime are both abstract[18,30,19,20,44] and application-based[21,22,23,24,26], work on the classical cloning process has been extremely limited and restricted to a purely mathematical approach[1,34,45,46]. There appears to be a belief that the classical cloning process is trivial, perhaps because it is so familiar. Computers routinely copy files, photocopying machines are widespread and the genetic information contained in DNA is replicated every time a cell divides. However, there are subtleties related to classical cloning[34] and even a classical no-cloning theorem[1] proved under certain, general assumptions. A good understanding ofthe copying of classical information is essential to appreciate the

quantum case and the relation between the two.

The discussion of cloning involves three coupled systems: a source, a target and a machine. The source contains the state to be cloned. The target is initially in a standard blank state and the machine is initially in a standard ready state, both independent of the source. The objective of cloning is to copy the state of the source into the target, without destroying the original. In the copying process, the machine state may be altered and has to be reset before the next copy can be made. Here, we consider the cloning process from a physical point of view, clarifying the conditions under which classical cloning is possible and explicitly constructing Hamiltonians which implement the cloning process.

Before going any further we need to define more precisely what we mean by a "state". A "state" in classical mechanics is defined as a point in phase space. A system in classical mechanics has a configuration space Q with local coordinates q^r and the phase space has twice the dimension (q^r, p_r) including coordinates as well as conjugate momenta. Phase spaces are even dimensional and allow us to define Poisson brackets between functions. In statistical physics, a state would be defined as a probability distribution on phase space. Daffertshofer et al.[1] have proved a classical no-cloning theorem when states are regarded as probability distributions. This proof is based on the invariance of the relative entropy (Kullback-Leibler divergence) under arbitrary diffeomorphisms of the phase space. It follows from their work that cloning of classical states is forbid-

den whenever the relative entropy of the total system is well defined. However, there are situations where the relative entropy of the system is ill defined, for example when the phase space distributions have delta function support and this permits a discussion of classical cloning.

Aaron Fenyes[34] studied the cloning process from the viewpoint of symplectic geometry. In his treatment, classical states are points in a symplectic manifold and the cloning process is a symplectomorphism. This provides a very general setting for the cloning process in classical mechanics. In the physics community, symplectic manifolds and symplectomorphisms are more usually referred to as phase spaces and canonical transformations. Here, we use the framework provided by Fenyes to study the classical cloning process in more detail.

Definition of the classical cloning process: Following[34], let M and N be symplectic manifolds. (A symplectic manifold is a manifold with a closed, non degenerate two-form ω_0. Diffeomorphisms that preserve the two form ω_0 are called symplectomorphisms.) Let (N, N, M) represent the source, target and machine respectively. Initially, we suppose that the target and machine are in standard states b and r. Given an arbitrary state $s \in N$ of the source, a cloning map is a symplectomorphism $\psi : N \times N \times M \to N \times N \times M$ such that $\psi(s, b, r) = (s, s, f(s, b, r))$ for all $s \in N$, where b, r are independent of s[34]. Here the manifold M acts as the copying machine, while the source and the target states are on the manifold N. The source state is s, the material to be copied

(for instance a birth certificate!); b the target state, which is initially blank, as are the A4 sheets in the tray of the copying machine; and the machine state is r (r for ready) before cloning. We would like to know whether there exists a cloning map for a given classical system (N, ω_0). What choice of the machine M is needed to achieve this? It is also of interest to determine how these maps can be generated in the laboratory by physical processes.

Let us suppose that that there is a cloning map ψ as above. Let us now fix $s = s_0$ and consider the linearised map ϕ that maps the tangent space of (s_0, b, r) to the tangent space of $(s_0, s_0, f(s_0, b, r))$. These tangent spaces are symplectic vector spaces and ϕ is a linear symplectic cloning map. Thus, the existence of ψ would imply the existence of linear symplectic cloning maps. Let us begin by addressing the simpler problem of linear symplectic cloning. Linearity results in a considerable simplification of the problem and permits explicit construction of cloning maps. As we will see later, this simple case illuminates the more general problem of classical cloning. It also covers the physically important case of harmonic oscillators, which are easily realised in an optics laboratory as modes of the electromagnetic field.

Let us start with the simplest example and choose M and N to be two dimensional symplectic vector spaces $(\mathbb{R}^2, \omega_0)$, so that we can view M and N as phase spaces, with each point in these spaces being labelled by a position and a mo-

mentum. Let $b = r = \begin{pmatrix} 0 \\ 0 \end{pmatrix}$, and $x = \begin{pmatrix} q \\ p \end{pmatrix}$. A linear symplectic cloning map on $\mathbb{R}^6$ is given by

$$\phi(s, b, r) = \left[\begin{array}{cc|cc|cc} 1 & 0 & 1 & 1 & -1 & 1 \\ 0 & 1 & 1 & 2 & 0 & 1 \\ \hline 1 & 0 & 0 & 1 & 0 & 1 \\ 0 & 1 & -1 & -1 & 1 & 0 \\ \hline 1 & 0 & 1 & 2 & -1 & 2 \\ 0 & -1 & 0 & -1 & -1 & -1 \end{array}\right] \begin{bmatrix} s \\ b \\ r \end{bmatrix}. \tag{2.43}$$

It is a cloning map because it satisfies $\phi(s, b, r) = (s, s, Fs)$, where $F = \begin{bmatrix} 1 & 0 \\ 0 & -1 \end{bmatrix}$. ϕ is a symplectic map as it satisfies the condition $\phi^T \Omega \phi = \Omega$, where Ω is the symplectic form on $\mathbb{R}^6$. Cloning by a machine is only possible if the dimension of M is greater than or equal to the dimension of N. A minimal choice is $M = N$. As emphasised by[34], cloning is impossible without the presence of the machine.

2.3.1 Cloning as a Canonical Transformation

In this section, we discuss a systematic procedure for the generation of cloning maps on the symplectic vector space $\mathbb{R}^2 \times \mathbb{R}^2 \times \mathbb{R}^2$. By definition, the cloning map $\phi : \mathbb{R}^6 \to \mathbb{R}^6$ must send $(s, b, r) \to (s, s, Fs)$ (where, $b = 0$ and $r = 0$

are at the origin). The two dimensional vector subspace V of $\mathbb{R}^6$ spanned by vectors of the form $\{s, 0, 0\}$ is mapped to the two dimensional subspace W of $\mathbb{R}^6$ spanned by vectors of the form $\{s, s, Fs\}$. In order for the map from V to W to be symplectic, F must be antisymplectic, i.e, it must reverse the symplectic structure. A simple choice for F is $F = \begin{bmatrix} 1 & 0 \\ 0 & -1 \end{bmatrix}$. We need to now extend this map to all of $\mathbb{R}^6$. Clearly V^c, the symplectic complement of V must map to W^c, the symplectic complement of W. A systematic procedure for constructing the map is the Gram-Schmidt procedure[47]. Following is the procedure to generate the cloning map above (2.43).

The cloning map is described by $(x, b, r) \rightarrow (x, x, Fx)$ (where, b and r are at the origin).

Let (e_i, f_j) and (E_i, F_j) be two bases. The symplectic cloning map is a map (a symplectomorphism) connecting these two basis sets. The symplectic form Ω is defined as follows:

$$\begin{aligned} \Omega(e_i, e_j) &= 0, \; \Omega(e_i, f_j) = \delta_{ij}, \\ \Omega(f_i, f_j) &= 0, \; \Omega(f_i, e_j) = -\delta_{ij}. \end{aligned} \tag{2.44}$$

Let us set $\{x, y\} \equiv \Omega(x, y)$. Let us consider

$$E_1 = e_1 + e_2 + e_3, \tag{2.45}$$

$$F_1 = f_1 + f_2 - f_3. \tag{2.46}$$

We now follow a method similar to the Gram-Schmidt Orthonormalization procedure and construct the following:

$$e_2' = e_2 - \{e_2, F_1\}E_1 + \{e_2, E_1\}F_1 = -e_1 - e_3, \tag{2.47}$$

$$e_3' = e_3 - \{e_3, F_1\}E_1 + \{e_3, E_1\}F_1 = e_1 + e_2 + 2e_3, \tag{2.48}$$

$$f_2' = f_2 - \{f_2, F_1\}E_1 + \{f_2, E_1\}F_1 = -f_1 + f_3, \tag{2.49}$$

$$f_3' = f_3 - \{f_3, F_1\}E_1 + \{f_3, E_1\}F_1 = 2f_3 - f_1 - f_2. \tag{2.50}$$

We now construct

$$E_2 = -e_2' - 2f_2' + f_3' = e_1 + e_3 + f_1 - f_2, \tag{2.51}$$

$$F_2 = e_3' - 3F_2' + f_3',$$

$$= e_1 + e_2 + 2e_3 + 2f_1 - f_2 - f_3. \tag{2.52}$$

We then construct

$$
\begin{aligned}
e_3'' &= e_2' - \{e_2', F_2\}E_2 + \{e_2', E_2\}F_2 \\
&= -e_1 - e_2 - 2e_3 - f_1 + f_3, && (2.53) \\
f_3'' &= f_2' - \{f_2', F_2\}E_2 + \{f_2', E_2\}F_2, \\
&= e_1 + e_3 - f_2 + f_3. && (2.54)
\end{aligned}
$$

We continue further to generate

$$
\begin{aligned}
E_3 &= -f_3'' = -e_1 - e_3 + f_2 - f_3, && (2.55) \\
F_3 &= -e_3'' = e_1 + e_2 + 2e_3 + f_1 - f_3. && (2.56)
\end{aligned}
$$

Our cloning map is given by Eq. (2.43).

Since the Gram-Schmidt procedure involves choices there is clearly ambiguity in the extension of the cloning map. What is the extent of this ambiguity? There is clearly $Sp(4)$ worth of ambiguity in mapping V^c to W^c. In addition, we also have the freedom to compose F with any other symplectic transformation in $\mathbb{R}^2$ of the machine. Thus there is a total of $Sp(4) \times Sp(2)$ worth of cloning maps in $\mathbb{R}^2$. Fenyes' construction extends easily to the case of $\mathbb{R}^{2n}$. The total ambiguity here is larger, $Sp(4n) \times Sp(2n)$.

Having found a linear cloning map, we would like to implement this transformation by a Hamiltonian, so that cloning can be realised in a laboratory. A symplectic map ϕ and its corresponding Hamiltonian H are related by

$$\phi = e^{Ht}. \tag{2.57}$$

Since we are working with linear spaces, it is natural to consider quadratic Hamiltonian functions. If x is a vector in $\mathbb{R}^6$, $(x^i, i = 1, 6)$, our Hamiltonian is a quadratic function

$$H(x) = 1/2 x^i h_{ij} x^j \tag{2.58}$$

with h_{ij} a real symmetric matrix $h_{ij} = h_{ji}$. Using Hamilton's equations we get an evolution

$$\dot{x}^i = \Omega^{ij} h_{jk} x^k \tag{2.59}$$

which is a linear transformation generated by $h^i{}_k = \Omega^{ij} h_{jk}$. Under time evolution for a time t, the vector x would be mapped to the vector $[\exp ht] x$ where h is the matrix $h^i{}_k$.

We will now explicitly construct Hamiltonians to implement the map (ϕ)

mentioned earlier and for the map discussed by Aaron Fenyes.

$$\phi = \begin{bmatrix} 1 & 0 & 1 & 0 & 0 & 0 \\ 0 & 1 & 0 & 0 & 0 & -1 \\ 1 & 0 & -1 & 0 & 1 & 0 \\ 0 & 1 & 0 & -1 & 0 & -1 \\ 1 & 0 & 0 & 0 & 1 & 0 \\ 0 & -1 & 0 & 1 & 0 & 2 \end{bmatrix}. \tag{2.60}$$

The map ϕ cannot be realised via a single time independent Hamiltonian [*]. Using the polar decomposition of symplectic matrices[48], we can write $\phi = \exp X \exp Y$ where X, Y are in the Lie algebra of the symplectic group. Writing $h_1 = X/\tau$ and $h_2 = Y/\tau$, we can express the cloning map as

$$\phi = e^{h_1 \tau} e^{h_2 \tau}, \tag{2.61}$$

where τ will be chosen later to suit our convenience. The Hamiltonian matrices

---

[*]Mathematically, this is because the exponential map from the Lie algebra of the symplectic group to the group is not surjective[48].

in explicit numerical form (rounded to three decimal places) are ,

$$
h_1\tau = \begin{bmatrix}
-0.209 & -0.003 & -0.206 & -0.332 & 0.206 & -0.128 \\
0.418 & 0.209 & -0.120 & -0.120 & -0.006 & 0.006 \\
0.120 & -0.332 & -0.738 & -0.254 & 0.284 & -0.583 \\
-0.120 & 0.206 & 1.066 & 0.738 & -0.535 & 0.738 \\
-0.006 & -0.128 & -0.738 & -0.583 & 0.409 & -0.505 \\
-0.006 & -0.206 & -0.535 & -0.284 & 0.254 & -0.409
\end{bmatrix}
\tag{2.62}
$$

$$
h_2\tau = \begin{bmatrix}
0.779 & -0.203 & -0.796 & 0.834 & 0.117 & 0.329 \\
0.101 & -0.779 & -1.438 & -0.412 & 1.107 & -1.741 \\
0.412 & 0.834 & -2.509 & -0.722 & 2.479 & 0.563 \\
-1.438 & 0.796 & 4.039 & 2.509 & -1.512 & 3.013 \\
1.741 & 0.329 & -3.013 & 0.563 & 1.534 & 0.958 \\
1.107 & -0.117 & -1.512 & -2.479 & -0.774 & -1.534
\end{bmatrix}
\tag{2.63}
$$

h_1 represents a pure shear transformation and h_2 a pure rotation in phase space.
The Hamiltonian functions are given by (2.58).

$$
\begin{aligned}
H_1 \;=\; & p_m(0.200135p_s - 0.454122p_t - 0.251032q_m - 0.134379q_s - 1.11724q_t) \\
& -0.208998p_s^2 + p_s(-0.0864358p_t - 0.134379q_m + 0.415041q_s - 0.451168q_t) \\
& -0.737739p_t^2 - 1.11724p_tq_m - 0.451168p_tq_s + 0.812358p_tq_t \\
& -0.409133q_m^2 - 0.200135q_mq_s + 0.454122q_mq_t \\
& +0.409133p_m^2 + 0.208998q_s^2 + 0.0864358q_sq_t + 0.737739q_t^2
\end{aligned}
$$

$$
\begin{aligned}
H_2 \;=\; & p_m(1.8583p_s - 0.53366p_t + 0.18342q_m + 1.43587q_s - 0.948606q_t) \\
& +0.779159p_s^2 + p_s(-0.384108p_t + 1.43587q_m - 0.101619q_s - 0.604052q_t) \\
& -2.50948p_t^2 - 0.948606p_tq_m - 0.604052p_tq_s + 3.31716p_tq_t \\
& +1.53428p_m^2 - 1.53428q_m^2 - 1.8583q_mq_s + 0.53366q_mq_t \\
& -0.779159q_s^2 + 0.384108q_sq_t + 2.50948q_t^2
\end{aligned}
$$

where (p_s, q_s), (p_t, q_t) and (p_m, q_m) pertain to the phase space variables corresponding to the source, the target and the machine respectively.

In a real physical process, the three systems (source, target and machine) will have their own Hamiltonian evolution. However, if we choose τ to be small (compared to any time scale present in the source, target and machine) we can
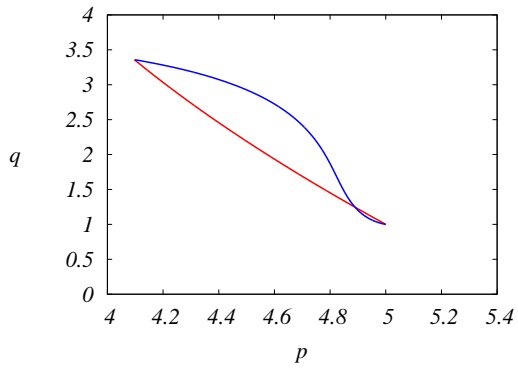
(a) Source
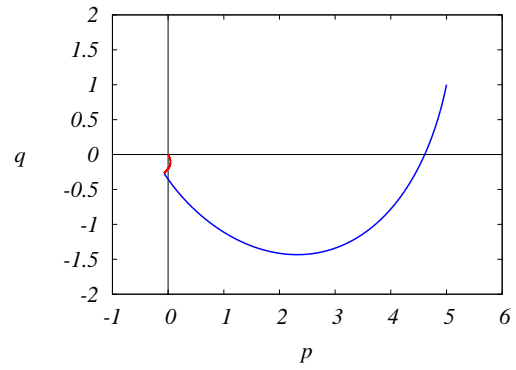
(b) Target
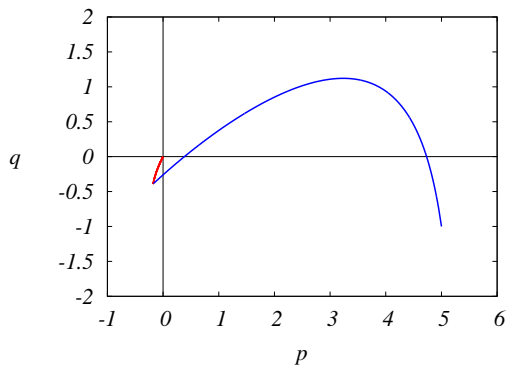
(c) Machine
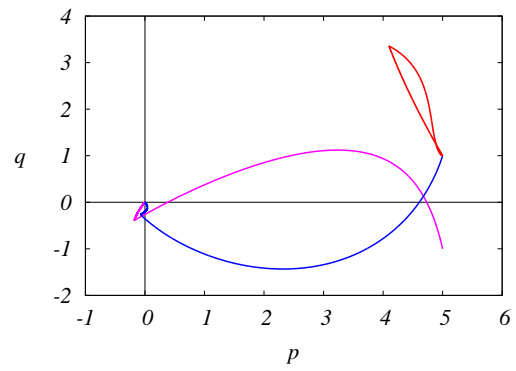
(d) Source (red), target (blue) and machine (magenta) together.

Figure 2.3: Evolution of states (in phase space) for the Hamiltonians mentioned in (2.62) (red) and (2.63) (blue).
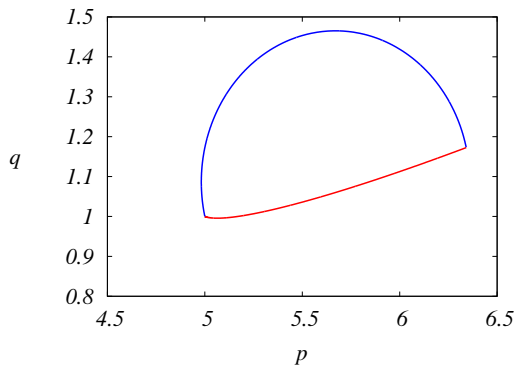
(a) Source
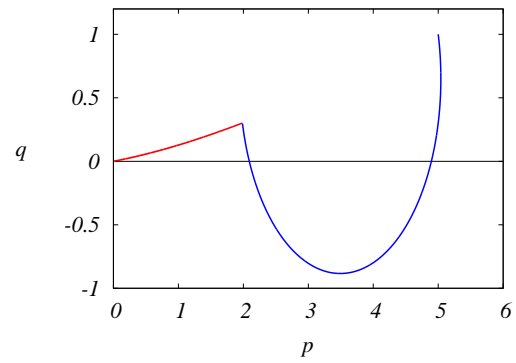
(b) Target
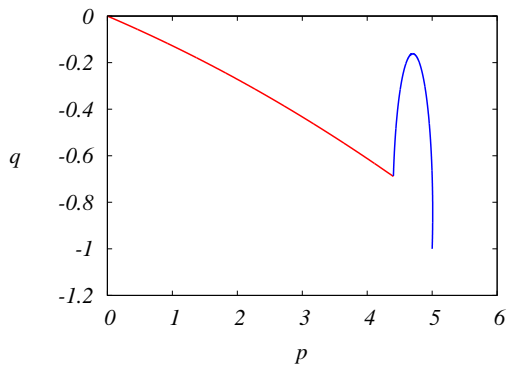
(c) Machine
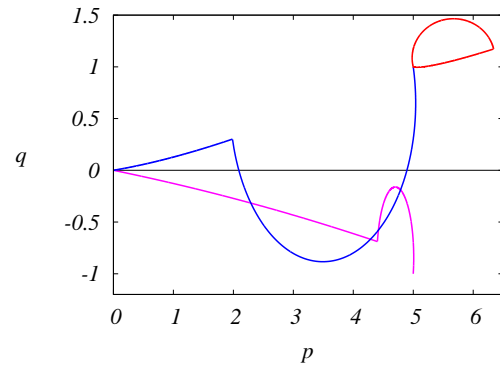
(d) Source (red), target (blue) and machine (magenta) together.

Figure 2.4: Evolution of states (in phase space) for the Hamiltonians corresponding to the symplectic map given by Aaron Fenyes (2.60).

ensure that the cloning Hamiltonians h_1 and h_2 dominate over the other terms. We can essentially assume that the evolution of the systems is "frozen" while cloning takes place.

Figure 2.3 shows the evolution of the source, the target, and the machine (in phase space) using the Hamiltonians in (2.62) and (2.63), for a time, $t = 2\tau$. From these figures we observe that, while the source returns to its original state after evolution i.e. $\begin{pmatrix} q \\ p \end{pmatrix}$, the target starts at the origin and goes to the state $\begin{pmatrix} q \\ p \end{pmatrix}$ making a perfect copy. The machine state also starts at the origin and it reaches $\begin{pmatrix} q \\ -p \end{pmatrix}$. If one considers the phase space area $A(\gamma) = \oint_\gamma pdq$ contained in an arbitrary loop γ in the source space, under cloning this loop is duplicated in the target space and it would seem that the phase space area has doubled. However, the machine is also affected and the image of γ in the machine phase space is such as to cancel out the duplication thereby preserving total phase space area. Thus we retain the original, and we have created a perfect clone and an anti-clone. The anti-clone contribution to the phase space area cancels the one from the clone, thus preserving the total phase space area.

Given three oscillators, one can, in principle create a perfect clone and anti-clone along the lines described above by tuning the coupling strengths read off

from (2.62,2.63). This would be a minimal cloning machine, since the machine has the same phase space as the source. In practice, this may need a large degree of control over the oscillators and their couplings. We will describe below a more practical (albeit non-minimal) scheme for realising the cloning process in the laboratory using non linear optics.

Similarly, Fig. 2.4 shows the evolution of the states under the Hamiltonian for the map by Aaron Fenyes (2.60)

2.3.3 MORE GENERAL CLONING MAPS

Fenyes' construction[34] provides cloning maps for $\mathbb{R}^{2n}$. What about other phase spaces that appear in classical mechanics for example, the phase space of the rigid rotor? We show that all such phase spaces also admit cloning maps and that the machine need be no larger than the system itself. Let Q be an n dimensional manifold and let $q_0 \in Q$ be a marked point. It is known that we can always embed Q in $\mathbb{R}^N$ for sufficiently large N. By a translation, let us arrange for the embedding to place q_0 at the origin of $\mathbb{R}^N$. Let us denote by Γ the phase space corresponding to Q. (Mathematically, $\Gamma = T^*Q$, the cotangent bundle over Q.) It now follows that Γ is symplectically embedded in $\mathbb{R}^{2N}$ and we know from the linear cloning theory that $\mathbb{R}^{2N}$ admits a cloning map which sends $\{(q,p),(q_0,0),(q_0,0)\}$ to $\{(q,p),(q,p),(q,-p)\}$. Restrict this map to points of Γ to find a cloning map for any classical phase space. Note that the

50

machine is also a copy of Γ: it is thus a minimal cloning scheme.

2.3.4 PROPOSED EXPERIMENT

As mentioned earlier, classical cloning can be realised by using techniques of non-linear optics[49]. In particular, one can use a four-wave mixing process like the Kerr effect to generate a clone and an anticlone, leaving the original unaltered. The basic physics[49] is that some materials have a nonlinear response to light waves incident on them. The "machine" here is considerably more complex than in the minimal cloning models of section II, since it includes two pump beams and a nonlinear material apart from the anticlone. We are concerned here with a third order nonlinear optics effect: the polarisation response of the material is cubic in the incident electric field: $\vec{P} = \epsilon_0 \chi^3 \vec{E}(\vec{E}.\vec{E})$, where ϵ_0 is the dielectric permittivity and $\chi^{(3)}$ the third order susceptibility. (It follows from symmetry arguments that the second order susceptibility $\chi^{(2)}$ vanishes for centrosymmetric materials.) The cloning machine consists of a non-linear sample illuminated by two strong" pump" beams. These serve to bring the response of the sample into the non-linear regime, acting rather like the bias voltage of a transistor. When this sample is further illuminated by a weak "signal" beam, we find that in addition to the signal beam (the source) the system generates two more beams, a clone beam and an anti-clone beam. We will describe the scheme more fully below.

Let us note first that a mode of the electromagnetic field is characterised by a wave vector $\vec{k}$ and a polarisation $\vec{\delta}$. We will keep the polarisation vector fixed along $\hat{z}$ in the discussion below. All our wave vectors will lie in the $x - y$ plane. A wave in the $\hat{k}$ direction can be described by the z component of its electric field $E = \hat{z}.\vec{E}$

$$E(\vec{r}, t) = Au(\vec{r}, t) + \overline{A}\overline{u}(\vec{r}, t) \qquad (2.64)$$

where $u(\vec{r}, t) = \exp i(\omega t - \vec{k}.\vec{r})$ and A is a complex number which describes the amplitude and phase of the beam.

Each mode of the field is an oscillator with frequency $\omega = \tilde{c}|\vec{k}|$, where $\tilde{c} = c/n(\omega)$ is the speed of light in the medium (which is assumed isotropic). The phase space of the oscillator is described by the real and imaginary parts of A (the two quadrature components of the wave), which are canonically conjugate to each other. The symplectic form can be written $d\overline{A} \wedge dA/(2i)$. This symplectic form is clearly reversed by the map $A \rightarrow \overline{A}$ taking A to $\overline{A}$.

We have supposed the medium to be isotropic, so that $\chi^{(3)}$ and $n(\omega)$, the refractive index are scalar. We suppose all beams in the experiment to have the same frequency ω. This has the practical advantage that it makes it easier to satisfy the phase matching conditions[49]. Let us consider three incident waves represented as follows:

$$E_j(\vec{r}, t) = A_j u_j(\vec{r}, t) + \overline{A}_j \overline{u}_j(\vec{r}, t) \qquad (2.65)$$

where $u_j(\vec{r}, t) = \exp i(\omega t - \vec{k}_j.\vec{r})$ with $j = 1, 2, 3$ and $\omega = \tilde{c}\vec{k}_j$. Here we consider the beam 1 to be the signal beam (corresponding to the source). The beams 2 and 3 are the pump beams and the emergent beams contain the clone and the anticlone. Third order nonlinear processes are based on the term $\epsilon_0\chi^{(3)}E^3$ in the expression for the polarisation. We are interested in the beams emerging at frequency ω. Expanding the cubic term E^3, the relevant terms in the polarisation are of the following form:

$$
\begin{aligned}
P_a &= \left[\epsilon_0\chi^{(3)}A_2A_3\right]\overline{A}_1 \exp i(\omega t - (\vec{k}_2 + \vec{k}_3 - \vec{k}_1).\vec{r}) \\
P_c &= \left[\epsilon_0\chi^{(3)}\overline{A}_2A_3\right]A_1 \exp i(\omega t - (\vec{k}_1 + \vec{k}_3 - \vec{k}_2).\vec{r}).
\end{aligned}
$$

Below we drop the constant terms in square brackets. These just indicate an overall change of amplitude and can be set to 1 by judicious choice of pump power.

We now have to choose the $\vec{k}_i$'s so as to satisfy the phase matching conditions, in both these beams. We choose the wave vectors such that $\vec{k}_2 + \vec{k}_3 = 0$ and $\vec{k}_1 = \vec{k}_2$. For this choice the two terms mentioned above reduce to

$$
E_a \propto \overline{A}_1 \exp i(\omega t + \vec{k}_1.\vec{r})), \tag{2.66}
$$

which corresponds to an anticlone and

$$E_c \propto A_1 \exp i(\omega t - \vec{k}_3.\vec{r}), \qquad (2.67)$$

which corresponds to a clone. These two emergent beams satisfy the phase matching conditions, since in each case $\omega = \tilde{c}|\vec{k}|$ holds.

In the above arrangement, the directions of all the beams are collinear, which makes it awkward in a laboratory situation. For experimental ease, one can slightly perturb the direction of the k_1 beam by setting $\vec{k_1} = \vec{k_2} + \vec{\delta}$, such that $\vec{\delta}.\vec{k_2} = 0$. Then $|\vec{k_1} + \vec{\delta}| \approx |\vec{k_1}|$ to first order in $|\delta|$ and thus we still satisfy the phase matching conditions, albeit approximately. With this new scheme, the anticlone beam emerges in the $\vec{k_a} = -\vec{k_1}$ direction, while the clone beam emerges in the $\vec{k_c} = \vec{k_3} + \vec{\delta}$ direction, while the original source beam continues in the $\vec{k_1}$ direction from the linear part of the response. Regarding ω as a carrier frequency we can use an Acousto-optic modulator (AOM) to impress a modulation on the signal A_1 so that A_1 depends on t on a slow timescale compared to the inverse carrier frequency. This results in an output in the clone channel (in the direction $\vec{k_c}$) proportional to $A_1(t)$ and in the anticlone channel (in the direction $\vec{k_a}$) proportional to $\overline{A}_1(t)$.

Daffertshofer et al.[1] have worked on classical no-cloning theorem on probability distributions using Liouvillian dynamics. They have considered the following evolution equation

$$\frac{\partial P}{\partial t} + \nabla.(\bar{v}P) = 0. \tag{2.68}$$

Then they show that $\frac{dK}{dt} = 0$, where K is the Kullback-Leibler (K.L) divergence given by $K(P_1, P_2) = \int dx \, P_1 \log \frac{P_1}{P_2}$. This is the basis for the "no-cloning theorem" they go on to prove.

Now let us consider the following case in phase space:

$$
\begin{aligned}
P_1 &= N_1 e^{-\beta_1[(p-p_0)^2+(q-q_0)^2]}, \\
P_2 &= N_2 e^{-\beta_2[(p-p_0)^2+(q-q_0)^2]},
\end{aligned} \tag{2.69}
$$

and the evolution equation is given by $\frac{\partial p}{\partial t} = -\alpha p$ and $\frac{\partial q}{\partial t} = -\alpha q$. This does not violate eq. (2.68). One can easily see that the K.L divergence for this evolution goes to 0 as $t \to \infty$ (because any distribution under this kind of evolution leads to a delta function at origin at very large times), meaning K.L divergence is not time independent.

The whole proof of the no-cloning theorem in[1] is based on the invariance of

the K.L divergence. Even the example they have considered in their paper in eq. (25) violates their theorem.

This problem arises because of two reasons

1. The equation considered is not the Liouville equation but the probability conservation equation. Equation (2.68) can be rewritten as

$$\frac{\partial P}{\partial t} + (\nabla.\bar{v})P + \bar{v}.(\nabla P) = 0. \qquad (2.70)$$

   For the Hamiltonian systems $(\nabla.\bar{v}) = 0$, which gives

$$\frac{\partial P}{\partial t} = \{P, H\}. \qquad (2.71)$$

   where H is the Hamiltonian of the system. This is indeed the Liouville equation.

2. While showing $\frac{dK}{dt} = 0$, they have just assumed $\frac{d\,(dpdq)}{dt} = 0$, without proving it anywhere. Even for this we need to have a divergence free field i.e, $(\nabla.\bar{v}) = 0 \implies \frac{d\,(dpdq)}{dt} = 0$.

Once we have a divergence free field the invariance of the K.L divergence follows directly. The rest of the proof in the paper[1] is all dependent upon just this condition. So, once we consider a non-divergent flow and Liouville equation we have a no-cloning theorem in classical statistical mechanics.

Till now we have assumed an ideal, noise free situation in which the state of a system is described by a point in phase space. To understand the classical cloning process in a more realistic context, we introduce thermal noise to the system and study how this affects the cloning process. In the ideal case, we had taken the states of the source, the target and the machine to be Dirac delta functions in the phase space. We now replace the delta functions with functions of finite width which are statistical mechanical probability distributions. For the sake of convenience, we consider the distributions to be Gaussian. We suppose the source to be a Gaussian peaked about (q_0, p_0). The source and machine are chosen to be Gaussians peaked around the origin.

The initial state of the total system (source, target, machine) is taken to be

$$P_{in}(x) = \mathcal{N} \exp \left[- (x - \mu)^T \mathcal{A} (x - \mu) \right] \tag{2.72}$$

where $x = \{q_s, p_s, q_t, p_t, q_m, p_m\}$ is a six dimensional vector, $\mu = \{q_0, p_0, 0, 0, 0, 0\}$ represents the means of the initial distributions and $\mathcal{A}$ a 6×6 diagonal matrix with diagonal entries $\{\alpha_s, \alpha_s, \alpha_t, \alpha_t, \alpha_m, \alpha_m\}$ and here and below, $\mathcal{N}$ is a normalisation constant. Under the cloning map $x \rightarrow \Lambda x$, the distribution of the

total system changes as $P_{fin}(x) = P_{in}(\Lambda^{-1}x) =$

$$\mathcal{N} \exp\left[- (\Lambda^{-1}x - \mu)^T \mathcal{A}(\Lambda^{-1}x - \mu)\right] \tag{2.73}$$

which can be rewritten as

$$P_{fin}(x) = \mathcal{N} \exp\left[- (x - \Lambda\mu)^T \mathcal{B}(x - \Lambda\mu)\right] \tag{2.74}$$

where $\mathcal{B} = (\Lambda^{-1})^T \mathcal{A}\Lambda^{-1}$. It is evident that the means of the distributions are succesfully cloned $\mu' = \Lambda\mu$. As we will see below, the variances are not faithfully cloned, in keeping with the classical no cloning theorem[1].

We can find the marginal distribution of the source by integrating over the target and machine. To do this we write $\mathcal{B}$ in block form

$$\mathcal{B} = \begin{bmatrix} a & c^t \\ c & b \end{bmatrix} \tag{2.75}$$

where a is a non-singular 2×2 matrix b a non-singular 4×4 matrix and c a rectangular 4×2 matrix and c^t its transpose. It is straightforward to compute the marginal for the source.

This yields for the source distribution after cloning:

$$P_{sf}(q_s, p_s) = \mathcal{N}_s \exp\left[- (x_s - \mu_s)^T \mathcal{C}_s (x_s - \mu_s)\right] \tag{2.76}$$

where $x_s = \{q_s, p_s\}$ is a 2 dimensional vector, and

$$\mathcal{C}_s = a - c^t b c \tag{2.77}$$

a 2×2 covariance matrix and $\mu_s = \{q_0, p_0\}$.

As an example, let us consider the target and the machine to be in a thermal state with temperature T with an oscillator Hamiltonian. In fact, let us set $k = m = 1$ in the oscillator Hamiltonian $H = \frac{p^2}{2m} + \frac{1}{2}kq^2$ so that the frequency is 1. The target Hamiltonian is $H_t = (q_t^2 + p_t^2)/2$ and the machine Hamiltonian is $H_m = (q_m^2 + p_m^2)/2$. The Gibbs state of the target and machine is

$$\mathrm{P} = \frac{1}{Z} e^{-\beta(H_t + H_m)}, \tag{2.78}$$

where $\beta = \frac{1}{k_B T}$ and Z a normalisation. We also set $\alpha_s = 1$ and since the state of the machine and target are thermal, we have $\alpha_t = \alpha_m = \alpha = \beta/2$

The explicit form of the covariance matrix $\mathcal{C}_s$ is

$$\mathcal{C}_s = \frac{1}{\Delta_s(\alpha)} \begin{bmatrix} \alpha^2 + 6\alpha & -4\alpha \\ \\ \\ -4\alpha & \alpha^2 + 4\alpha \end{bmatrix} \tag{2.79}$$

where $\Delta_s(\alpha) = \alpha^2 + 10\alpha + 8$.

A very similar calculation, marginalising over the source and the machine gives the target state as

$$P_{tf}(q_t, p_t) = \mathcal{N}_t \exp - \left[(x_t - \mu_s)^T \mathcal{C}_t (x_t - \mu_s) \right] \tag{2.80}$$

where $x_t = \{q_t, p_t\}$ is a 2 dimensional vector, $\mathcal{C}_t$ a 2×2 covariance matrix and $\mu_t = \mu_s = \{q_0, p_0\}$. The explicit form of the covariance matrix $\mathcal{C}_t$ is

$$\mathcal{C}_t = \frac{1}{\Delta_t(\alpha)} \begin{bmatrix} \alpha^2 + 3\alpha & \alpha \\ \\ \\ \alpha & \alpha^2 + 2\alpha \end{bmatrix} \tag{2.81}$$

where $\Delta_t(\alpha) = \alpha^2 + 5\alpha + 5$.

As the general formulae make clear, in the limit of zero temperature $(\beta \rightarrow \infty)$, α goes to infinity and the covariance matrices of both the source and the target go to the initial distribution: the cloning is perfect. However, at finite temperature, there is corruption of the source as well as the target. There is also a spurious correlation between momentum and position introduced by the cloning process. Thus, the cloning is imperfect, as expected from the classical no-cloning theorem for classical systems with statistical distributions.

Similar conclusions emerge from our numerical analysis, which also shows how presence of statistical mechanical noise affects the cloning process (see A.1). When noise is introduced either in the machine or the target state, the original gets corrupted and the copy (which is distinct from the corrupted original) is not perfect. For illustration, we describe only three cases. The means of the initial state to be copied are $\mu_p = 8$ and $\mu_q = 5$.

When the noise is introduced either in the machine or the target state, the original gets corrupted and the copy (which is distinct from the corrupted original) is not perfect. But when the noise is introduced only at the source, we are still able to generate a perfect copy without destroying the original, in the sense that we are able to make a perfect copy of a statistical mechanical distribution (see fig 2.5) when the target and the machine are ideal.

Figure 2.6 shows the distributions of the states after cloning when the machine is at a temperature $T = 10^{23}K$ and the source and the target are delta

functions. Here it can be observed that all the three distributions are different from the original and from each other. These are binormal distributions and the most general form can be written as

$$P(p,q) = \frac{e^{-\left(\frac{(p-\mu_p)^2}{2\sigma_p^2(1-\rho^2)} - \frac{\rho(p-\mu_p)(q-\mu_q)}{\sigma_p\sigma_q(1-\rho^2)} + \frac{(q-\mu_q)^2}{2\sigma_q^2(1-\rho^2)}\right)}}{2\pi\sqrt{1-\rho^2}\sigma_p\sigma_q}, \tag{2.82}$$

where, μ_p, μ_q are the means and σ_p, σ_q are the standard deviations along p and q and ρ is the correlation between p and q.

Now we see how the process gets corrupted when the noise is present in more than one subsystem. One thing to be observed here is not only the original gets corrupted, but it is different from the imperfect copy we have made. Figure 2.7 shows the distributions of the states after cloning when both the source and the target are at a temperature $T = 10^{23}K$. One can notice that in both the cases (Figures 2.6 and 2.7), while the clones are imperfect, the means of the cloned states and the machine state are (μ_p, μ_q), $(\mu_p, \mu_q)(\mu_p, -\mu_q)$ i.e, the means are exactly where the perfect copies would be if the temperatures are 0.

To calculate the imperfectness of the cloning process we use fidelity. The fidelity[7] for classical probability distributions is given by
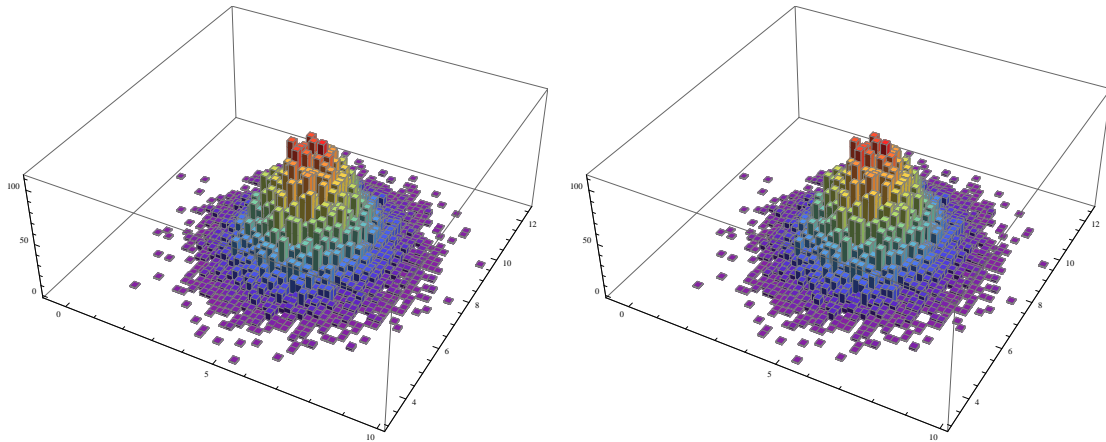
(a) Source with the means $(5, 8)$, the standard deviations $(1.17473, 1.17473)$, and the Correlation 0.

(b) Target with the means $(5, 8)$, the standard deviations $(1.17473, 1.17473)$, and the Correlation 0.
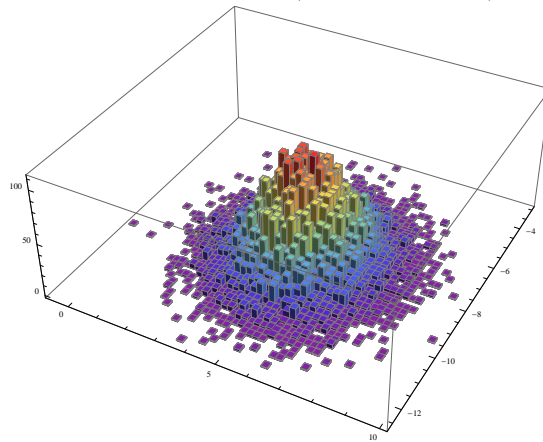
(c) Machine with the means $(5, -8)$, the standard deviations $(1.17473, 1.17473)$, and the Correlation 0.

Figure 2.5: Histograms showing the distributions of the states in phase space after cloning, when noise is present only in the source.
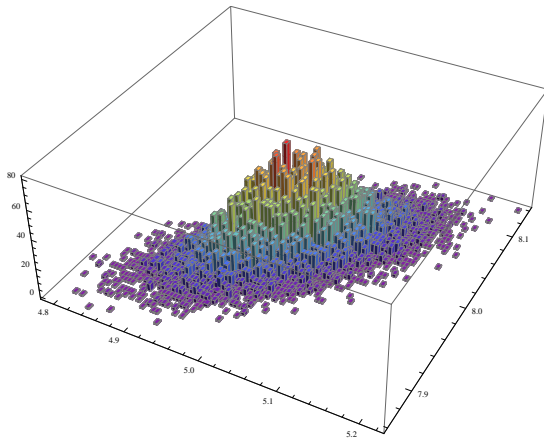
(a) Source with the means $(5, 8)$, the standard deviations $(0.0523467, 0.0371259)$, and the Correlation 0.708061.
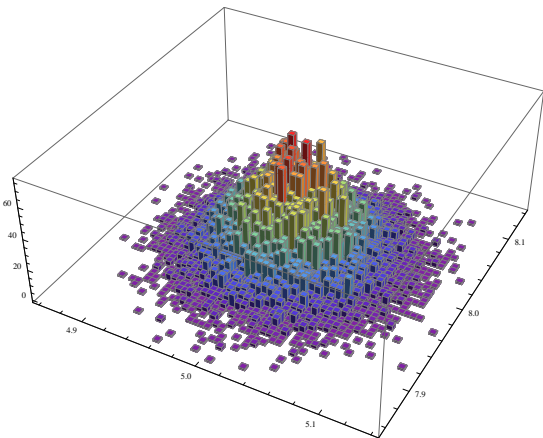
(b) Target with the means $(5, 8)$, the standard deviations $(0.0371259, 0.0369647)$, and the Correlation 0.00165714.
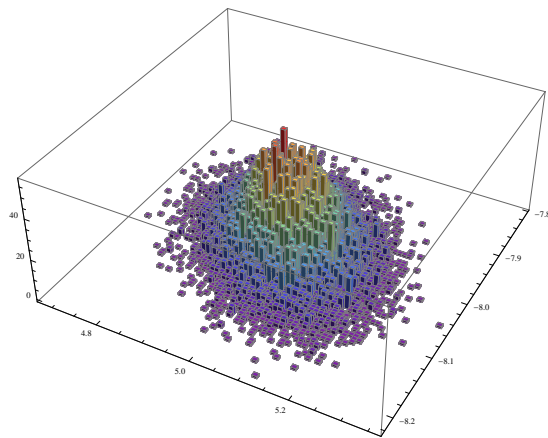
(c) Machine with the means $(5, -8)$, the standard deviations $(0.0828892, 0.0524335)$, and the Correlation -0.320408.

Figure 2.6: Histograms showing the distributions of the states in phase space after cloning, when noise is present only in the machine.
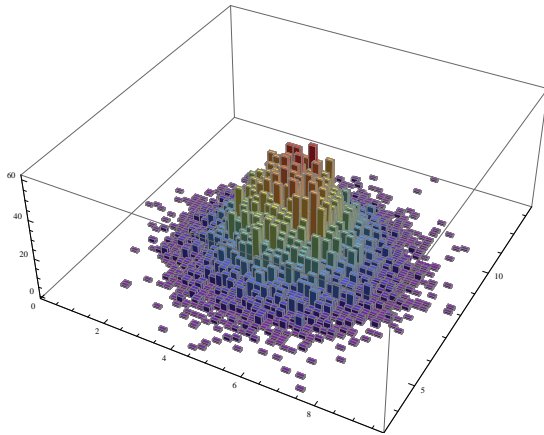
(a) Source before cloning, with the means $(5, 8)$, the standard deviations $(1.17473, 1.17473)$, and the Correlation 0.

(b) Source after cloning, with the means $(5, 8)$, the standard deviations $(2.03552, 2.86569)$, and the Correlation 0.710686.
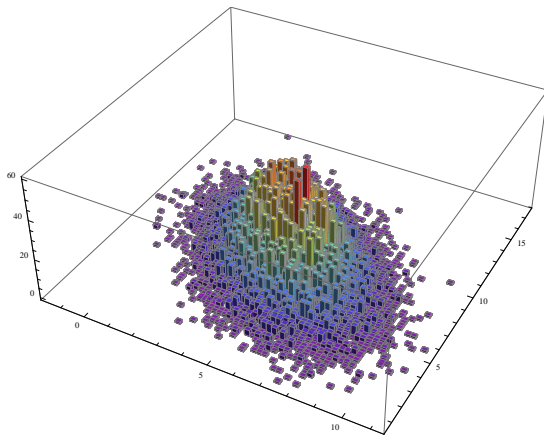
(c) Target with the means $(5, 8)$, the standard deviations $(1.65905, 2.01198)$, and the Correlation -0.413202.
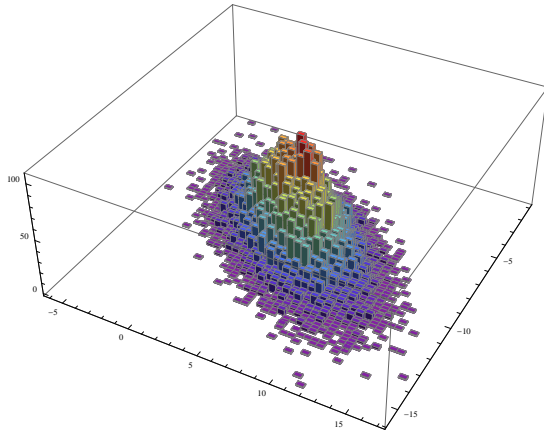
(d) Machine with the means $(5, -8)$, the standard deviations $(2.87228, 1.64867)$, and the Correlation -0.582384.
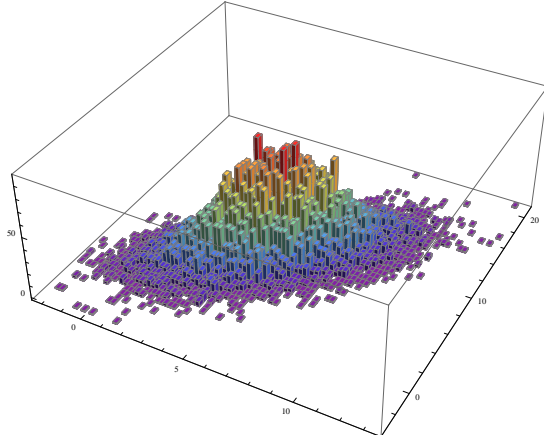
Figure 2.7: Histograms showing the distributions of the states in phase space before cloning (a) and after cloning (b, c, d), when noise is present in both the source and the target.

$$f = \sum_x \sqrt{p_x q_x}, \text{ for discrete distributions,}$$

$$= \int_{-\infty}^{\infty} \sqrt{p(x)q(x)}dx, \text{ for continuous distributions.} \qquad (2.83)$$

This can be generalised to any number of variables.

In the case where there is no noise in the source but is present in the target or the machine, we get the fidelity to be zero. This is because there is no overlap between a delta distribution and a Gaussian. We get fidelity, $f = 1$, when there is noise only at the source.

The calculation of fidelity is not straight forward when the noise is present in more than one sub system. In this case we not only have to see how good the copy is, but also calculate how much the original got corrupted. So we calculate two fidelities, one between the original and the corrupted states and another between the original and the copy states. The total fidelity is given by the product of these fidelities. We calculated the fidelity in the case of fig. 2.7, where there is noise in both the source and the target states, to be $f = 0.714$.

Needless to say, that we recover the limit of perfect cloning when we set the widths of the target and the machine distributions to zero i.e, when the source, the target and the machine all correspond to delta distributions.

To have a noise that affects the cloning process and fidelity, we need to have

β^{-1} of the same order of magnitude as the energy of the harmonic oscillator. To achieve this, the temperature of the system has to be higher than $10^{20}K$. The temperature of a typical physical process is usually of the order of $10^3 K$ to 10^4K, which generates too small a noise to affect the classical cloning process. This tells us that the classical cloning processes are not affected significantly by thermal noise. This is the reason why we are able to copy classical information without much problem in our daily experience.

2.6 Conclusion

The study of quantum cloning process has led to a better understanding of quantum mechanics. But the systems considered are highly idealised. In this chapter, we studied how the cloning process gets affected when the systems is not ideal. To achieve this we introduce thermal noise in the system and see how the fidelity gets affected. In the process we find that the traditionally used fidelity does not show the effects of temperature. Hence, we use a slightly different form of fidelity to analyse the effects of temperature.

Then we look at the classical limit of the the quantum cloning process by taking both the number of input photons and the number of copies generated, to infinity. Here the fidelity definition used traditionally brings a better understanding. We find that in the classical limit the fidelity reaches one, implying that perfect cloning is possible.

This leads us to the question of the classical cloning process. Here, we have presented a discussion of classical cloning and its subtleties. We have given a systematic method for generating all possible linear cloning maps for $\mathbb{R}^2$ and illustrated this method with an explicit example. We have gone beyond earlier literature[34,1] in constructing explicit Hamiltonians generating a cloning map. We then propose a realisable experiment to demonstrate a classical cloning process in the laboratory, using non-linear optics. We have studied the effect of statistical noise on the cloning process. An important off shoot from this work is a proof that any phase space emerging from a configuration manifold Q (as a cotangent bundle T^*Q) admits a cloning map, in fact with a minimal machine size.

It is not presently clear whether *all* symplectic manifolds admit cloning maps. For example S^2 can be given a symplectic structure, with the area on the standard sphere being the symplectic two-form. But it is obviously not the cotangent bundle of any manifold, since it is compact. We leave it for future work to determine whether general symplectic manifolds admit cloning maps and what size of machine would be required for this.

How does the cloning of states differ between quantum and classical mechanics? Intuition would suggest that our inability to clone is an essentially quantum phenomenon. Classical states, viewed as points in phase space, can be measured to any desired accuracy and therefore reproduced; unlike quantum states

which are disturbed by measurement. However, some expositions (the current Wikipedia version for example) of the quantum no cloning theorem do not include a "machine" or any ancillary degrees of freedom. They seek to copy the source state by a Unitary transformation of the source-target system. This is a misleading argument, since under the same conditions, classical cloning is also forbidden[34] under Hamiltonian evolution. Duplication of an arbitrary classical state also implies duplication of the phase space area of an arbitrary loop $A(\gamma)$ $(A(\gamma) \to 2A(\gamma))$. The machine *is* needed to cancel the excess phase space area. As we have seen, the presence of the machine renders cloning possible. The machine must at least be as large as the system to the cloned, but could be larger. In contrast, even with a machine present, quantum cloning is impossible by Unitary transformations, in accord with our intuition.

It is interesting to note that a clone state is always accompanied by an "anticlone" state. In the minimal cloning model, the anticlone is the final state of the machine, which is a time reversed version of the original state $(q, p) \to (q, -p)$. In our proposed experiment, we have taken care to ensure that the anticlone is also manifestly present in one of the emergent beams. From the optics point of view, this is a "phase conjugate beam". In fact, our proposed experiment is modeled very closely on the setup used in phase conjugation. A discussion of anticlone states also appears in Ref.[44] which treats quantum cloning.

In our discussion of a "state" in classical mechanics, we first introduced a state

as a point in phase space or as a statistical distribution with delta function concentration at a phase point. More general states in the statistical mechanical sense emerged from convex combinations of these "states". It is illuminating to compare this situation with quantum mechanics, where "pure states" are rays in Hilbert space, or equivalently one dimensional projections. Convex combinations of "pure states" yield all possible quantum states or density matrices. In quantum mechanics, the no-cloning theorem applies even to "pure states". In the classical case, "pure states" can be cloned, but statistical mixtures of "pure states" cannot. This seems to be an essential difference between the classical and quantum cases.

Another point worth stressing is that both thermal and quantum fluctuations spoil our ability to clone. This can be seen operationally in the proposed experiment. Any thermal noise occuring in the pump beams will automatically leave its mark in both the clone beam and the source beam. A similar effect happens with quantum fluctuations. Zero point fluctuations in the electromagnetic field will cause spontaneous emission in the emergent beams and so spoil the cloning process. We expect our study to generate interest in experimentally testing these ideas.

"There is no royal road to science, and only those who do not dread the fatiguing climb of its steep paths have a chance of gaining its luminous summits."

Karl Marx

3

Role of resource limitation in quantum measurements

Quantum mechanics is a very successful theory for describing the microscopic world of atoms. However, ever since its inception there are certain fundamental aspects of quantum theory that have remained obscure. This has to do with

the relation between unitary evolution which is central to the theory, and the measurement process, which gives us information about the quantum system. The challenge that remains is a self-consistent formulation of quantum theory which explains unitary evolution and outcomes of a measurement within a single framework.

Bohr had taken a semiclassical approach in which he viewed the apparatus classically and treated the system (spin) quantum mechanically. Such a point of view is unsatisfactory since at a fundamental level the world is governed by quantum mechanics. Here, we present a completely quantum mechanical analysis of the Stern-Gerlach experiment. Our purpose is to explore, in a simple solvable context, the idea that coarseness of the experimental probes is responsible for *apparent* non-unitarity in the measurement process.

We focus on the Stern-Gerlach experiment as a context for understanding the measurement process in quantum mechanics without invoking any *ad hoc* assumption beyond pure unitary evolution. Let us begin by summarising the Stern-Gerlach experiment. The set up consists of a beam of silver atoms (spin-$\frac{1}{2}$ particles) moving along the z direction passing through an inhomogeneous magnetic field along the y direction. Two spots appear on the screen corresponding to the y component of the spin, $S_y = \frac{1}{2}$ and $S_y = -\frac{1}{2}$. There have been a few analytical studies of this experiment in the past couple of decades[50,51,52,53,54,55,56,57]. Some studies[56] invoke Ehrenfest's Theorem to address the issue of measure-

ment in a Stern-Gerlach setup. There have also been detailed analyses of the Stern-Gerlach experiment from the point of view of environment induced decoherence[50,51,55,58]. Here we invoke the new idea that there is an inherent *coarseness* in the detection process. The role of coarseness of the measurement process in the quantum to classical transition has been explored in the past[59,60,61]. In[59,60] coarseness of the measurement process has been investigated by using the Leggett-Garg inequality as a way of probing the quantum to classical transition. We present an analysis which offers a new perspective on the Stern-Gerlach experiment from the point of view of the coarseness of the measurement process.

3.1 The Measurement Process

Let us summarise the measurement process in quantum mechanics. Our system is initially in a coherent superposition of states $|S\rangle = \sum_i c_i |S_i\rangle$ in an orthonormal basis which diagonalises the quantity being measured. To begin with, the system plus apparatus is in the product state $|\psi\rangle = |S\rangle|A\rangle$, in which the system and apparatus are unentangled. It is useful to logically break up the measurement process into three steps. The first step in the measurement process entails coupling between the quantum system and the measuring apparatus so that the total state evolves unitarily to an entangled state $U|\psi\rangle = \sum_i c_i |S_i\rangle|A_i\rangle^*$. This

---

*We note that in general, the $|A_i\rangle$ s need not be orthonormal.

state can be represented as a pure density matrix

$$\rho = |\psi\rangle\langle\psi| = \sum_{ij} c_j^* c_i |S_i\rangle|A_i\rangle\langle S_j|\langle A_j| \tag{3.1}$$

After the second step, the density matrix of the system takes the impure form

$$\tilde{\rho} = \sum_i |c_i|^2 |S_i\rangle\langle S_i| \tag{3.2}$$

which is interpretable as a classical mixture of states. Finally, the impure diagonal density matrix (3.2) goes over to a pure state $c_i|S_i\rangle\langle S_i|c_i^*$. The first step can be explained entirely in terms of unitary evolution and therefore is not controversial. The final step sometimes called "collapse", has been debated extensively as the "quantum measurement problem". This singling out of one outcome from many possibilities is not addressed here. Let us note that, even in classical probability theory, there is a singling out of one from several outcomes. We address here the second step; the transition from quantum superpositions to classical mixtures. Here, we investigate the Stern-Gerlach experiment from the perspective of coarse quantum measurement (CQM), in which we recognise the fact that all experiments are constrained by bounded resources. We model these constraints by using a screen whose size and spatial resolution are fixed. The spatial resolution of the screen is given by the pixel size and the size of the screen determines the total number of pixels. Experimentally one can only say that an atom

was incident on our screen somewhere within a pixel. Fixing these resources imposes ultraviolet as well as infrared cutoffs on the experimental probes. Here we are more concerned with the short distance cutoff.

3.2   ANALYSIS OF THE STERN-GERLACH SETUP

Consider silver atoms with spin-$\frac{1}{2}$ at rest in the laboratory, in a magnetic field given by

$$B = (B_0 y, B_0 x, 0).$$

Notice that this field is both divergence and curl free. We confine the atoms to the x-z plane and thus set $y = 0$. Figure 3.1 shows a schematic diagram of the Stern-Gerlach setup we are discussing here.

The Hamiltonian for the system is

$$H = \frac{p^2}{2m} - \boldsymbol{\mu}.B \tag{3.3}$$

where $\boldsymbol{\mu} = g\mu_B \frac{\hbar}{2}\boldsymbol{\sigma}$, with g the Landé g factor and μ_B the Bohr magneton. The stationary solution satisfies:

$$H\psi = E\psi \;\left(\psi = \psi(x,z),\; \psi(x,0) = e^{-\frac{x^2}{2\sigma^2}}\right) \tag{3.4}$$

Restricting to the x-z plane by setting $y = 0$, the Hamiltonian can be written
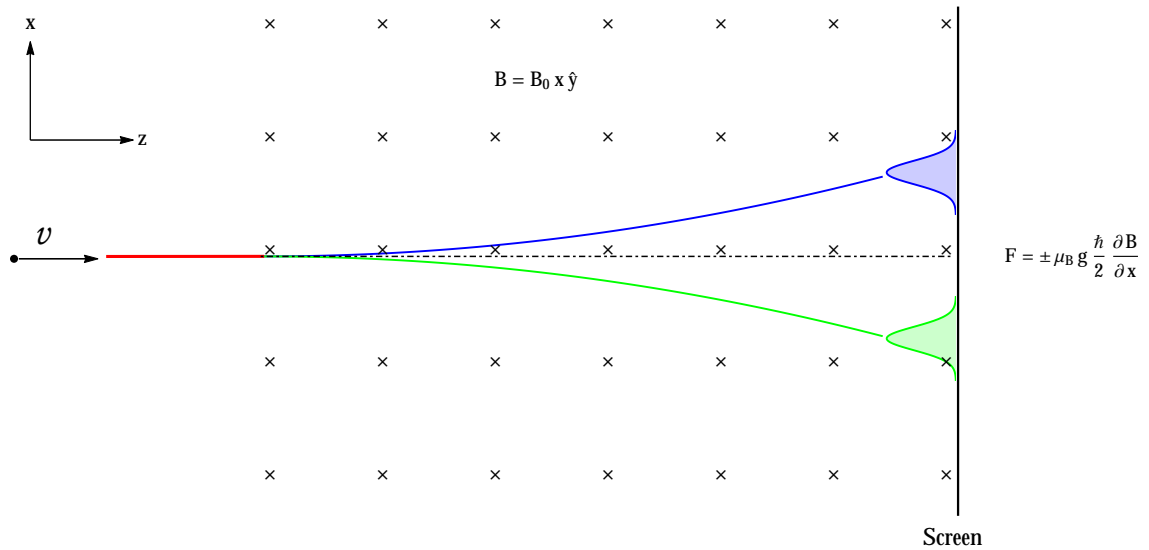
Figure 3.1: The Stern-Gerlach setup.

more explicitly as

$$H = \frac{p_x^2 + p_z^2}{2m} + xF\sigma_y \tag{3.5}$$

where, $F = -g\mu_B \frac{\hbar}{2}B_0$ and if we assume a solution of the form $\psi(x,z) =$

$\phi(x, z)\, e^{ikz}$ (since this is a propagating wave along the z-direction), Eq.(3.4) in the paraxial approximation reduces to the following:

$$i\hbar \left(\frac{k\hbar}{m} \right) \frac{\partial \phi}{\partial z} = -\frac{\hbar^2}{2m} \frac{\partial^2 \phi}{\partial x^2} + xF\sigma_y\phi \qquad (3.6)$$

if we set $E = \frac{k^2\hbar^2}{2m}$.

This equation can be identified with the time dependent Schrödinger equation, by setting $t = \frac{zm}{k\hbar}$:

$$i\hbar \frac{\partial \phi}{\partial t} = -\frac{\hbar^2}{2m} \frac{\partial^2 \phi}{\partial x^2} + xF\sigma_y\phi \qquad (3.7)$$

Since the eigenvalues of σ_y are $+1$ and -1 we get the corresponding components of the spinor ϕ as ϕ_+ and ϕ_-, respectively. Thus Eq.(3.7) reduces to:

$$i\hbar \frac{\partial \phi_+}{\partial t} = -\frac{\hbar^2}{2m} \frac{\partial^2 \phi_+}{\partial x^2} + xF\phi_+ \qquad (3.8)$$

$$i\hbar \frac{\partial \phi_-}{\partial t} = -\frac{\hbar^2}{2m} \frac{\partial^2 \phi_-}{\partial x^2} - xF\phi_- \qquad (3.9)$$

To solve these equations we move to an accelerated frame along the x-axis and employ the following transformations in x, t and ϕ, which reduce the above equations to a free particle equation for $\tilde{\phi}_\pm(\xi, T)$ where ξ is related to x as fol-

lows:

$$x = \xi \pm \frac{1}{2}aT^2 \tag{3.10}$$

and

$$t = T \tag{3.11}$$

Thus we have:

$$\phi_\pm(x, t) = \tilde{\phi}_\pm(\xi, T)\, e^{if(\xi,T)} \tag{3.12}$$

We outline the solution to Eq.(3.8).Substituting Eqs. (3.10), (3.11) and (3.12) in Eq.(3.8) we reduce Eq(3.8) to a free particle equation and find f and a :

$$f = \frac{maT}{\hbar}(\xi + \frac{1}{3}aT^2),\; a = -\frac{F}{m} \tag{3.13}$$

The kernel (propagator) for the free particle problem corresponding to Eq.(3.8) can be obtained using path integral approach[62]:

$$\tilde{K}(x, x_i; t) = \sqrt{\frac{m}{2\pi i \hbar t}}\, e^{i\frac{m(x - x_i)^2}{2\hbar t}} \tag{3.14}$$

where x is the position at time t and x_i is position at $t_i = 0$. We can find the propagator for the Hamiltonian under consideration by applying the following transformation.

$$K(x, x_i; t) = e^{if(x,t)}\tilde{K}(x, x_i; t) \tag{3.15}$$

which gives the required propagator[63,62]:

$$K^{++}(x, x_i; t) = \sqrt{\frac{m}{2\pi i\hbar t}} \exp\left\{i\left(\frac{m}{2\hbar t}(x - x_i)^2 - \frac{Ft}{2\hbar}(x + x_i) - \frac{F^2 t^3}{24m\hbar}\right)\right\}$$

(3.16)

The solution to Eq.(3.8) can be cast as follows:

$$\phi_+(x, t) = \int_{-\infty}^{\infty} K^{++}(x, x_i, t)\, \phi_+(x_i, 0)\, dx_i$$

(3.17)

After solving Eq.(3.17) we get the final solution for ϕ_+. We employ the same procedure to find ϕ_-. The solutions are:

$$\phi_+(x, t) = \sqrt{\frac{m\sigma}{(m\sigma^2 + i\hbar t)\sqrt{\pi}}}$$

(3.18)

$$\times \exp\left\{-\frac{m(x^2 + \frac{a^2}{12\hbar}(4im\sigma^2 - \hbar t)t^3 + \frac{axt}{\hbar}(-2im\sigma^2 + \hbar t))}{2(m\sigma^2 + i\hbar t)}\right\}$$

$$\phi_-(x, t) = \sqrt{\frac{m\sigma}{(m\sigma^2 + i\hbar t)\sqrt{\pi}}}$$

(3.19)

$$\times \exp\left\{-\frac{m(x^2 + \frac{a^2}{12\hbar}(4im\sigma^2 - \hbar t)t^3 - \frac{axt}{\hbar}(-2im\sigma^2 + \hbar t))}{2(m\sigma^2 + i\hbar t)}\right\}$$

In general, one can consider a further evolution beyond the region where the magnetic field is present and consider free evolution which leads to solutions of

the form given below:

$$|\phi_+(x,t)|^2 = \sqrt{\frac{m^2\sigma^2}{(m^2\sigma^4 + \hbar^2 t^2)\pi}} \exp\left\{ -\frac{m^2[x - \frac{1}{2}at_1{}^2 - at_1(t - t_1)]^2}{(m^2\sigma^4 + \hbar^2 t^2)} \right\}$$

$$(3.20)$$

$$|\phi_-(x,t)|^2 = \sqrt{\frac{m^2\sigma^2}{(m^2\sigma^4 + \hbar^2 t^2)\pi}} \exp\left\{ -\frac{m^2[x + \frac{1}{2}at_1{}^2 + at_1(t - t_1)]^2}{(m^2\sigma^4 + \hbar^2 t^2)} \right\}$$

$$(3.21)$$

where t_1 is the amount of time spent by the atom in the magnetic field and t is the total time of evolution. We view the spin as a quantum system and the position of the silver atom as the apparatus or pointer. The above formulation results in a separation in *time* of the two spin states. This can be mapped to the formulation, of a typical experiment, where the separation of the spins happens in *space* and we will sometimes use the spatial notation and language with the understanding that $t = zm/k\hbar$, where $\hbar k = \sqrt{2mE}$. Here the symbols $+$ and $-$ refer to the two components ϕ_+ and ϕ_- of the Pauli spinor ϕ. The final wave function is got by "folding" the initial Gaussian with the propagator matrix. It has the form

$$\phi(x,t) = c_+\phi_+(x,t)|+\rangle + c_-\phi_-(x,t)|-\rangle,$$

where $|+\rangle$ and $|-\rangle$, are eigenstates of σ_y and $\phi_+(x, t)$ and $\phi_-(x, t)$ are Gaussian wave packets. We can identify two relevant time scales: $\tau_1 = \sqrt{\frac{2\sigma}{a}}$, the time over which the centers of mass of the two wave packets separate and $\tau_2 = \frac{m\sigma^2}{\hbar}$, the timescale over which the individual wavepackets spread. We use the values $m = 1.79 \times 10^{-25} kg$, $F = 9.27 \times 10^{-22} N$ and $\sigma = 10^{-6} m$ which are experimentally reasonable. Typical values for the two time scales are $\tau_1 = 10^{-5}s$ and $\tau_2 = 10^{-3}s$.

Figure 3.2 shows the evolution of the wave packet from $t = 0$ sec to $t = 30\mu$ sec, for the values mentioned above. At $t = 0$ sec the two components of the wave packet (pertaining to the two spin components) are overlapping and at $t = 30\mu$ sec the two components of the wave packet are well separated.

We restrict our discussion to a situation where the detection screen is placed at a location just at the point where the atom exits the magnetic field. However, in general, one can have a further free evolution of the separated wave packets beyond this region in the field free space.

The full density matrix is of the form:

$$\rho_{\alpha\beta}(x, x') = c_\alpha \phi_\alpha(x) c_\beta^* \phi_\beta^*(x'), \qquad (3.22)$$

where α and β take values $+$ and $-$. In Eq.(3.22) we have suppressed the time dependence in the notation.
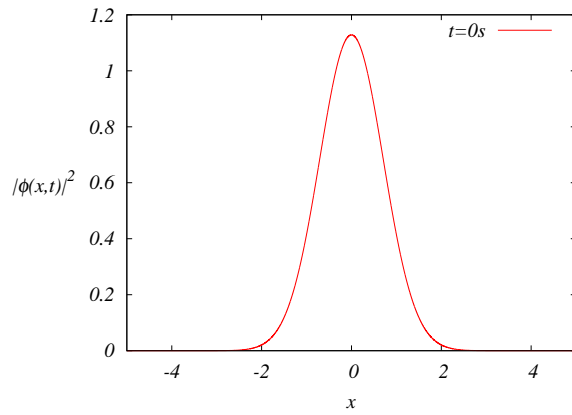
(a) $t = 0$ sec
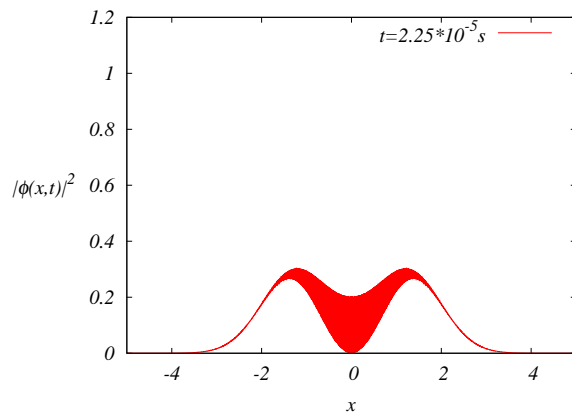
(b) $t = 22.5 \, \mu$ sec
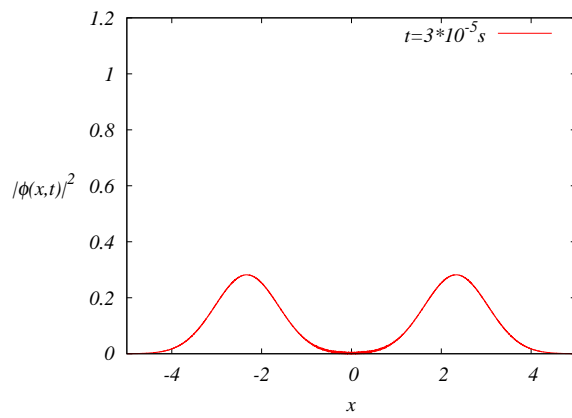
(c) $t = 30 \, \mu$ sec

Figure 3.2: Evolution of the wave packet with respect to time.

We now use the fact that the detection is done *coarsely* i.e., any screen placed for the detection of an atom is pixelated. We take the width of the pixel Δ to be 10^{-6}m (same order as the smallest pixel available). For the sake of simplicity we set $c_+ = c_- = 1/\sqrt{2}$. The full density matrix can be written as

$$\rho(x, x') = \frac{1}{2} \begin{pmatrix} \phi_+(x)\phi_+^*(x') & \phi_+(x)\phi_-^*(x') \\ \phi_-(x)\phi_+^*(x') & \phi_-(x)\phi_-^*(x') \end{pmatrix}. \tag{3.23}$$

The coarse-grained density matrix, $\bar{\rho}(x, x')$ can be written as

$$\bar{\rho}(x, x')_{\alpha\beta} = \frac{1}{\Delta} \int_{-\Delta/2}^{\Delta/2} \rho_{\alpha\beta}(x + u, x' + u)du, \tag{3.24}$$

where $\alpha, \beta = \pm$. The off diagonal terms $\rho_{+-}(x + u, x' + u)$ and $\rho_{-+}(x + u, x' + u)$ are oscillatory due to a term $e^{ix2\pi/d}$, which oscillates on a length scale $d = \frac{\hbar}{2Ft}$, which is about 10^{-8}m. Since the oscillation length scale is smaller than the size of the pixel (10^{-6}m), on coarse graining the off-diagonal elements average to zero (see A.2), resulting in a diagonal density matrix

$$\bar{\rho}(x, x') = \frac{1}{2} \begin{pmatrix} \phi_+(x)\phi_+^*(x') & 0 \\ 0 & \phi_-(x)\phi_-^*(x') \end{pmatrix}. \tag{3.25}$$
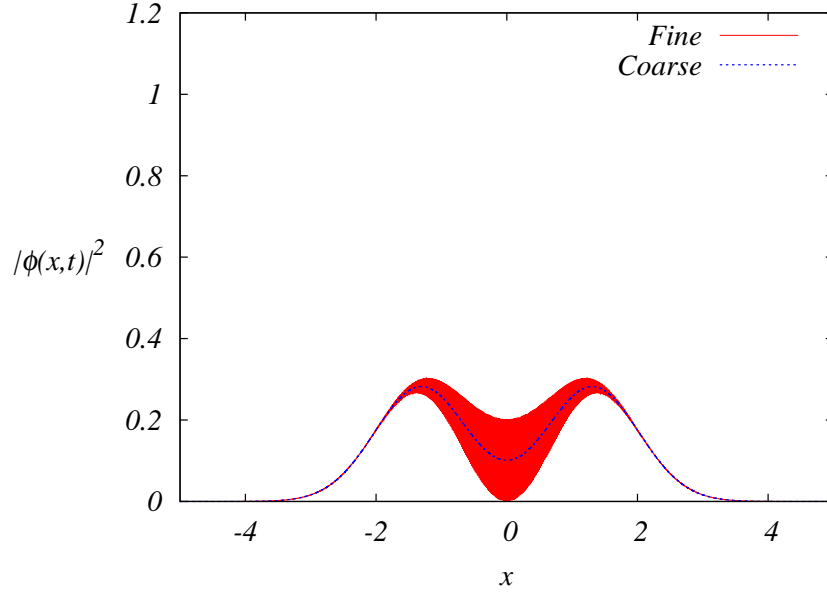
Figure 3.3: The spatial distribution of the wave packet at $t = 22.5 \, \mu$ sec, before and after the coarse graining.

Setting $x = x'$, we can write the coarse grained density matrix as

$$
\bar{\rho} = \begin{pmatrix} P_+(X) & 0 \\ 0 & P_-(X) \end{pmatrix} = \frac{1}{2L\sqrt{\pi}} \begin{pmatrix} e^{-\left(\frac{x-\frac{at^2}{2}}{L}\right)^2} & 0 \\ 0 & e^{-\left(\frac{x+\frac{at^2}{2}}{L}\right)^2} \end{pmatrix}.
\qquad (3.26)
$$

where, $L = \frac{m\sigma}{\sqrt{(m^2\sigma^4 + t^2\hbar^2)}}$. In Fig 3.3 we have plotted both the exact wave packet and the coarse-grained one for comparison.

What can one learn from a coarse measurement? Let us suppose as is usual in experiments that we only detect the position of the silver atom with low resolution and do not measure the momentum at all. We assign relative probabilities $P_\pm(X) = 1/2 \int_{-\Delta/2}^{\Delta/2} |\phi_\pm(X + u)|^2 du$ corresponding to an atom of spin $\pm$ detected at X, by integrating over a pixel of width Δ around X. By detecting an atom at pixel X we do gain information about the spin. If we set, $P(X) = P_+(X) + P_-(X)$ and define $q_\pm(X) = P_\pm(X)/P(X)$ (conditional probabilities for the silver atom being detected at the pixel X), the entropy of the spin probability distribution is $S(X) = -q_-(X) \log q_-(X) - q_+(X) \log q_+(X)$. The information we gain (See Fig 3.4) is thus given by

$$I(X) = \log 2 - S(X) \tag{3.27}$$

$$= \log(2) - \frac{\left(\frac{x+\frac{at^2}{2}}{L}\right)^2}{1 + e^{\frac{2at^2x}{L^2}}} - \frac{\left(\frac{x-\frac{at^2}{2}}{L}\right)^2}{1 + e^{-\frac{2at^2x}{L^2}}} - \log\left(e^{-\left(\frac{x+\frac{at^2}{2}}{L}\right)^2} + e^{-\left(\frac{x-\frac{at^2}{2}}{L}\right)^2}\right)$$

per event at X. Note that the arrivals at X values away from 0 give us more information.

The mean information per event is given by[3]:
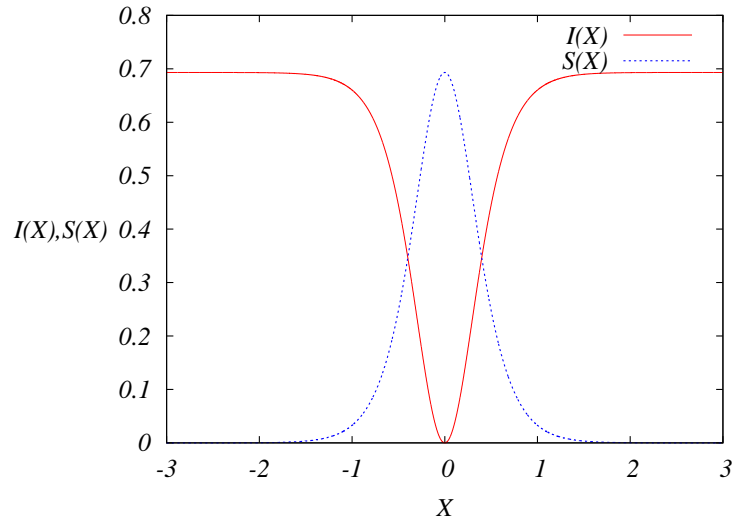
(a) $t = 22.5\,\mu\sec$
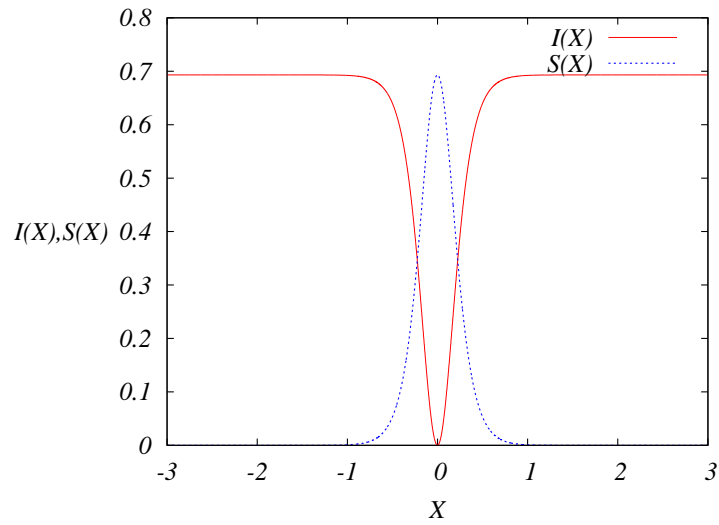
(b) $t = 30\,\mu\sec$

Figure 3.4: Information extracted $I(X)$ (in red) and entropy $S(X)$ (in blue) versus X (position of the detection of atom).
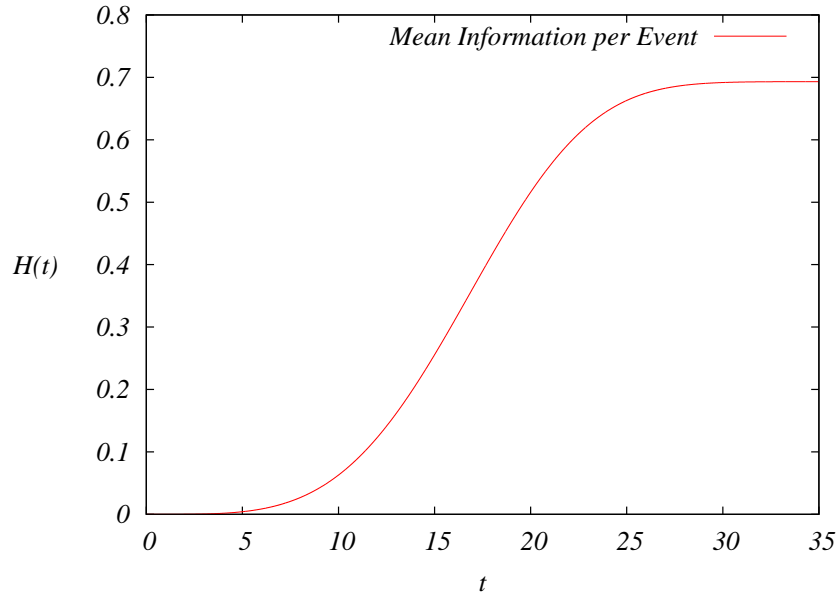
Figure 3.5: Mean information per event $\mathcal{H}$ versus time in μ sec.

$$
\begin{aligned}
\mathcal{H} &= \int P(X)I(X)dX \tag{3.28} \\
&= \log 2 - \int P(x) \log P(x)dx + \int P_+(x) \log P_+(x)dx + \int P_-(x) \log P_-(x)dx.
\end{aligned}
$$

It follows from Eq.(3.28) that $\mathcal{H}$ starts out from zero at $t = 0$ and approaches $\log 2$ (see A.3) over a timescale of $\tau_1 = 10^{-5}$s (See Fig. 3.5). The fact that $\mathcal{H}$ is positive means that we do gain some information about the spin of the atoms by detecting their positions, even before the two wave packets have separated cleanly.

Here we have addressed the Quantum Measurement Process in the context of the Stern-Gerlach experiment. An exact solution of the Schrödinger equation permits us to analyse unitary evolution in an idealised mathematical model of the experiment. Coarse Quantum Measurement (CQM) is based on the idea that every measurement is done with limited resources of resolution. The key conclusion of our analysis is that the apparent loss of unitarity in a quantum measurement is a consequence of the coarseness of the experimental probes. Previous literature on coarse measurements[59,60,61] has not applied the idea to understand the classic Stern-Gerlach experiment which is of great interest as a paradigm for quantum measurement.

In the context of statistical mechanics, the authors of Ref.[4,64] note that entropy is a subjective notion depending upon the resources available to the experimenter, to distinguish between statistical states. This follows the Bayesian approach to probability theory. The view we advocate is very similar in the context of quantum mechanics. The idea of "coarse measurement" is clearly a subjective one. Depending on the resources available to the experimenter, the evolution may appear unitary or otherwise. Thus, with a high enough resolution, one can always detect interference effects. When the interference between the two wave packets is detectable, we must conclude that the spin is *both* up and down si-

multaneously. This does not constitute a measurement of the spin component σ_y. In a low-resolution experiment, the interference *apparently* gets washed out and we can obtain information about the spin. This is the regime of interest here.

Some of the quantum measurement literature concerns itself with von Neuman measurements, which can be regarded as instantaneous. One talks about "before" and "after", but not during the measurement. Exceptions are weak[65] and nonideal measurements[66]. In weak measurements one tries to continuously extract information from a quantum system causing minimal disturbance using a weak probe, that does not destroy the interference pattern. In coarse measurements, one explicitly loses the interference pattern. Regarding nonideal measurements Ref.[66] discusses the subtleties in the notion of distinguishability of apparatus states: even states which are orthogonal in the Hilbert space sense can have considerable spatial overlap. In contrast, our focus is on how a coarse measurement results in the apparent loss of coherence of the final wavepacket in a Stern-Gerlach setup. As has been emphasised by Ref.[59], the coarse measurement approach is conceptually different from the decoherence paradigm. Decoherence involves interaction with environmental degrees of freedom. Information is lost from the system by tracing over the environment. The coarse measurement approach does not invoke new degrees of freedom or new dynamics. It is essentially kinematical, dealing with the experimenter's inability to measure

or control fine details.

There have been other parallel developments[67,68] which address the issue of imperfect measurements. In[67] the authors model the detector as a phase randomizer or dephaser, which leads to a mixed state density matrix starting from a pure state density matrix. In[68], the formalism of coarse-graining has been framed in a formal mathematical language. We go beyond this discussion by providing a physical basis in terms of resource limitation. Ref.[68] also touches upon the issue of non-idealness as in Ref.[66]. There has even been a suggestion[69] that the "reduction of the wavepacket" happens just when the atom enters the magnetic field.

In the actual experimental setup for the Stern-Gerlach experiment, the atoms are heated in an oven to about $450K$. At this temperature, the two spin states of the silver atom are in an incoherent or classical superposition of the two spin states. As a result, the interference effects dealt with here will not be visible. To see the quantum interference effects discussed here, the internal state of the atom must be in a *coherent* superposition of spin states. An optical analogue of the Stern-Gerlach experiment[70] may be a more practical candidate for realising this experiment.

4

Quantum advantage in measurements

The state of a quantum system is never completely revealed through the measurement process. However, if the observer has the information that the system is prepared in any of two given states, the task at hand becomes that of distinguishing the two given quantum states[71,72,73,74,75] using the measurement process. In this chapter we explore the issue of distinguishability of quantum states

in the context of quantum measurement.

In general, quantum states are represented by density matrices. To tell whether a given system is in state ρ_1 or ρ_2, we have to perform a measurement. By making a single measurement, the states cannot be distinguished with certainty unless the states are both pure and orthogonal to one another (See section 2.2.4 in Ref[7]). There have been studies[76,77,78] on minimising the error in distinguishing the states. People have worked on the idea of using a large number of quantum states in order to achieve greater distinguishability. Here we use Umegaki's quantum relative entropy[79] as a measure of distinguishability between quantum states.

One encounters a similar situation in the classical domain, in the cases of checking whether a coin is fair or not, estimating the parameters of a distribution, drug trials, etc. Our ability to distinguish probability distributions increases with the number of trials. Kullback-Leibler (KL) divergence provides an operational manner to distinguish between probability distributions[3,80,81].

Another example of the use of a distinguishability measure occurs in the theory of colours[82,83]. The space of colours is two-dimensional (assuming normal vision) and one can see this on a computer screen in several graphics softwares. The sensation of colour is determined by the relative proportion of the RGB values, which gives us two parameters. The extent to which one can distinguish neighbouring colours is usually represented by MacAdam ellipses[82,84,83], which

are contours on the chromaticity diagram which are just barely distinguishable from the centre. These ellipses give us a graphical representation of an operationally defined Riemannian metric on the space of colours. The flat metric on the Euclidean plane would be represented by circles, whose radii are everywhere the same. As it turns out, the metric on the space of colours is not flat and the MacAdam ellipses vary in size, orientation and eccentricity over the space of colours. This analogy is good to bear in mind, for we provide a similar visualisation of the geometry of state space based on entropic considerations.

Here we demonstrate an improved experimental strategy for discriminating between two quantum states using relative entropy. This is a new direction hitherto unexplored in the existing literature[85,86,87,88,89].

4.1 Statistical Inference using Kullback-Leibler (KL) divergence

Consider a random variable $X = \{x_1, x_2, \ldots, x_n\}$, with $P = \{p_1, p_2, \ldots, p_n\}$ as the empirical probability distribution obtained from repeated measurements. Let $Q = \{q_1, q_2, \ldots, q_n\}$ be the statistical model we consider for the Random variable X. The question of interest is the number of trials needed to be able to distinguish (at a given confidence level) between our assumed probability distribution and the measured probability distribution. A popular measure for distinguishing between the expected distribution and the measured distribution is given by the relative entropy or the KL divergence (KLD) which is widely used

in the context of distinguishing classical probability distributions[80].

Let us consider the case where we perform N measurements to obtain the empirical distribution. What is the probability that the observed distribution P is obtained by the model distribution Q? This is what we call the likelihood function,

$$L(N|Q) = \frac{N!}{\prod N_i!} \prod q_i^{N_i},\tag{4.1}$$

where, N_i is the number of times the experiment returns the value x_i and $p_i = N_i/N$. If we take the average of the logarithm of this likelihood function and use Stirling's approximation for large N we get the following expression:

$$\frac{1}{N} \log L(N|Q) = -D_{KL}(P\|Q),\tag{4.2}$$

where, $D_{KL}(P\|Q) = \sum p_i \log \frac{p_i}{q_i}$. Thus $D_{KL}(P\|Q)$ gives us the divergence of the measured distribution from the model distribution. The KL divergence is positive and vanishes if and only if the two distributions P and Q are equal.

The relative entropy (or KLD) gives an operational measure of how distinguishable two distributions are, quantified by the number of trials needed to distinguish two distributions at a given confidence level. However, the KLD is not a distance function on the space of probability distributions: it is not symmetric between the distributions P and Q. One may try to symmetrize this

function, but then, the result does not satisfy the triangle inequality. However, in the infinitesimal limit, when Q approaches P, the relative entropy can be Taylor expanded to second order about P. The Hessian matrix does define a positive definite quadratic form, at P and thus a Riemannian metric on the space of probability distributions. For a classical probability distribution $P = \{p_i, i = 1, 2, \ldots, d\}$, the Fisher-Rao metric[3,90] is given by

$$ds^2 = \sum_i \frac{dp_i^2}{p_i} \tag{4.3}$$

and this forms the basis of classical statistical inference and the famous χ-squared test. The Riemannian metric then defines a distance function, based on the lengths of the shortest curves connecting any two states P and Q.

4.2 Measurements on single qubits: Emergence of the Bures metric

Let us now consider the quantum problem of distinguishing between two states ρ_1 and ρ_2. Take the case of an n-dimensional quantum system and a collection of measurement operators $\{\hat{M}_i\}$.

$$\hat{M}_i = |m_i\rangle\langle m_i|, \ i = 1, \ldots, n$$

where, $|m_i\rangle$s form a complete basis, implying $\sum_i |m_i\rangle\langle m_i| = \mathbb{I}$.

The probability p_i of density matrix ρ collapsing on to $|m_i\rangle$ is given by

$$p_i = \text{Tr}\left[\rho|m_i\rangle\langle m_i|\right] \tag{4.4}$$

Here we consider the case of a qubit on the Bloch sphere, where

$$\rho = \frac{\mathbb{I} + \vec{n}.\vec{\sigma}}{2}, \; \hat{M}_\pm = \frac{\mathbb{I} \pm \vec{m}.\vec{\sigma}}{2} \tag{4.5}$$

$$p_+ = \frac{1 + \vec{n}.\hat{m}}{2}, \; p_- = \frac{1 - \vec{n}.\hat{m}}{2} \tag{4.6}$$

where, $\hat{m}$ is the unit vector along the measurement direction, $\vec{n}$ corresponds to the state ρ on the Bloch sphere, and $\vec{\sigma} = (\sigma_x, \sigma_y, \sigma_z)$ represent Pauli matrices.

Here $\rho_1 = \frac{\mathbb{I} + X.\sigma}{2}$ plays the role of P above and $\rho_2 = \frac{\mathbb{I} + Y.\sigma}{2}$ that of Q. A new ingredient in the quantum problem is that we can choose our measurement basis. Suppose that we are given a string of N qubits all in the same state, which may be either ρ_1 or ρ_2. A possible strategy is to make projective measurements on individual qubits, in the basis of $\hat{M}_i$, analogous to measuring the spin component in the direction $\hat{m}$. For each choice of $\hat{m}$ we find $p_\pm = \frac{1 \pm X.\hat{m}}{2}$ and $q_\pm = \frac{1 \pm Y.\hat{m}}{2}$ and we can compute the KL-Divergence or the classical relative entropy of the two distributions as :

$$S_m(\rho_1\|\rho_2) = p_+ \log \frac{p_+}{q_+} + p_- \log \frac{p_-}{q_-}. \tag{4.7}$$

We will now choose $\hat{m}$ in such a way as to maximize our discriminating power *i.e* $S_m(\rho_1\|\rho_2)$. This gives us,

$$\delta S_m = \frac{\partial S}{\partial \hat{m}}\delta\hat{m} = \lambda\delta\hat{m}, \tag{4.8}$$

which can be rewritten as

$$\frac{\partial S_m}{\partial a_1}X + \frac{\partial S_m}{\partial a_2}Y = \lambda\delta\hat{m}, \tag{4.9}$$

where $a_1 = \hat{m}.X$ and $a_2 = \hat{m}.Y$. Since δS_m is a linear combination of X and Y we find that $\hat{m}$ must lie in the plane containing X and Y, as shown in Fig 4.1. Without loss of generality, we can suppose this to be the $x - z$ plane, so that $X_2 = Y_2 = \hat{m}_2 = 0$. We can replace $\hat{m} = (\cos\beta, 0, \sin\beta)$ by the angle β. ρ_1 and ρ_2 can be expressed, in the measurement basis as

$$\rho_1 = \frac{1}{2}\begin{pmatrix} 1 + r_1\cos\beta & r_1\sin\beta \\ r_1\sin\beta & 1 - r_1\cos\beta \end{pmatrix}, \tag{4.10}$$

$$\rho_2 = \frac{1}{2}\begin{pmatrix} 1 + r_2\cos(\theta + \beta) & r_2\sin(\theta + \beta) \\ r_2\sin(\theta + \beta) & 1 - r_2\cos(\theta + \beta) \end{pmatrix}, \tag{4.11}$$

which gives us $p_\pm = \frac{1}{2}(1 \pm r_1\cos\beta)$ and $q_\pm = \frac{1}{2}(1 \pm r_2\cos(\theta + \beta))$. Thus, the classical relative entropy between ρ_1 and ρ_2 can be written as

$$S_m(r_1, r_2, \theta, \beta) = \left(\frac{1 + r_1 \cos \beta}{2}\right) \log \left(\frac{1 + r_1 \cos \beta}{1 + r_2 \cos (\theta + \beta)}\right) \quad (4.12)$$
$$+ \left(\frac{1 - r_1 \cos \beta}{2}\right) \log \left(\frac{1 - r_1 \cos \beta}{1 - r_2 \cos (\theta + \beta)}\right).$$
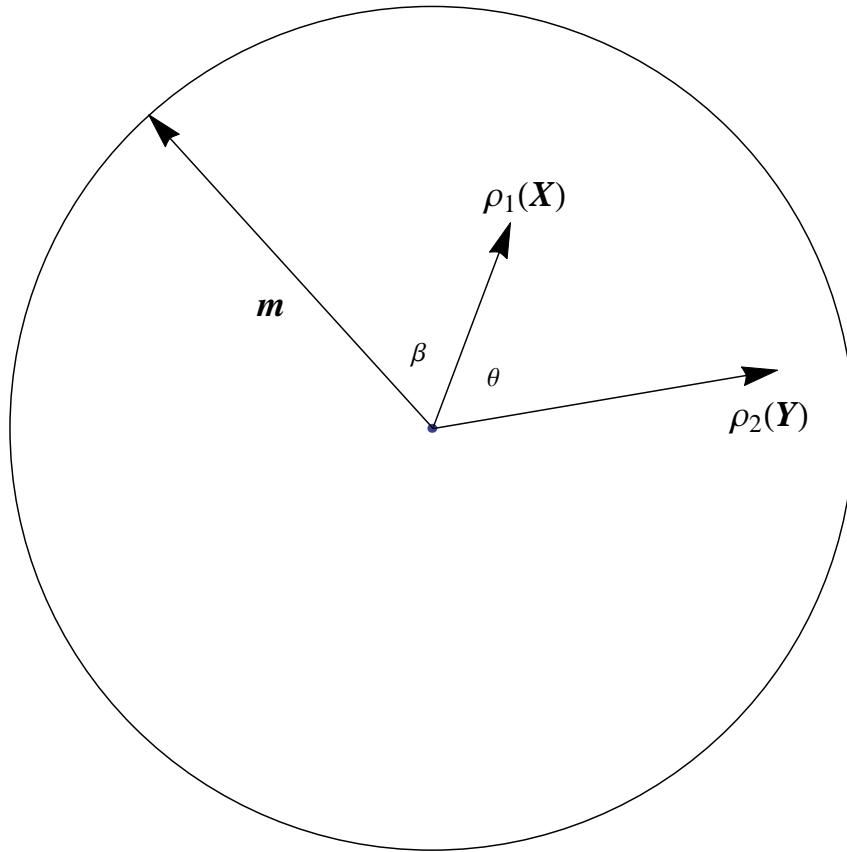
Figure 4.1: The plane of the Bloch sphere containing the vectors corresponding to the states ρ_1 and ρ_2.

The relative entropy between two density matrices is a function of the measurement basis parametrised by β. Plotting $S(\beta)$ (Fig 4.2), we find that the
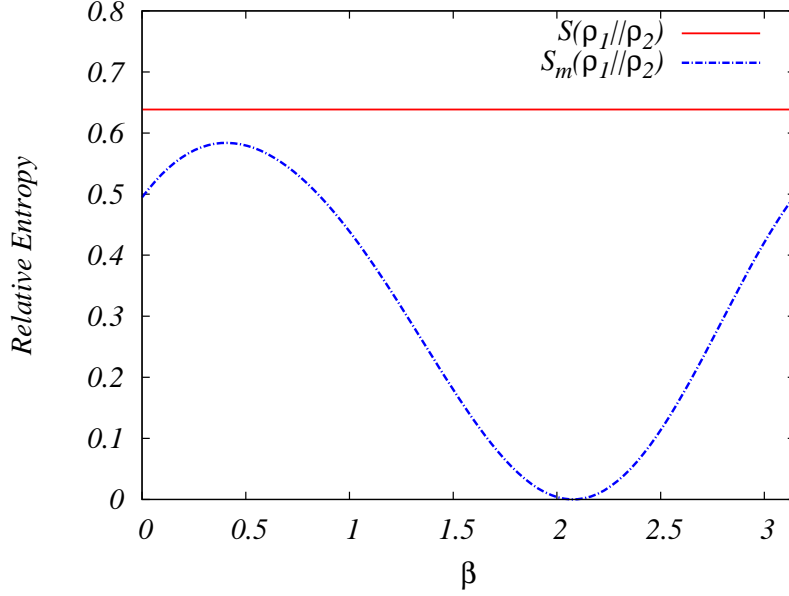
Figure 4.2: The classical $S_m(\rho_1 \| \rho_2)$ and the quantum $S(\rho_1 \| \rho_2)$ relative entropies between ρ_1 and ρ_2 plotted against β.

maximum distinguishability is attained at $\beta = \beta^*$. This is clearly the most advantageous choice of β. The value of S_m at the maximum is denoted by $S^*(r_1, r_2, \theta) = S_m(r_1, r_2, \theta, \beta^*(r_1, r_2, \theta))$. $S^*(r_1, r_2, \theta)$ gives us the optimal choice for state discrimination when we measure qubits, one at a time. Here for the analysis we chose $r_1 = 0.9, r_2 = 0.5$ and $\theta = \frac{\pi}{2}$. The maximum occurs at $\beta^* = 0.41$. As we can see in Fig 4.2, $S^*(r_1, r_2, \theta)$ is never more than Umegaki's quantum relative entropy[79].

$$
\begin{aligned}
S(\rho_1 \| \rho_2) &= \mathrm{Tr}[\rho_1 \log \rho_1 - \rho_1 \log \rho_2] & (4.13)\\
S(r_1, r_2, \theta) &= \frac{1}{2} \log\left(\frac{1 - r_1^2}{1 - r_2^2}\right) + \frac{r_1}{2}\left(\log\left(\frac{1 - r_1}{1 + r_1}\right) + \cos\theta \log\left(\frac{1 - r_2}{1 + r_2}\right)\right).
\end{aligned}
$$
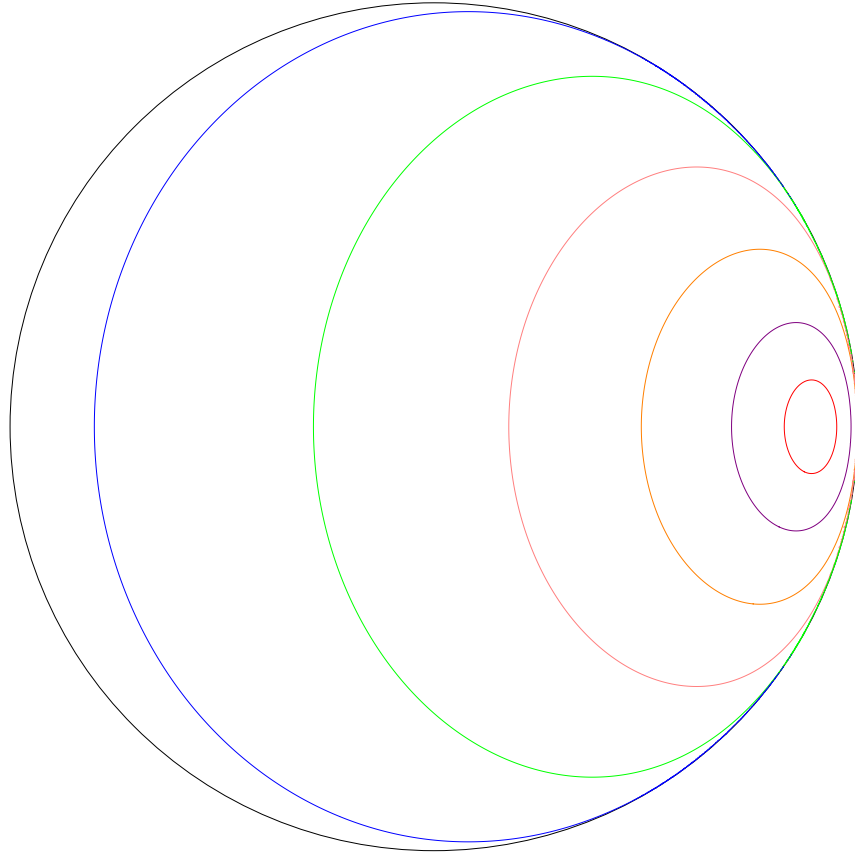
Figure 4.3: Contours of constant quantum relative entropy.

Figure 4.3 shows the contours of constant relative entropy, i.e., for the chosen state of $r_1 = 0.9$, Fig 4.3 shows all the states that are equally distinguishable using quantum relative entropy in one colour. The outer boundary in black represents the set of pure states, where the quantum relative entropy diverges.

Figure 4.4 shows a comparison between the quantum relative entropy $S(r_1, r_2, \theta)$ and the optimised classical relative entropy $S^*(r_1, r_2, \theta)$, for the values $r_1 = 0.9$ and $r_2 = 0.9$. Note that the quantum relative entropy in general exceeds the
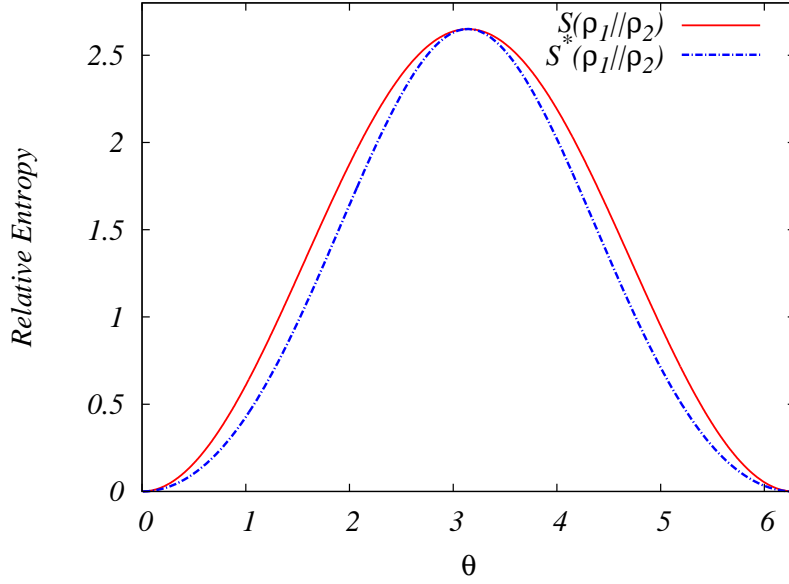
Figure 4.4: The quantum relative entropy $S(r_1, r_2, \theta)$ and the optimised classical relative entropy $S^*(r_1, r_2, \theta)$ as a function of θ.

classical one. Equality between $S^*(\rho_1\|\rho_2)$ and $S(\rho_1\|\rho_2)$ happens if and only if $[\rho_1, \rho_2] = 0$ $(\theta = 0, \pi, 2\pi \approx 0)$ *i.e,* when the two density matrices commute with each other. This difference is what we call the *Quantum Advantage*:

$$\Omega(\rho_1\|\rho_2) = S(\rho_1\|\rho_2) - S^*(\rho_1\|\rho_2). \tag{4.14}$$

We now take the infinitesimal limit and replace (ρ_1, ρ_2) by $(\rho, d\rho)$ and rep-

resent ρ by (r, θ) and $d\rho$ by $(dr, d\theta)$. dp_+ and dp_- are:

$$\left.\begin{aligned} dp_+ &= \frac{\cos\beta dr - r\sin\beta d\theta}{2}, \\ dp_- &= \frac{r\sin\beta d\theta - \cos\beta dr}{2}. \end{aligned}\right\} \tag{4.15}$$

Considering the classical relative entropy (4.7) between infinitesimally separated states and doing a Taylor expansion, gives us the Fisher-Rao metric (4.3), which is given by

$$ds^2 = \frac{dp_+^2}{p_+} + \frac{dp_-^2}{p_-}. \tag{4.16}$$

Substituting dp_+, dp_-, p_+ and p_-, from (4.15), we get

$$ds^2 = \frac{(dr - r\tan\beta d\theta)^2}{1 - r^2 + \tan^2\beta}. \tag{4.17}$$

Keeping r, dr, $d\theta$ fixed and optimising with respect to β we find

$$\tan\beta^* = -\frac{r\left(1 - r^2\right)}{dr/d\theta}. \tag{4.18}$$

Substituting $\tan\beta^*$ in (4.17) we get the expression for the metric

$$ds^2 = \frac{dr^2}{1 - r^2} + r^2 d\theta^2. \tag{4.19}$$

Returning to three dimensions using spherical symmetry we get an expression

for the metric

$$ds^2 = \frac{dr^2}{1 - r^2} + r^2(d\theta^2 + \sin^2\theta d\phi^2). \qquad (4.20)$$

In the above derivation, we have defined the distinguishability metric in the tangent space by optimising over all measurement bases. The metric we arrive at is the Bures-Helstrom (BH) metric ([91,92,93], Ref.[94] and references therein), which was introduced by Bures[91] from a purely mathematical point of view. Its relevance to quantum state discrimination was elucidated by Helstrom[92]. It plays the role of the Fisher-Rao metric in quantum physics, *if one restricts oneself to measuring one qubit at a time.*

Let the quantum relative entropy, $\mathcal{S}(\rho_1(\boldsymbol{\lambda}_1)\|\rho_2(\boldsymbol{\lambda}))$ be a function on the space of density matrices which is positive and vanishes if and only if $\rho_2 = \rho_1$[7]. Let us consider $\mathcal{S}(\rho_1(\boldsymbol{\lambda}_1)\|\rho_2(\boldsymbol{\lambda}))$ as a function of its second argument. If we now take the infinitesimal limit as $\rho_2 \to \rho_1$ (similar to the case of classical relative entropy), we can Taylor expand the relative entropy function. The Hessian (the third term of the Taylor expansion), which is second order in $\Delta\lambda$, gives us the metric $g_{ij} = \frac{\partial^2 \mathcal{S}}{\partial \lambda^j \partial \lambda^i}$. The form of this metric[95] in the case of a qubit is

$$ds^2 = \frac{dr^2}{1 - r^2} + \left[\frac{r}{2} \log\left(\frac{1+r}{1-r}\right)\right](d\theta^2 + \sin^2\theta d\phi^2). \qquad (4.21)$$

This metric has been discussed earlier by Bogoliubov, Kubo and Mori (BKM) in the context of statistical mechanical fluctuations[96,97]. Using the BKM and

the BH metrics, the quantum advantage can be defined as

$$\Omega(\rho, \rho+d\rho) = ds^2_{BKM} - ds^2_{BH} = \left[\frac{r}{2}\log\left(\frac{1+r}{1-r}\right) - r^2\right](d\theta^2 + \sin^2\theta d\phi^2).$$

$$(4.22)$$

Taking spherical symmetry into account, this can be written as $\left[\frac{r}{2}\log\left(\frac{1+r}{1-r}\right) - r^2\right]d\theta^2$.

4.3 Quantum advantage : Measurements on Multiple Qubits

Let us now take the "thermodynamic" limit of large N. Given N qubits, which may be a state $\rho_1^{\otimes N}$ or $\rho_2^{\otimes N}$ we can choose a measurement basis in the Hilbert space $\mathcal{H}^{\otimes N}$. The optimisation over measurement bases is now over an enlarged set. Earlier we were restricted to bases of the form $b^{\otimes N}$ which are separable in the Hilbert space $\mathcal{H}^{\otimes N}$. We now have the freedom to include entangled bases and this implies

$$\frac{S^*(\rho_1^{\otimes N}\|\rho_2^{\otimes N})}{N} \geq S^*(\rho_1\|\rho_2).$$

$$(4.23)$$

In fact[98], no matter how small the separation between the distinct states ρ_1 and ρ_2, as $N \to \infty$, $\frac{1}{N}S^*(\rho_1^{\otimes N}\|\rho_2^{\otimes N}) \to S(\rho_1\|\rho_2)$, where $S(\rho_1\|\rho_2)$ is Umegaki's quantum relative entropy. As we see in Fig 4.4, this is greater than or equal to the classical relative entropy, so the appropriate relative entropy to use in the thermodynamic limit is Umegaki's relative entropy.

To illustrate the quantum advantage that comes from grouping qubits before measuring them, we numerically study an example for $N = 2$ and $\rho_1, \ \rho_2$ distinct and well separated. The quantum state of the combined system is now given by $\tilde{\rho} = \rho \otimes \rho$, where ρ can refer to either ρ_1 or ρ_2. In choosing a measurement basis to distinguish $\tilde{\rho}_1$ from $\tilde{\rho}_2$, we now have the additional advantage that we can choose bases which are not separable. This extra freedom gives us the quantum advantage which comes from entanglement. For example, let us choose $(r_1, r_2, \theta) = (0.9, 0.5, \pi/2)$ so that $X = \{r_1, 0, 0\}$, $Y = \{r_2/\sqrt{2}, 0, r_2/\sqrt{2}\}$ and the direction $\hat{m}$ in the x-z plane $\hat{m} = \{\cos \beta, 0, \sin \beta\}$. Let the corresponding 1-qubit basis which diagonalizes $\hat{m}.\boldsymbol{\sigma}$ be $|+\rangle, |-\rangle$. We now construct the non separable basis $|b_1\rangle = \frac{|+-\rangle + |-+\rangle}{\sqrt{2}}$, $|b_2\rangle = \frac{|+-\rangle - |-+\rangle}{\sqrt{2}}$, $|b_3\rangle = |++\rangle$ and $|b_4\rangle = |--\rangle$. Note that two of these basis states are maximally entangled Bell states and two are completely separable. (Curiously, using all basis states as Bell states leads to no improvement over the separable states.) We numerically compute the relative entropy and optimise over β. This leads to an improvement over measurements conducted on one qubit at a time. The improvement is seen in the value of the relative entropy per qubit, which increases from 0.5839 in the one qubit strategy to 0.5856 in the two-qubit strategy.

In fact, this number can be further improved. By numerical Monte-Carlo searching (see A.4), we have found bases (which don't have the clean form above) which yield a relative entropy of 0.5863 per qubit. Our Monte-Carlo search is

simplified by the observation that one can by a unitary transformation bring any two states described by X and Y to the x-z plane of the Bloch ball so that we are working over the real numbers rather than complex numbers. Over the reals, unitary matrices are orthogonal matrices. We start with an initial basis in the four-dimensional real Hilbert space of the composite system and then rotate the basis by a random orthogonal matrix close to the identity. We then compute the relative entropy using the new basis and accept the move if the new basis has larger relative entropy and reject it otherwise. This gives us a monotonic rise in the relative entropy and drives us towards the optimal basis in the two-qubit Hilbert space.

The method extends easily to three qubits and more, although the searches are more time-consuming. We have numerically observed that measuring three qubits at a time results in a further improvement over the two-qubit measurement strategy. However, this number (0.5880) still falls short of the quantum relative entropy which is 0.6385. The classically optimised relative entropy S_N^* for N qubits considered as a single system satisfies the inequality $\frac{1}{N}S_N^* \leq S_Q$[98] where S_Q is the quantum relative entropy. As $N \to \infty$ the inequality is saturated. Thus the gap between the classically optimised relative entropy and the quantum relative entropy (Figures 4.2 and 4.4) progressively reduces as one increases the number of qubits measured at a time.

Figure 4.5 represents the geometry of the qubit state space. Here we draw and
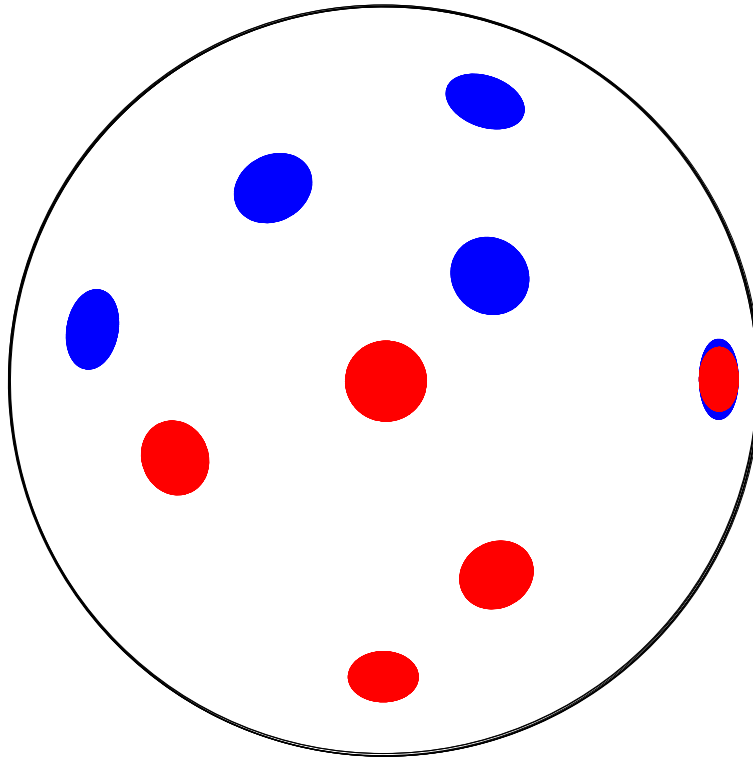
Figure 4.5: The qubit state space with contours (analogous to MacAdam ellipses) for the relative entropy, $S = 0.005$.

compare optimised classical relative entropy (blue contours, see A.5) and quantum relative entropy (red contours, see A.6). This is analogous to the MacAdam ellipses in the space of colours. These contours indicate that all states that fall

inside the region are indistinguishable from the reference state. To draw the contours, we set the the value of the relative entropy to 0.005, below which the states are indistinguishable. The contour on the right shows both classical and quantum relative entropies superposed (same reference state). Note that the red contour is *inside* the blue contour and the region that falls only on blue contour represents the quantum advantage. For superposed contours the states falling in the blue region but not red region are distinguishable using quantum relative entropy but not classical relative entropy. This tells us that, for a given relative entropy (below which the states are indistinguishable), we can distinguish more states using quantum relative entropy than classical relative entropy. Thus there is an advantage in using the quantum relative entropy instead of classical relative entropy in distinguishing quantum states.

4.4 Proposed Experimental Realisation

The strategy described above can be experimentally realised with current technology using cold atoms in traps. Experimental realisations of the quantum advantage are within reach. There have been studies involving measurements for quantum state discrimination[73,74,75], where the upper limit of the state distinguishability is set by the classical relative entropy. In order to exploit the quantum advantage discussed here, we need to measure in an entangled basis of the two-qubit system. The entangled basis $|b_i\rangle$ mentioned here, is related to the

separable basis $|++\rangle$, $|+-\rangle$, $|-+\rangle$, $|--\rangle$ by a unitary transformation U in the four dimensional Hilbert space. One can equivalently apply U to the separable state $\tilde{\rho} = \rho \otimes \rho$. This creates an entangled state $U^\dagger \tilde{\rho} U$, which can then be measured in the separable basis using a projective measurement. Consider a pair of qubits subject to the Hamiltonian

$$H = \vec{\sigma_1}.\vec{B_1} + \vec{\sigma_2}.\vec{B_2} + J(t)\vec{\sigma_1}.\vec{\sigma_2}, \qquad (4.24)$$

which is a standard Heisenberg Hamiltonian for spins. This Hamiltonian evolution produces the unitary transformation U for suitable choice of $J(t)$.

This entangling unitary transformation U is the square root of the SWAP operation $U = \sqrt{SWAP}$. U has already been experimentally realised in[99] by creating a system in the laboratory subject to the Hamiltonian (4.24). The method used in[99] is to load ^{87}Rb atoms in pairs into an array of double-well potentials. The experimenters have control over all the parameters in the Hamiltonian. They can generate the transformation U at will by using a $\pi/4$ pulse for $J(t)$ by using radio frequency, site selective pulses to address the qubits in pairs (See Table 1 of[99]), thus effecting the entangling unitary transformation U.

4.5 CONCLUSION

We have used the quantum relative entropy as a starting point which measures our ability to distinguish two quantum states. Our use of the quantum relative

entropy is motivated by the fact that it has both physical and operational significance. Other measures of entropy do exist, like for example, the α-divergence. Hasegawa[100] has derived a Riemannian metric using the α-divergence as the starting point. As discussed here, relative entropy has an operational significance in the context of quantum measurement which makes it an attractive candidate for deriving a metric on the space of quantum states. Umegaki's relative entropy is additive for independent systems, (unlike the α-divergence) and also has a well defined physical interpretation in terms of statistical physics.

Questions addressed here were raised but not fully answered in an early paper of Peres and Wootters[101]. At that time it was not fully clear whether there was a one qubit strategy which could compete with the multi-qubit strategy. Subsequent works have made it clear[102,98] that the best one qubit strategy is inferior to the multi-qubit strategy. As N goes to infinity, we approach the bound set by the quantum relative entropy in distinguishing the states, which is superior to the one set by the optimised classical relative entropy. We propose an experimental strategy for realising the quantum relative entropy using entanglement.

There is a divergence in relative entropy that occurs as one approaches the limit of pure states. It is natural to ask if this is a genuine singularity or one caused by our choice of coordinates. It is easily seen that the singularity is genuine. The divergence of relative entropy as one approaches $r = 1$ (pure states) has a physical interpretation. It means that pure states are much easier to dis-

criminate between, than mixed states. Conversely, even a small corruption of the purity of quantum states will seriously undermine our ability to distinguish between them.

The quantum advantage described here is strongly connected to the commutation properties of the density matrices ρ_1 and ρ_2. For commuting matrices, it is evident that the optimal basis should simultaneously diagonalize both the states and then the quantum advantage disappears. In fact, there is a correlation between the quantum advantage and the *quantumness* defined in[103,104] as $Q(\rho_1, \rho_2) = 2\text{Tr}([\rho_1, \rho_2]^2)$ in terms of the commutator of two density matrices ρ_1 and ρ_2, using the Hilbert-Schmidt norm as a distinguishability measure on the space of density matrices. In particular, in the case analysed here, considering ρ_2 in the neighbourhood of ρ_1, we find that $Q(\rho_1, \rho_2) = r^4 d\theta^2$.

In the context of quantum metrology[105,106] the idea that a quantum procedure leads to an improved sensitivity in parameter estimation compared to its classical counterpart has been explored. The central limit theorem dictates that the average error propagates as $\Delta/\sqrt{N}$, where N is the number of samples or probes and Δ^2 is the variance associated with each probe.

While this is true in a classical probe of a quantum system, this can be improved by using, what we call a quantum probe. A quantum probe can be present either during the measurement process or at the input itself. They argue that the presence of a quantum probe at the measurement end does not yield any

different result, but a quantum probe at the input betters the precision to $1/N$, which is called the Heisenberg limit. They go on to show that this is the true limit in case of estimating a quantum parameter using certain protocols.

In the context of quantum metrology[105,106], researchers are interested in estimating only one parameter, which cannot be used in the comparison of states. We need at least three parameters for distinguishing two qubits. In our work, we are interested in distinguishability of quantum states. In quantum metrology, N (the number of measurements on the qubits) is advantageous in scaling the error with the factor $1/N$. In contrast, here we are interested in the measurement or realisation of Δ which stems from the relative entropy.

"The noblest pleasure is the joy of understanding."

Leonardo da Vinci

5

Optimal Information Extraction from a Quantum State

In classical probability theory a natural question that comes up is the following: How accurately can one estimate the parameters of a probability distribution[107]. This arises in drug testing, predicting election results etc. For example, a shoe

manufacturer needs the distribution of shoe sizes of his customers for effective control over the manufacturing process. In estimating the probability distribution one need not study the entire dataset. Instead one can consider a small sample such that it is as random as possible. Our work explores related questions in quantum states. How does one infer a quantum state by random sampling? Here we are interested in estimating the parameters of a quantum state through the measurement process and address questions related to the entropy of the state after measurement.

The result of a quantum measurement is dependent on the measurement basis. Projective measurements give us only the probabilities associated with the measured state[8,36]. So, in order to achieve the optimal result, we need to choose the basis in which the state is diagonalised. If we do not have any prior information regarding the state we are measuring, the process of choosing the basis gets to be completely random. This raises the question of the extent to which we deviate from the true state when we choose an arbitrary basis. The question we like to pose is the following: in the case of an unknown quantum state how can we maximise the information that we can extract regarding the state.

To address this question we choose to compare the Von Neumann entropy[8] of the state before and after measurement with respect to the basis of measurement. The entropy of the state gives us the uncertainty (or the lack of knowledge) regarding the state in question, which decreases after the measurement.

In contrast, the information gain (knowledge regarding the state) increases after the measurement.

5.1 INFORMATION GAIN

Given any quantum state ρ, the Von Neumann entropy is defined as $S = -\text{Tr}[\rho \log \rho]$. Prior to making any measurement the observer has no knowledge of the state. This leaves us with maximum uncertainty in guessing the state. This corresponds to the maximally mixed state. In the case of a d dimensional system, the entropy of a maximally mixed state is given by $\log d$. Using this we define a new term called *Information Gain* (I)[108], which measures what we learned from the measurements.

Now let us consider the relative entropy between two states ρ and σ

$$S(\rho\|\sigma) = \text{Tr}[\rho \log \rho - \rho \log \sigma] \tag{5.1}$$

where, ρ represents the state to be estimated and σ is our guess for what the state is. We define Information gain (I) as the relative entropy between ρ and σ, where σ is the maximally mixed state. This gives us

$$I = \log d + \text{Tr}\rho \log \rho. \tag{5.2}$$

This formula can also be achieved by directly subtracting the Von Neumann

entropy of the state from that of the maximally mixed state.

Let us consider the case of a qubit on the Bloch sphere[7].

$$\rho = \frac{\mathbb{I} + \vec{n}.\vec{\sigma}}{2}, \ \hat{M}_{\pm} = \frac{\mathbb{I} \pm \hat{m}.\vec{\sigma}}{2} \tag{5.3}$$

$$p_+ = \frac{1 + \vec{n}.\hat{m}}{2}, \ p_- = \frac{1 - \vec{n}.\hat{m}}{2} \tag{5.4}$$

Where, $\hat{m}$ is the unit vector along the measurement direction and $\vec{\sigma} = (\sigma_x, \sigma_y, \sigma_z)$ represent Pauli matrices. The density matrix ρ can be expressed in the measurement basis as

$$\rho = \frac{1}{2} \begin{pmatrix} 1 + r\cos\theta & r\sin\theta \\ r\sin\theta & 1 - r\cos\theta \end{pmatrix} \tag{5.5}$$

where $r = |\vec{n}|$ and $\cos\theta = \vec{n}.\hat{m}$.

The entropy $(-\mathrm{Tr}[\rho\log\rho])$ calculated from these probabilities will be the least when $\hat{m}$ and $\vec{n}$ are parallel. Information gain after measurement is given by

$$I = \log 2 - S = \log 2 + p_+ \log p_+ + p_- \log p_-. \tag{5.6}$$

This will always be less than the maximum unless one makes a measurement in the basis where $\hat{m}$ and $\vec{n}$ are parallel. Here we wish to compute the average information gain, where $\vec{n}$ is fixed and $\hat{m}$ can be any unit vector on the Bloch

sphere.

$$I = \log 2 + \left(\frac{1 + r\cos\theta}{2}\right)\log\left(\frac{1 + r\cos\theta}{2}\right) + \left(\frac{1 - r\cos\theta}{2}\right)\log\left(\frac{1 - r\cos\theta}{2}\right)$$

$$(5.7)$$

$$
\begin{aligned}
\langle I \rangle &= \frac{\int_0^\pi \int_0^{2\pi} I \sin\theta d\theta d\phi}{\int_0^\pi \int_0^{2\pi} \sin\theta d\theta d\phi} = \log 2 + \frac{1}{2}\int_0^\pi (p_+ \log p_+ + p_- \log p_-)\sin\theta d\theta \\
&= \frac{1}{2r}\left[(1 + r)^2 \log(1 + r) - (1 - r)^2 \log(1 - r)\right] - \frac{1}{2} \qquad (5.8)
\end{aligned}
$$

This gives us the average information gain, where a state is measured in a completely arbitrary basis.

Let us now consider the case where measurements are made on two qubits at a time i.e. we make measurements on $\rho \otimes \rho$. Calculating probabilities in the separable basis gives us the probabilities

$$
\begin{aligned}
p_{|++\rangle} &= \frac{(1 + r\cos\theta)^2}{4}, \quad p_{|+-\rangle} = \frac{1 - r^2\cos^2\theta}{4} \\
p_{|--\rangle} &= \frac{(1 - r\cos\theta)^2}{4}, \quad p_{|-+\rangle} = \frac{1 - r^2\cos^2\theta}{4}
\end{aligned}
$$

Similarly, measuring in the Bell basis gives us the probabilities

$$p_{\frac{|++\rangle+|--\rangle}{\sqrt{2}}} = \frac{1+r^2}{4}, \quad p_{\frac{|++\rangle-|--\rangle}{\sqrt{2}}} = \frac{1+r^2\cos 2\theta}{4}$$

$$p_{\frac{|+-\rangle-|-+\rangle}{\sqrt{2}}} = \frac{1-r^2}{4}, \quad p_{\frac{|+-\rangle+|-+\rangle}{\sqrt{2}}} = \frac{1-r^2\cos 2\theta}{4}$$

Measuring in a separable basis doesn't change the information extracted. Measuring in the Bell basis does not always reveal more information, in fact it does worse than the separable basis in general. To gain an improvement we choose a basis which is a combination of both the Bell and separable states, given by $|++\rangle, |--\rangle, \frac{|++\rangle+|--\rangle}{\sqrt{2}}, \frac{|+-\rangle-|-+\rangle}{\sqrt{2}}$ [95]. The Information gain after measurement in this basis is

$$
\begin{aligned}
I &= \frac{1-r^2\cos 2\theta}{8}\log\left(\frac{1-r^2\cos 2\theta}{4}\right) + \frac{1-r^2}{8}\log\left(\frac{1-r^2}{4}\right) \\
&\quad + \left(\frac{1+r\cos\theta}{2}\right)^2\log\left(\frac{1+r\cos\theta}{2}\right) \\
&\quad + \left(\frac{1-r\cos\theta}{2}\right)^2\log\left(\frac{1-r\cos\theta}{2}\right) + \log 2
\end{aligned}
\tag{5.9}
$$

The average information gain is given by
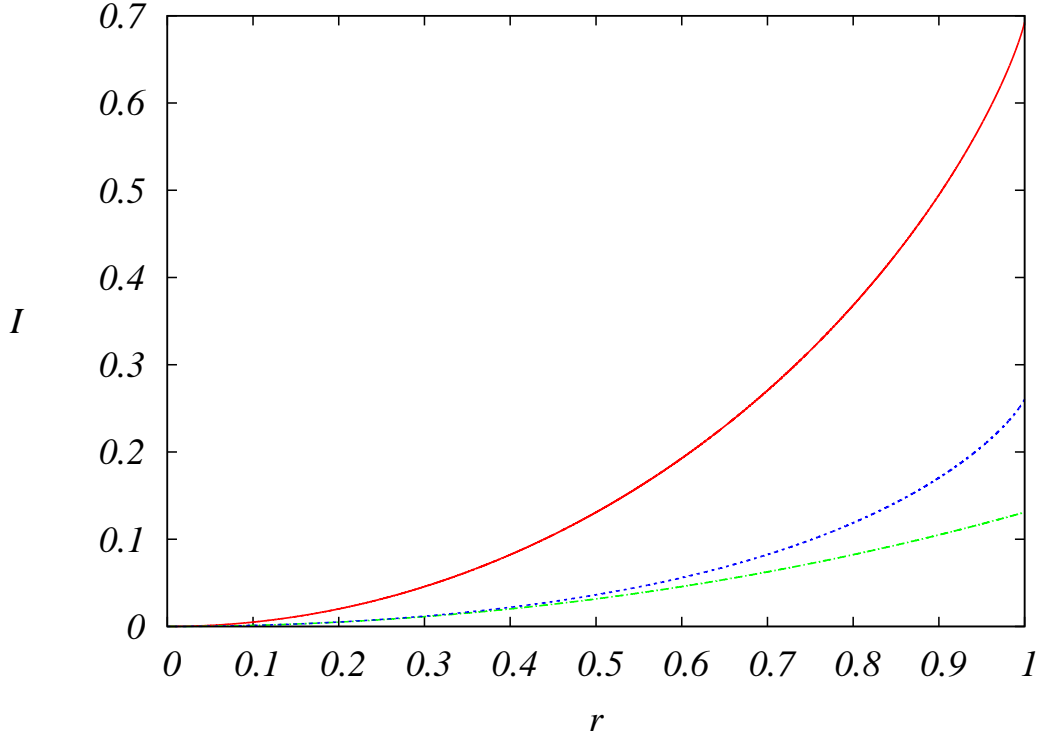
Figure 5.1: Comparison between maximum information extractable (red) and information extracted after measurement using a two qubit strategy (blue) and a one qubit strategy (green), for fixed $\theta = \pi/3$, as a function of r.

$$
\begin{aligned}
\langle I \rangle &= \frac{\frac{3}{2}(r-1)^3 \log(1-r) + \frac{3}{2}(r+1)^3 \log(r+1) - 4r\left(r^2+3\right)(1+\log 8)}{76r} \\
&+ \frac{r\sqrt{r^2+1}\left(3\left(r^2+3\right)\log(1-r) - 2\left(r^2(4+\log 8)+6+\log 512\right)\right)}{76r\sqrt{r^2+1}} \\
&+ \frac{3r\sqrt{r^2+1}\left(r^2+3\right)\log(r+1) + 3\sqrt{2}\left(r^2+1\right)^2 \log\left(\frac{1+3r^2+2\sqrt{2}r\sqrt{r^2+1}}{2\sqrt{2}r\sqrt{r^2+1}-1-3r^2}\right)}{76r\sqrt{r^2+1}} \\
&+ \log 2 + \frac{\left(1-r^2\right)}{2}\log\left(\frac{1-r^2}{4}\right)
\end{aligned}
\tag{5.10}
$$
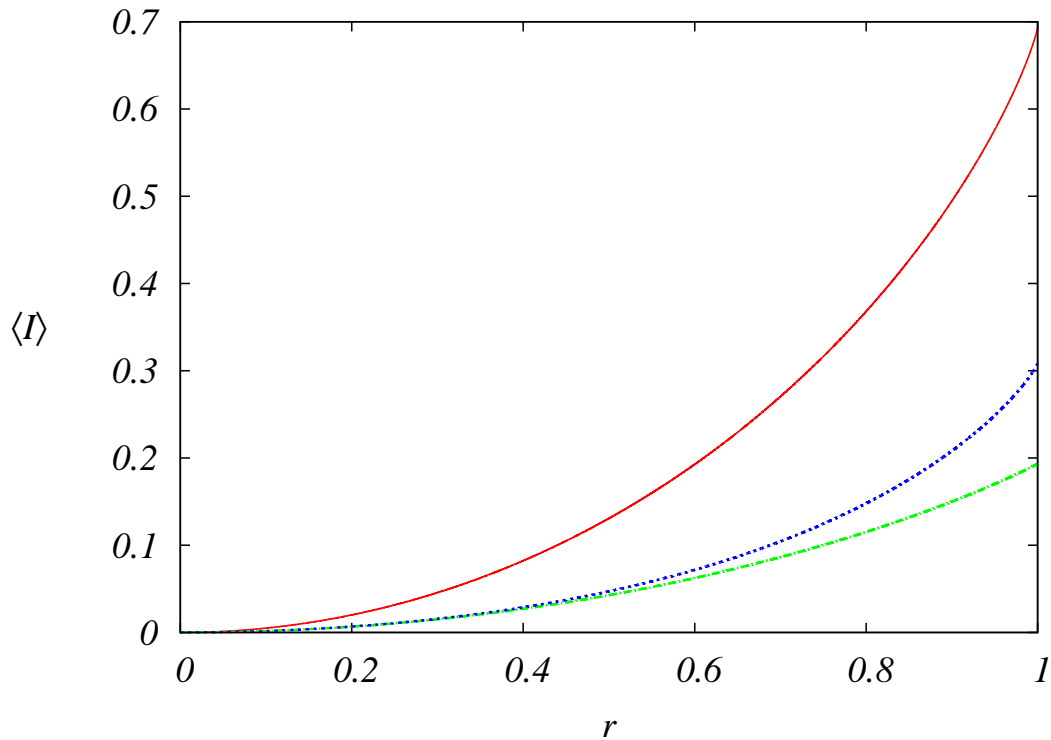
Figure 5.2: Comparison between maximum information extractable (red) and average information extracted after measurement using a two qubit strategy (blue) and a one qubit strategy (green), as a function of r.

In Fig 5.1 we have plotted the information extracted as a function of r for a fixed θ. Here we have compared the maximum information available (5.2) (red) with the information extracted after measurement in a one qubit strategy (5.7) (green) and a two qubit strategy (5.9) (blue). Similarly, in Fig 5.2 we have plotted and compared the maximum information available (5.2) (red) with the average information extracted after measurement in a one qubit strategy (5.8) (green) and a two qubit strategy (5.10) (blue).

In Figures 5.3 and 5.4 we have shown how the information extracted after mea-
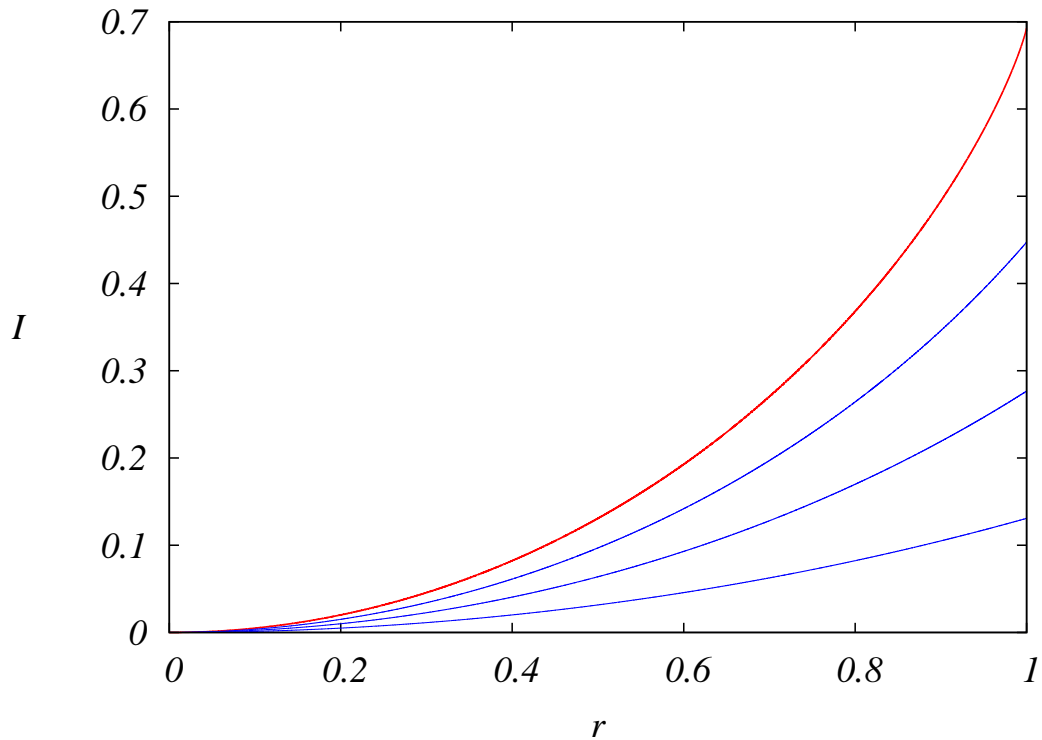
Figure 5.3: Information extracted using a one qubit strategy for the angles, $\theta = \pi/2, \pi/3, \pi/4, \pi/6, 0\,(red)$.

surement in a one qubit strategy (5.8) and a two qubit strategy (5.10) changes with the change in the angle θ, respectively.

5.2 CONCLUSION

In this chapter we start with the notion of information gain and relate it to the quantum measurement process.

In particular we consider the case of a qubit and concretise our ideas in this context. We compare the actual information gained in a measurement process
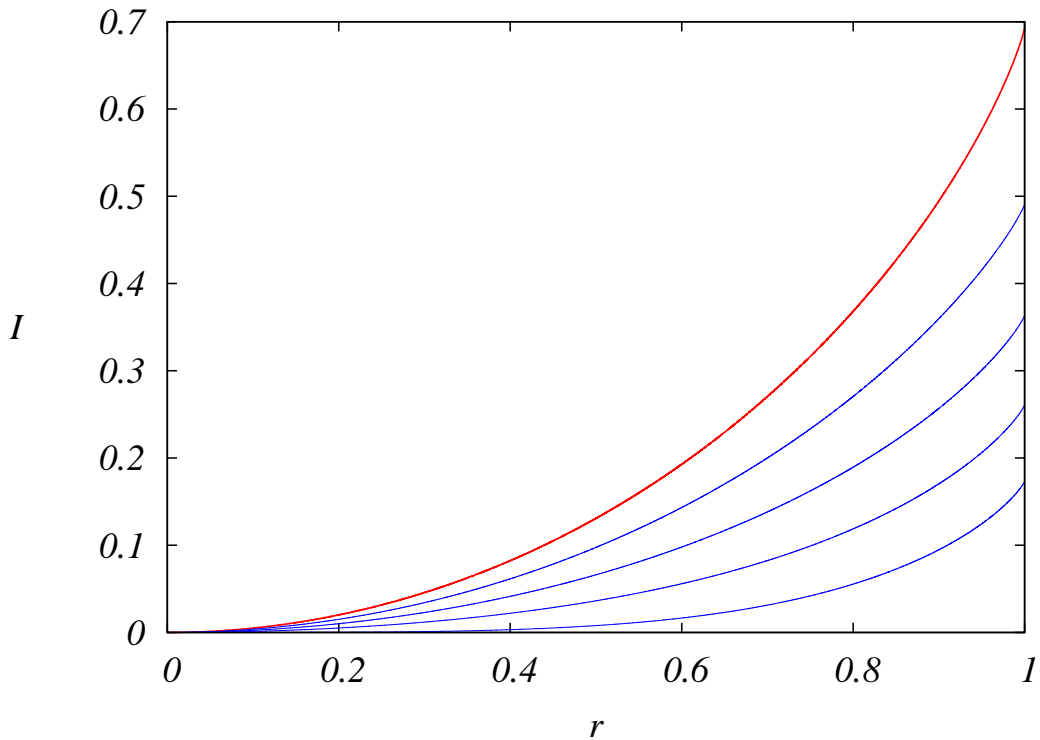
Figure 5.4: Information extracted using a two qubit strategy for the angles, $\theta = \pi/2, \pi/3, \pi/4, \pi/6, 0(red)$.

with the amount of information extractable.

Furthermore, we move from a one qubit measurement strategy to a two qubit measurement strategy to improve the information gain. Finally we compare the average information gain in a one qubit strategy and a two qubit strategy.

We find that we definitely gain by invoking a two qubit strategy. So, we can extrapolate this idea to a multi qubit strategy involving more than two qubits to optimise the information gain in a measurement.

"If I have seen further than others, it is by standing upon the shoulders of giants."

Isaac Newton

6
Conclusion

The central goal of this thesis has been to investigate aspects of classical and quantum cloning and issues related to the measurement process.

The thesis is organised in six chapters as follows:

1. Introduction.

2. Classical and Quantum Cloning.

3. Role of resource limitation in quantum measurements.

4. Quantum advantage in measurements.

5. Optimal Information Extraction from a Quantum State.

6. Conclusion.

In Chapter II, we studied quantum cloning using atom-photon interactions. Then we introduced thermal noise in the system at the atomic level and the photon level to see the effects on the fidelity of the cloning process. We find that the fidelity definition used traditionally in the literature does not distinguish between the processes with and without the thermal noise. Hence, we use a slightly different form of fidelity that brings out the effects of temperature.

Then we study the classical limit of the cloning process by taking both the number of photons and atoms to infinity. This gives us, as expected a perfect cloning process with fidelity one.

In future we would like to replace the photon with classical light and study its interaction with the atomic system.

This leads us to the study of the cloning process in the classical regime. Although perfect cloning is possible in the classical regime, the physics behind the process is not trivial. We study the classical cloning process using symplectic maps. We demonstrate a procedure which generates symplectic maps required

for the cloning process. We also generate a Hamiltonian to realise the symplectic map for conjugate variables p, q and study the process in phase space. Later we replaced the delta functions with probability distributions and how this corrupts the cloning process. We use fidelity to check to what extent the process corrupts the original and the copy.

The measurement process is a fundamental aspect of quantum mechanics. In Chapter III, we study the effects of coarse graining on the measurement process and study how it affects the information obtained from the measurement process. For this we use a Stern-Gerlach setup. Here we treat the system (spin) quantum mechanically and the apparatus (magnetic field and the position of the silver atom) classically. We do a coarse graining on the screen (where we detect the silver atom) i.e, the screen is pixelated. We show that this coarse graining process leads to an apparent loss of unitarity in the quantum measurement process.

After the wave packet is passed through the magnetic field, we show how coarse graining using a pixelated screen washes away the coherent terms.

In Chapter IV, we study distinguishability of quantum states using measurements. Here we use relative entropy as the distinguishability measure because of its connection to the likelihood theory. We study this in the case of qubits on the Bloch sphere. We study how well we can distinguish two qubits after measurement. This depends upon the basis in which we choose to measure the

state. We choose the basis in which the relative entropy between the states is maximum after the measurement. We found that this is less than the quantum relative entropy between the states (except when the states commute with each other), which provides higher distinguishability. So, we came up with a strategy of measuring multiple qubits at a time that improves upon the optimised classical relative entropy. We propose an experiment using cold atoms to realise how a multi-qubit strategy provides a better distinguishability that a single qubit strategy.

In Chapter V, we study how to extract maximum information from a given state, when no information regarding the state is available. The probabilities measured depend upon the basis in which we choose to measure. But when we don't have any information regarding the state which we are measuring, the choice of the basis becomes completely arbitrary. This leads to a reduction of the information extracted from the state available. We define information extracted as $I = \log 2 - S$, in the case of qubits, where S is the entropy of the state. We use a similar strategy used in[95] to increase the information extracted. We also calculated the average information extracted for a given qubit, averaged over the entire Bloch sphere. Here we compare and show how measuring multiple qubits at a time enables us to extract more information compared to measuring one qubit at a time.

A

Programs

Mathematica program for numerical analysis to see how the presence of statistical mechanical noise affects the cloning process.

$$p = 5;$$

$$q = 8;$$

$$m = 1;$$

$$k = 1;$$

$$T1 = 10^{23}; (*\text{Temperature of the source.}*)$$

$$T2 = 10^{23}; (*\text{Temperature of the target.}*)$$

$$T3 = 10^{23}; (*\text{Temperature of the machine.}*)$$

$$L1 = \{\};$$

$$R = \{\};$$

$$M = \{\};$$

$$H = \{\};$$

$$\text{For}[i = 1, i < 2 \times 10^4, i++,$$

$$\text{p1} = \text{RandomVariate}\left[\text{NormalDistribution}\left[0, \sqrt{mT1k_B}\right], 1\right][[1]];$$

$q_1 = \text{RandomVariate}\left[\text{NormalDistribution}\left[0, \sqrt{\dfrac{T_1 k_B}{k}}\right], 1\right][[1]];$

$p_2 = \text{RandomVariate}\left[\text{NormalDistribution}\left[0, \sqrt{m T_2 k_B}\right], 1\right][[1]];$

$q_2 = \text{RandomVariate}\left[\text{NormalDistribution}\left[0, \sqrt{\dfrac{T_2 k_B}{k}}\right], 1\right][[1]];$

$p_3 = \text{RandomVariate}\left[\text{NormalDistribution}\left[0, \sqrt{m T_3 k_B}\right], 1\right][[1]];$

$q_3 = \text{RandomVariate}\left[\text{NormalDistribution}\left[0, \sqrt{\dfrac{T_3 k_B}{k}}\right], 1\right][[1]];$

$\Lambda = \{\{1, 0, 1., 1, -1, 1\}, \{0, 1, 1, 2, 0, 1\}, \{1, 0, 0, 1, 0, 1\},$

$\{0, 1, -1, -1, 1, 0\}, \{1, 0, 1, 2, -1, 2\}, \{0, -1, 0, -1, -1, -1\}\};$

$S = \{p + p1, q + q1, p2, q2, p3, q3\};$

$f = \Lambda.S;$

$L_1 = \text{Append}[L_1, \{p + p1, q + q1\}];$

$R = \text{Append}[R, \{f[[1, 1]], f[[1, 2]]\}];$

$M = \text{Append}[M, \{f[[1, 3]], f[[1, 4]]\}];$

$H = \text{Append}[H, \{f[[1, 5]], f[[1, 6]]\}];\,]$

$m = 1.79 \times 10^{-25};$

$a = 5178.77;$

$\hbar = 1.054 \times 10^{-34};$

$\sigma = 10^{-6};$

$t = 2.25 \times 10^{-5};$

$x = 2 \times 10^{-6}; (*Position \ of \ the \ pixel.*)$

$$\int_0^{-10^6} \left(\int_0^{-10^6} \sqrt{\frac{m^2 \sigma^2}{\pi \left(m^2 \sigma^4 + t^2 \hbar^2 \right)}} \exp \left(-\frac{m^2 \sigma^2 \left(x - \frac{1}{2} a t^2 \right)^2}{\left(m^2 \sigma^4 + t^2 \hbar^2 \right)} \right) du \right) dv;$$

This program gives us gives the value registered by the pixel. Expression inside the integral can be changed to calculate all the density matrix elements.

$m = 1.79 \times 10^{-25}$;

$a = 5178.77$;

$\hbar = 1.054 \times 10^{-34}$;

$\sigma = 10^{-6}$;

$$P_+(x) = \frac{m\sigma \times \exp\left(-\frac{m^2\sigma^2\left(x-\frac{at^2}{2}\right)^2}{m^2\sigma^4+t^2\hbar^2}\right)}{2\sqrt{\pi\left(m^2\sigma^4+t^2\hbar^2\right)}};$$

$$P_-(x) = \frac{m\sigma \times \exp\left(-\frac{m^2\sigma^2\left(\frac{at^2}{2}+x\right)^2}{m^2\sigma^4+t^2\hbar^2}\right)}{2\sqrt{\pi\left(m^2\sigma^4+t^2\hbar^2\right)}};$$

$r = N[\text{Table}[\{10^6 t, \text{NIntegrate}[P_-\log P_- + P_+\log P_+ - (P_- + P_+)\log(P_- + P_+),$

$\{x, -10^{-5}, 10^{-5}\}] + \log(2)\}, \{t, 0, 5 \times 10^{-5}, 10^{-8}\}]]$

This program numerically calculates the mean information per event, $\mathcal{H}$.

$r1 = .9; r2 = .5; \text{the} = \dfrac{\pi}{2};$

$rho1 = \{\{(1 + r1)/2, 0\}, \{0, (1 - r1)/2\}\};$

$rho2 = \{\{(1 + r2Cos[the])/2, r2Sin[the]/2\}, \{r2Sin[the]/2, (1 - r2Cos[the])/2\}\};$

$A = \text{Table}[\text{RandomReal}[], \{i, 1, 4\}, \{j, 1, 4\}];$

$\text{Banti} = A - A^{\mathsf{T}}; \text{O1} = \text{MatrixExp}[\text{Banti}];$

$\text{Rho1} = \text{KroneckerProduct}[\text{rho1}, \text{rho1}];$

$\text{Rho2} = \text{KroneckerProduct}[\text{rho2}, \text{rho2}];$

$\text{B1} = \text{O1}.\{1, 0, 0, 0\}; \text{B2} = \text{O1}.\{0, 1, 0, 0\};$

$\text{B3} = \text{O1}.\{0, 0, 1, 0\}; \text{B4} = \text{O1}.\{0, 0, 0, 1\};$

$\text{eps} = 0.001; \text{L1} = \{\text{Stw}\};$

$\text{For}[j = 1, j < 20000, j\text{++},$

$\text{A1} = \text{Table}[\text{RandomReal}[], \{i, 1, 4\}, \{j, 1, 4\}];$

$\text{Banti1} = \text{A1} - \text{A1}^{\mathsf{T}}; \text{O2} = \text{MatrixExp}[\text{Banti1} \times \text{eps}];$

$\text{B1p} = \text{O2}.\text{B1}; \text{B2p} = \text{O2}.\text{B2}; \text{B3p} = \text{O2}.\text{B3}; \text{B4p} = \text{O2}.\text{B4};$

$\text{P1} = \text{B1}.\text{Rho1}.\text{B1}; \text{P2} = \text{B2}.\text{Rho1}.\text{B2}; \text{P3} = \text{B3}.\text{Rho1}.\text{B3}; \text{P4} = \text{B4}.\text{Rho1}.\text{B4};$

$\text{Q1} = \text{B1}.\text{Rho2}.\text{B1}; \text{Q2} = \text{B2}.\text{Rho2}.\text{B2}; \text{Q3} = \text{B3}.\text{Rho2}.\text{B3}; \text{Q4} = \text{B4}.\text{Rho2}.\text{B4};$

$$\text{Stw} = \text{P\textsc{i}}\log\left(\frac{\text{P\textsc{i}}}{\text{Q\textsc{i}}}\right) + \text{P2}\log\left(\frac{\text{P2}}{\text{Q2}}\right) + \text{P3}\log\left(\frac{\text{P3}}{\text{Q3}}\right) + \text{P4}\log\left(\frac{\text{P4}}{\text{Q4}}\right);$$

P\textsc{i}p = B\textsc{i}p.Rho\textsc{i}.B\textsc{i}p;

P2p = B2p.Rho\textsc{i}.B2p;

P3p = B3p.Rho\textsc{i}.B3p;

P4p = B4p.Rho\textsc{i}.B4p;

Q\textsc{i}p = B\textsc{i}p.Rho2.B\textsc{i}p;

Q2p = B2p.Rho2.B2p;

Q3p = B3p.Rho2.B3p;

Q4p = B4p.Rho2.B4p;

$$\text{Stwp} = \text{P\textsc{i}p}\log\left(\frac{\text{P\textsc{i}p}}{\text{Q\textsc{i}p}}\right) + \text{P2p}\log\left(\frac{\text{P2p}}{\text{Q2p}}\right) + \text{P3p}\log\left(\frac{\text{P3p}}{\text{Q3p}}\right) + \text{P4p}\log\left(\frac{\text{P4p}}{\text{Q4p}}\right);$$

If[Stwp > L\textsc{i}[[−1]], B\textsc{i} = B\textsc{i}p; B2 = B2p; B3 = B3p; B4 = B4p; ,];

L\textsc{i} = Append[L\textsc{i}, Stwp];]

This program can be extended to the case of measuring three qubits at a time.

A.5 Fortran program for numerically calculating Macadam ellipses of classical relative entropy.

c MacadamC.F

c Macadam Ellipses for Classical Relative Entropy

c

```fortran
c Created by Anirudh reddy on 14/04/17.
c C1(r1=0.9,x=0.84,0.95)
c C2(r1=0.8,x=0.72,0.87)
c C3(r1=0.6,x=0.5,0.7)
c C4(r1=0.4,x=0.3,0.5)
c C5(r1=0.0,x=-0.1,0.1)

    implicit none
integer i, j, K
real S, Sopt, r1, x, y, phi, p1, p2, q1, q2
real, parameter :: pi = 4.*atan(1.)
real, dimension(2,2) :: rho1, rho2
real, dimension(2,1) :: b1, b2
real, dimension(1,1) :: junk
character*100 filename

    write(filename,"(A6)") "C4.txt"
open(111, file=filename)
r1 = 0.4
rho1 = reshape((/ (1.+r1)/2., 0., 0., (1.-r1)/2. /), shape(rho1))
do i = 0, 200
```

```fortran
x = 0.3 + i*2*0.0005

do j = 0, 200

y = -0.15 + j*3*0.0005

S = 0.

do k = 0, 36000

phi = 0. + k*2.*pi/36000

rho2 = reshape((/ (1.+x)/2., y/2.,

y/2., (1.-x)/2. /), shape(rho2))

b1 = reshape((/ cos(phi), sin(phi) /), shape(b1))

b2 = reshape((/ -sin(phi), cos(phi) /), shape(b2))

junk = matmul(matmul(transpose(b1), rho1), b1)

p1 = junk(1,1)

junk = matmul(matmul(transpose(b2), rho1), b2)

p2 = junk(1,1)

junk = matmul(matmul(transpose(b1), rho2), b1)

q1 = junk(1,1)

junk = matmul(matmul(transpose(b2), rho2), b2)

q2 = junk(1,1)

Sopt = p1*log(p1/q1) + p2*log(p2/q2)

if (Sopt .gt. S) then

S = Sopt
```

```
endif

enddo

if (S .lt. 0.005) then

write(111,*) y,x

endif

enddo

enddo

close(111)

write(*,*) "Yay! The code is complete. :P"

end
```

A.6   Fortran program for numerically calculating Macadam ellipses of Quantum relative entropy.

```
c MacadamQ.F
c Macadam Ellipses for Quantum Relative Entropy
c
c Created by Anirudh reddy on 14/04/17.
c M1(r1=0.9,x=0.84,0.95)
c M2(r1=0.8,x=0.72,0.87)
c M3(r1=0.6,x=0.5,0.7)
```

```
c M4(r1=0.4,x=0.3,0.5)
c M5(r1=0.0,x=-0.1,0.1)

      implicit none
integer i, j
real*8 S, r1, x, y
character*100 filename


      write(filename,"(A6)") "M5.txt"
open(111, file=filename)

r1 = 0.0
do i = 0, 200
x = - 0.1 + i*2*0.0005
do j = 0, 200
y = -0.1 + j*2*0.0005
S=(-((1.+r1*x/Sqrt(x**2+y**2))/2.)*Log((1.+Sqrt(x**2+y**2))/2.)
-(1.-r1*x/Sqrt(x**2+y**2))/2.*Log((1.-Sqrt(x**2+y**2))/2.)
+(1.+r1)/2.*Log((1.+r1)/2.)+(1.-r1)/2.*Log((1.-r1)/2.))
if (S .lt. 0.005) then
write(111,*) y,x
endif
```

```
enddo
enddo
close(111)
end
```

References

[1] A. Daffertshofer, A. R. Plastino, and A. Plastino. Classical no-cloning theorem. *Phys. Rev. Lett.*, 88:210601, May 2002.

[2] C. E. Shannon. A mathematical theory of communication. *Bell System Technical Journal*, 27(3):379–423, 1948.

[3] Thomas M. Cover and Joy A. Thomas. *Elements of Information Theory (Wiley Series in Telecommunications and Signal Processing)*. Wiley-Interscience, 2006.

[4] E. T. Jaynes. Information theory and statistical mechanics. *Phys. Rev.*, 106:620–630, May 1957.

[5] R. Landauer. Irreversibility and heat generation in the computing process. *IBM Journal of Research and Development*, 5(3):183–191, July 1961.

[6] Charles H. Bennett. The thermodynamics of computation—a review. *International Journal of Theoretical Physics*, 21(12):905–940, 1982.

[7] M.A. Nielsen and I.L. Chuang. *Quantum Computation and Quantum Information*. Cambridge Series on Information and the Natural Sciences. Cambridge University Press, 2000.

[8] J. Von Neumann. *Mathematical Foundations of Quantum Mechanics*. Investigations in physics. Princeton University Press, 1955.

[9] Charles H. Bennett, Gilles Brassard, Claude Crépeau, Richard Jozsa, Asher Peres, and William K. Wootters. Teleporting an unknown quantum state via dual classical and einstein-podolsky-rosen channels. *Phys. Rev. Lett.*, 70:1895–1899, Mar 1993.

[10] Lov K. Grover. A Fast quantum mechanical algorithm for database search. 1996.

[11] David Deutsch and Richard Jozsa. Rapid solution of problems by quantum computation. *Proceedings of the Royal Society of London A: Mathematical, Physical and Engineering Sciences*, 439(1907):553–558, 1992.

[12] Peter W. Shor. Polynomial-time algorithms for prime factorization and discrete logarithms on a quantum computer. *SIAM J. Comput.*, 26(5):1484–1509, October 1997.

[13] W. K. Wootters and W. H. Zurek. A single quantum cannot be cloned. *Nature*, 299(5886):802–803, Oct 1982.

[14] D. Dieks. Communication by epr devices. *Physics Letters A*, 92(6):271 – 272, 1982.

[15] Nick Herbert. Flash—a superluminal communicator based upon a new kind of quantum measurement. *Foundations of Physics*, 12(12):1171–1179, 1982.

[16] A. Peres. How the no-cloning theorem got its name. *Fortschritte der Physik*, 51(4-5):458–461, 2003.

[17] Gian Carlo Ghirardi and T Weber. Quantum mechanics and faster-than-light communication: Methodological considerations. *Il Nuovo Cimento B (1971-1996)*, 78(1):9–20, 1983.

[18] V. Bužek and M. Hillery. Quantum copying: Beyond the no-cloning theorem. *Phys. Rev. A*, 54:1844–1852, Sep 1996.

[19] N. Gisin and S. Massar. Optimal quantum cloning machines. *Phys. Rev. Lett.*, 79:2153–2156, Sep 1997.

[20] R. F. Werner. Optimal cloning of pure states. *Phys. Rev. A*, 58:1827–1832, Sep 1998.

[21] J. Kempe, C. Simon, and G. Weihs. Optimal photon cloning. *Phys. Rev. A*, 62:032302, Aug 2000.

[22] Christoph Simon, Gregor Weihs, and Anton Zeilinger. Optimal quantum cloning via stimulated emission. *Phys. Rev. Lett.*, 84:2993–2996, Mar 2000.

[23] Sylvain Fasel, Nicolas Gisin, Grégoire Ribordy, Valerio Scarani, and Hugo Zbinden. Quantum cloning with an optical fiber amplifier. *Phys. Rev. Lett.*, 89:107901, Aug 2002.

[24] Antía Lamas-Linares, Christoph Simon, John C. Howell, and Dik Bouwmeester. Experimental quantum cloning of single photons. *Science*, 296(5568):712–714, 2002.

[25] Heng Fan, Gregor Weihs, Keiji Matsumoto, and Hiroshi Imai. Cloning of symmetric d-level photonic states in physical systems. *Phys. Rev. A*, 66:024307, Aug 2002.

[26] Shubhrangshu Dasgupta and G. S. Agarwal. Improving the fidelity of quantum cloning by field-induced inhibition of the unwanted transition. *Phys. Rev. A*, 64:022315, Jul 2001.

[27] Sadegh Raeisi, Wolfgang Tittel, and Christoph Simon. Proposal for inverting the quantum cloning of photons. *Phys. Rev. Lett.*, 108:120404, Mar 2012.

[28] Chi-Sheng Niu and Robert B. Griffiths. Optimal copying of one quantum bit. *Phys. Rev. A*, 58:4377–4393, Dec 1998.

[29] Nicolas J. Cerf. Pauli cloning of a quantum bit. *Phys. Rev. Lett.*, 84:4497–4500, May 2000.

[30] Vladimír Bužek and Mark Hillery. Universal optimal cloning of arbitrary quantum states: From qubits to quantum registers. *Phys. Rev. Lett.*, 81:5003–5006, Nov 1998.

[31] Dagmar Bruß. Optimal eavesdropping in quantum cryptography with six states. *Phys. Rev. Lett.*, 81:3018–3021, Oct 1998.

[32] Masato Koashi and Nobuyuki Imoto. No-cloning theorem of entangled states. *Phys. Rev. Lett.*, 81:4264–4267, Nov 1998.

[33] Nicolas J. Cerf and Philippe Grangier. From quantum cloning to quantum key distribution with continuous variables: a review (invited). *J. Opt. Soc. Am. B*, 24(2):324–334, Feb 2007.

[34] Aaron Fenyes. Limitations on cloning in classical mechanics. *Journal of Mathematical Physics*, 53(1):012902, 2012.

[35] Charles H. Bennett and Gilles Brassard. Quantum cryptography: Public key distribution and coin tossing. *Theoretical Computer Science*, 560, Part 1:7 – 11, 2014. Theoretical Aspects of Quantum Cryptography â�’ celebrating 30 years of {BB84}.

[36] W. Heisenberg. *The Physical Principles of the Quantum Theory*. Dover Books on Physics and Chemistry. Dover Publications, 1949.

[37] E. Joos and H. D. Zeh. The emergence of classical properties through interaction with the environment. *Zeitschrift für Physik B Condensed Matter*, 59(2):223–243, 1985.

[38] David Bohm. A suggested interpretation of the quantum theory in terms of "hidden" variables. i. *Phys. Rev.*, 85:166–179, Jan 1952.

[39] Bryce S. DeWitt. Quantum mechanics and reality. *Physics Today*, 23(9):30–35, 1970.

[40] Angelo Bassi. Models of spontaneous wave function collapse: what they are, and how they can be tested. *Journal of Physics: Conference Series*, 701(1):012012, 2016.

[41] RAFAEL D. SORKIN. Quantum mechanics as quantum measure theory. *Modern Physics Letters A*, 09(33):3119–3127, 1994.

[42] Rafael D. Sorkin. Quantum measure theory and its interpretation. In *Physics and experiments with linear colliders. Proceedings, 3rd Workshop, Morioka-Appi, Japan, September 8-12, 1995. Vol. 1, 2*, 1995.

[43] S. Baghbanzadeh and A.T. Rezakhani. Temperature effects on quantum cloning of states and entanglement. *Physics Letters A*, 373(8):821 – 825, 2009.

[44] Valerio Scarani, Sofyan Iblisdir, Nicolas Gisin, and Antonio Acín. Quantum cloning. *Rev. Mod. Phys.*, 77:1225–1256, Nov 2005.

[45] Nicholas J. Teh. On classical cloning and no-cloning. *Studies in History and Philosophy of Science Part B: Studies in History and Philosophy of Modern Physics*, 43(1):47 – 63, 2012.

[46] Keiji Matsumoto. An asymptotic theory of cloning of classical state families. *arXiv e-prints*, page arXiv:1107.1090, July 2011.

[47] D. McDuff and D. Salamon. *Introduction to Symplectic Topology*. Oxford mathematical monographs. Clarendon Press, 1998.

[48] H. Hilgert and K. Neeb. *Structure and Geometry of Lie Groups*. Springer, 2012.

[49] Geoffrey New. *Introduction to Nonlinear Optics*. Cambridge University Press, 2011.

[50] A Venugopalan, Deepak Kumar, and R Ghosh. Environment-induced decoherence i. the stern-gerlach measurement. *Physica A: Statistical Mechanics and its Applications*, 220(3–4):563 – 575, 1995.

[51] Anu Venugopalan. Decoherence and schrödinger-cat states in a stern-gerlach-type experiment. *Phys. Rev. A*, 56:4307–4310, Nov 1997.

[52] Michel Gondran and Alexandre Gondran. A complete analysis of the stern-gerlach experiment using pauli spinors. *arXiv preprint quant-ph/0511276*, 2005.

[53] M. Hannout, S. Hoyt, A. Kryowonos, and A. Widom. Quantum measurement theory and the stern–gerlach experiment. *American Journal of Physics*, 66(5), 1998.

[54] D. E. Platt. A modern analysis of the Stern-Gerlach experiment. *American Journal of Physics*, 60:306–308, April 1992.

[55] G. P. Berman, G. D. Doolen, P. C. Hammel, and V. I. Tsifrinovich. Static stern-gerlach effect in magnetic force microscopy. *Phys. Rev. A*, 65:032311, Feb 2002.

[56] Marco Frasca. Stern-gerlach experiment and bohm limit. *arXiv preprint quant-ph/0402072*, 2004.

[57] M. O. Scully, E. L. Willis, and A. Barut. On the theory of the stern-gerlach apparatus. *Foundations Of Physics*, 17:575, 1987.

[58] P. Gomis and A. Pérez. A study of decoherence effects in the Stern-Gerlach experiment using matrix Wigner functions. *arXiv preprint quant-ph/1507.08541*, July 2015.

[59] Johannes Kofler and Caslav Brukner. Classical world arising out of quantum physics under the restriction of coarse-grained measurements. *Phys. Rev. Lett.*, 99:180403, Nov 2007.

[60] Hyunseok Jeong, Youngrong Lim, and M. S. Kim. Coarsening measurement references and the quantum-to-classical transition. *Phys. Rev. Lett.*, 112:010402, Jan 2014.

[61] Sadegh Raeisi, Pavel Sekatski, and Christoph Simon. Coarse graining makes it hard to see micro-macro entanglement. *Phys. Rev. Lett.*, 107:250401, Dec 2011.

[62] Richard Feynman and A. R. Hibbs. *Quantum Mechanics and Path Integrals*. McGraw-Hill, 1965.

[63] Bailey C. Hsu, Manuel Berrondo, and Jean-François S. Van Huele. Stern-gerlach dynamics with quantum propagators. *Phys. Rev. A*, 83:012109, Jan 2011.

[64] Jr. Walter T. Grandy. *Entropy and the Time Evolution of Macroscopic Systems*. Oxford University Press, 2008.

[65] A. A. Clerk, M. H. Devoret, S. M. Girvin, Florian Marquardt, and R. J. Schoelkopf. Introduction to quantum noise, measurement, and amplification. *Rev. Mod. Phys.*, 82:1155–1208, Apr 2010.

[66] Dipankar Home, Alok Kumar Pan, Md Manirul Ali, and A S Majumdar. Aspects of nonideal stern–gerlach experiment and testable ramifications. *Journal of Physics A: Mathematical and Theoretical*, 40(46):13975, 2007.

[67] L. S. Schulman. Book review: Decoherence and quantum measurements, by mikio namiki. *Foundations of Physics*, 29(11):1807–1810, 1999.

[68] Paul Busch, Marian Grabowski, and Pekka J. Lahti. *Operational Quantum Physics*. Springer Publishing Company, Incorporated, 1st edition, 2013.

[69] Michael Devereux. Reduction of the atomic wavefunction in the stern–gerlach magnetic field. *Canadian Journal of Physics*, 93(11):1382–1390, 2015.

[70] N. W. M. Ritchie, J. G. Story, and Randall G. Hulet. Realization of a measurement of a "weak value". *Phys. Rev. Lett.*, 66:1107–1110, Mar 1991.

[71] S. Amari. *Information Geometry and Its Applications*. Applied Mathematical Sciences. Springer Japan, 2016.

[72] Yong Siah Teo. *Introduction to Quantum-State Estimation*. World Scientific, 2015.

[73] Anthony Chefles. Quantum state discrimination. *Contemporary Physics*, 41(6):401–424, 2000.

[74] Masao Osaki, Masashi Ban, and Osamu Hirota. Derivation and physical interpretation of the optimum detection operators for coherent-state signals. *Phys. Rev. A*, 54:1691–1701, Aug 1996.

[75] Stephen M. Barnett and Sarah Croke. Quantum state discrimination. *Adv. Opt. Photon.*, 1(2):238–278, Apr 2009.

[76] A. S. Kholevo. On asymptotically optimal hypothesis testing in quantum statistics. *Theory of Probability & Its Applications*, 23(2):411–415, 1979.

[77] Lane P. Hughston, Richard Jozsa, and William K. Wootters. A complete classification of quantum ensembles having a given density matrix. *Physics Letters A*, 183(1):14 – 18, 1993.

[78] Paul Hausladen and William K. Wootters. A pretty good measurement for distinguishing quantum states. *Journal of Modern Optics*, 41(12):2385–2390, 1994.

[79] Hisaharu Umegaki. Conditional expectation in an operator algebra. iv. entropy and information. *Kodai Math. Sem. Rep.*, 14(2):59–85, 1962.

[80] Jonathon Shlens. Notes on kullback-leibler divergence and likelihood. *CoRR*, abs/1404.2000, 2014.

[81] Shinto Eguchi and John Copas. Interpreting kullback-leibler divergence with the neyman-pearson lemma. *Journal of Multivariate Analysis*, 97(9):2034 – 2040, 2006. Special Issue dedicated to Prof. Fujikoshi.

[82] I. Bengtsson and K. Zyczkowski. *Geometry of Quantum States: An Introduction to Quantum Entanglement.* Cambridge University Press, 2007.

[83] Joseph W. Weinberg. The geometry of colors. *General Relativity and Gravitation*, 7(1):135–169, 1976.

[84] David L. MacAdam. Visual sensitivities to color differences in daylight*. *J. Opt. Soc. Am.*, 32(5):247–274, May 1942.

[85] Dénes Petz. Geometry of canonical correlation on the state space of a quantum system. *Journal of Mathematical Physics*, 35(2), 1994.

[86] Dénes Petz. Covariance and fisher information in quantum mechanics. *Journal of Physics A: Mathematical and General*, 35(4):929, 2002.

[87] Hiroshi Hasegawa. Exponential and mixture families in quantum statistics: Dual structure and unbiased parameter estimation. *Reports on Mathematical Physics*, 39(1):49 – 68, 1997.

[88] Anna Jenčová. Geodesic distances on density matrices. *Journal of Mathematical Physics*, 45(5), 2004.

[89] M. R. Grasselli and R. F. Streater. On the uniqueness of the chentsov metric in quantum information geometry. *Infinite Dimensional Analysis, Quantum Probability and Related Topics*, 04(02):173–182, 2001.

[90] Paolo Facchi, Ravi Kulkarni, V.I. Man'ko, Giuseppe Marmo, E.C.G. Sudarshan, and Franco Ventriglia. Classical and quantum fisher information in the geometrical formulation of quantum mechanics. *Physics Letters A*, 374(48):4801 – 4803, 2010.

144

[91] Donald Bures. An extension of kakutani's theorem on infinite product measures to the tensor product of semifinite w^*-algebras. *Trans. Amer. Math. Soc. 135 (1969), 199-212*, 1969.

[92] C.W. Helstrom. Minimum mean-squared error of estimates in quantum statistics. *Physics Letters A*, 25(2):101 – 102, 1967.

[93] Samuel L. Braunstein and Carlton M. Caves. Statistical distance and the geometry of quantum states. *Phys. Rev. Lett.*, 72:3439–3443, May 1994.

[94] Åsa Ericsson. Geodesics and the best measurement for distinguishing quantum states. *Journal of Physics A: Mathematical and General*, 38(44):L725, 2005.

[95] K. Shivam, A. Reddy, J. Samuel, and S. Sinha. Entropy and Geometry of Quantum States. *ArXiv e-prints*, September 2016.

[96] Dénes Petz and Gabor Toth. The bogoliubov inner product in quantum statistics. *Letters in Mathematical Physics*, 27(3):205–216, 1993.

[97] R. Kubo, M. Toda, and N. Hashitsume. *Statistical Physics II, Nonequilibrium Statistical Mechanics*. Berlin:Springer, 1991.

[98] V. Vedral. The role of relative entropy in quantum information theory. *Rev. Mod. Phys.*, 74:197–234, Mar 2002.

[99] Marco Anderlini, Patricia J. Lee, Benjamin L. Brown, Jennifer Sebby-Strabley, William D. Phillips, and J. V. Porto. Controlled exchange interaction between pairs of neutral atoms in an optical lattice. *Nature*, 448(7152):452–456, Jul 2007.

[100] Hiroshi Hasegawa. Î±-divergence of the non-commutative information geometry. *Reports on Mathematical Physics*, 33(1):87 – 93, 1993.

[101] Asher Peres and William K. Wootters. Optimal detection of quantum information. *Phys. Rev. Lett.*, 66:1119–1122, Mar 1991.

[102] Fumio Hiai and Dénes Petz. The proper formula for relative entropy and its asymptotics in quantum probability. *Comm. Math. Phys.*, 143(1):99–114, 1991.

[103] P. Iyengar, G. N. Chandan, and R. Srikanth. Quantifying quantumness via commutators: an application to quantum walk. *ArXiv e-prints*, December 2013.

[104] L. Ferro, P. Facchi, R. Fazio, F. Illuminati, G. Marmo, V. Vedral, and S. Pascazio. Measuring quantumness: from theory to observability in interferometric setups. *ArXiv e-prints*, January 2015.

[105] Vittorio Giovannetti, Seth Lloyd, and Lorenzo Maccone. Quantum metrology. *Phys. Rev. Lett.*, 96:010401, Jan 2006.

[106] Marcin Zwierz, Carlos A. Pérez-Delgado, and Pieter Kok. General optimality of the heisenberg limit for quantum metrology. *Phys. Rev. Lett.*, 105:180402, Oct 2010.

[107] E. Walter and Luc Pronzato. *Identification of parametric models from experimental data.* Springer ; Masson, Berlin ; New York : Paris, 1997.

[108] Anirudh Reddy, Joseph Samuel, Kumar Shivam, and Supurna Sinha. Coarse quantum measurement: An analysis of the stern-gerlach experiment. *Physics Letters A*, 380(11):1135 – 1140, 2016.